ISSN Print 0970 - 3268
ISSN Online 2582 - 2020

The Journal of the Indian Association of Sedimentologists

The Indian Association of Sedimentologists

Volume 39 No. 2 July - December, 2022

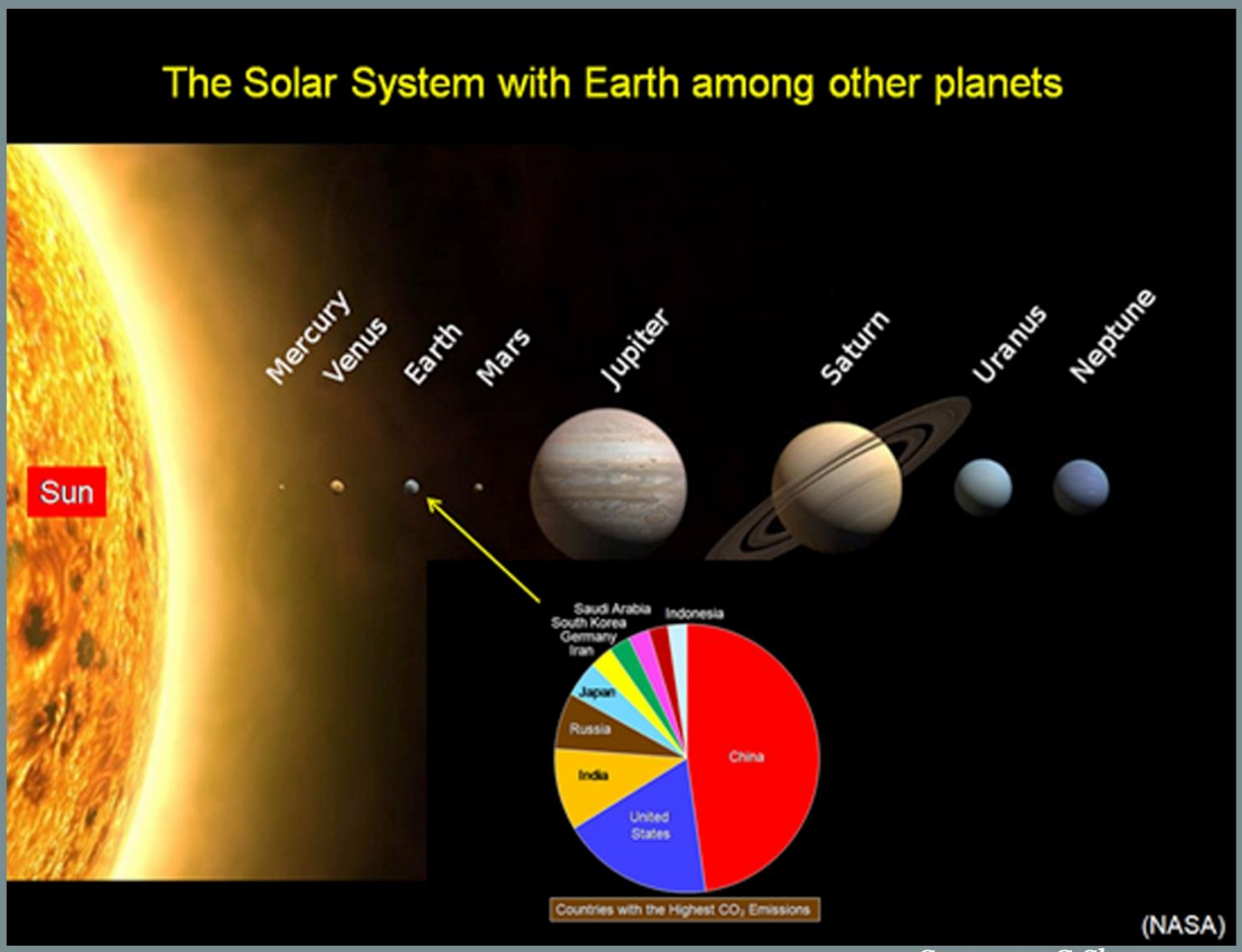

Courtesy: G Shanmugam

ISSN Print 0970 – 3268
ISSN online 2582 - 2020

The journal of the Indian Association of Sedimentologists

DOI:
https://doi.org/ 10.51710/jias.v39iII

The Journal of the Indian Association of Sedimentologists (IAS) is both an international open access online and print journal and is leader in its field and publishes ground-breaking research from across the spectrum of sedimentology, sedimentary geology, sedimentary geochemistry, experimental and theoretical sediment transport, mass movement fluxes, modern and ancient sedimentary environments, sequence – cyclo – chrono – and chemostratigraphy, sediment – biological interaction, palaeosols, diagenesis, stable isotope geochemistry, environmental sedimentology, neo-tectonics, geo-hazards, stratigraphy, palynology, sedimentary mineral resources and hydrocarbons, and allied branches of sedimentary - stratigraphic research. It also publishes review articles, editorials, conference reports, tributes, announcements, advertisements, etc. It is currently distributed to universities and research laboratories in India and abroad. Access is open to complete electronic journal archive. Subscribers also have the option to buy the printed journal at subsidized cost.

Indian Association of Sedimentologists

TABLE OF CONTENTS

JOURNAL INDIAN ASSOCIATION OF SEDIMENTOLOGISTS ISSN NO 2582 – 2020
Vol. 39, Issue 2, 2022, pp. 1-2
DOI: https://doi.org/10.51710/jias.v39iII.267

Geology of Wetlands: key for their conservation and development

Wetlands are prevalent in all types of landscapes around the world and constitute landforms, soil units, water features and faunal and floral communities. Wetlands sustain flora and fauna in the surface layer and they are dynamic and changing as such are reffered to as living landforms. Wetlands provide natural solutions for achieving "the Paris Climate Goals, Global Biodiversity Framework, and Sustainable Development Goals". Unfortunately wetlands have not received due attention by geologists even though geology and geological processes are at the baseline for their evolution and development. The main reason is a poor understanding of wetland landforms. Wetlands can develop only in regions where water accumulates, and the underlying surface/bed rock is impervious. They constitute unusual landforms developed by biogenic materials (solid materials, biological or organic mostly peat, gas and water) predominantly formed by biological processes.

Wetlands can be broadly classified as 1) mineral wetlands which generally develop in high-energy environments and 2) peatland wetlands which dvelop in low-energy environments. They either go through terrestrialization or paludification during the course of their development. Wetlands as landscape and economic resource are important and will continue to remain so in the future. They are intimately connected to the surroundings within their individual basins and watersheds. The geology of wetlands focuses on understanding these relationships (Moore, 2001). Sustainable use and management of wetlands are of paramount importance to conserve and enhance these resources to serve the needs of the associated faunal and floral communities and, protect the environment and health of human society.

India has nearly 4.6% of its land as wetlands which cover an area of 15.26 million hectares which constitute largest network of wetlands and Ramsar sites in South Asia. The 49 Ramsar sites in the country cover an area of 10, 93,636 hectares as of February 2022. The Indian wetland ecosystems are distributed in different geographical regions; most of these are directly or indirectly linked with major river systems (the Ganges, Cauvery, Krishna, Godavari and Tapti). There are 27,403 wetlands in India including 23,444 inland wetlands and 3,959 coastal wetlands. These cover around 4.63 percent of India's land area, with paddy cultivation accounting for 70% of that. The natural wetlands in India include high-altitude wetlands in the Himalaya, flood plains of major river systems, saline and transient wetlands in dry and semi-arid regions, and coastal wetlands (lagoons, backwaters, estuaries, mangroves, swamps, and coral reefs, etc.).

With the increasing awreness about global warming, climate change and their adverse impact on human society, wetland science has gained importance, refinement and has been widely recognised as a distinct and unique discipline in the environmental sciences. What is now needed to conserve this resource and its sustainable management is to understand the intricacies of wetland landforms, its hydrodynamics, biogeochemistry, fauna and flora, ecology and its linkages with climate, natural and anthropogenic interferences. In order to learn the intricacies of these elements of wetlands, role of geology and geological processes form the baseline for advancement in wetland science.

During 1900s geologists initiated to work on wetland geology but today geologists need to be involved with wetlands and to play their leading role, especially in view of current environmental and economic issues, like climate change, landscape development and rehabilitation, sustainable use of wetland resource, surface water and groundwater conservation and management, and health of human society. Geologists' interest in wetland geology should go beyond their narrow historical role with regard to peat as an economic resource, and must engage with much broader issues in understanding the origin, character, development, and management of the overall wetland resource. The new outlook and inputs from geologists will go a long way for plans and designs to ensure that wetlands remain intact, and engineers are enable in restoring and sustaining wetlands. This new outlook will indeed provide solution to the challenges of working with wetlands in the landscape and inventing nature-sensitive technologies and codes of debvelopment of wetlands.

Climate determines the sustainability of wetlands because it can both supply and remove water from them. If either of the two factors, geological setting or climate, impacts storage of water on the land surface, a wetland will not form. In case any one of these factors changes, the existing wetlands will perish. Low land wetlands termed as "Mineral wetlands" occur in high-energy settings and often exchange water with lakes, rivers or oceans in their vicinity. On the other hand, highland wetlands termed as peatlands occur in low-energy settings and are more independent of adjacent extraneous landscape units. Geology of the surrounding landscapes impact the evolution and development differently in these two cases. Peatlands are important repositories of paleoenvironmental

information (Warner and Bunting, 1996). As such, they can be long-term time capsules of climatic changes, geomorphic changes, natural catastrophes and human activities. The signatures preserved in peat and organic sediment or geochemical markers in the peat and deep interstitial waters are the primary tools for reconstructing the past events.

Human activities may be responsible for setting up conditions conducive to wetland formation or promoting its developmental processes (e.g. Warner et al., 1989). Geologists have an important role to play in assessing human impacts on wetlands, because not all intact wetlands are as natural as we think. In particular they have a major role to play in assessing peatland carbon stocks, characterizing the dynamics of carbon cycling, and developing predictive models of carbon and climate change (Frolking et al., 2001; Blodau, 2002). Some wetlands may overlie important groundwater aquifers, which support numerous wetlands and important aquifers used by the dense population around them (e. g., Sharpe et al., 2002). Wetlands are important for protecting surface and ground waters and drinking water supplies from complex biogeochemical trasformations which occur in them and attinuate contaminants in runnoff water coming from variety of human activities (i.e. Devito et al., 2000).

Geologists have also a role to play in our national carbon inventory because the net carbon stored in our wetlands greatly exceeds the carbon stored in our forests and agricultural soils.

Wetland sediments are a sealed archive of the historical information to be unravelled. The sequence of sediment types and their contained fossils provides a detailed record of how a particular wetland developed and enables the scientist to reconstruct the course of succession at that site. The microscopic fossils (diatoms, pollen grains) in the sediments can provide additional information about the changing conditions (past landscapes, modern polution problem, increasing acidity of rainfall, provide information about the evolution and development of living organisms and ecosystems) as the succession proceeds.

Wetland geology is far more relevant and important than is generally assumed. geology cource needs to be included in school curriculam which delas with wetlands. More emphasis should be laid on wetland science by including courses on Quaternary and environmental geology and on related subjects at the university level. State and Central governments need share a greater responsibility for care of valuable wetland resource for conservation and protection. Much more efforts need to be taken by the professionals to raise awareness among average citizens and governments of the relevance of conservation and protection of wetlands as biological landforms.

References

Blodau, C., 2002, Carbon cycling in peatlands – A review of processes and controls: Environmental Reviews, v. 10, p. 111-134.

Devito, K.J., Fitzgerald, D., Hill, A.R., and Aravena, R., 2000, Nitrate dynamics in relation to lithology and hydrologic flow path in a river riparian zone: Journal of Environmental Quality, v. 29, p. 1075-1084.

Frolking, S., Roulet, N.T., Moore, T.R., Richard, P.J.H., Lavoie, M. and Muller,S.D., 2001, Modelling northern peatland decomposition and peat accumulation: Ecosystems, v. 4, p. 479-498.

Moore, P.D., 2001, Wetlands: Facts on File Inc., N.Y., 200 p.

Sharpe, D.R., Hinton, M.J., Russell, H.A.J., and Desbarnts, A.J., 2002, The need for basin analysis in regional hydrogeological studies: Oak Ridges Moraine, southern Ontario: Geoscience Canada, v. 29, p. 3-20.

Warner, B.G. and Bunting, M.J. 1996, Indicators of rapid environmental change in northern peatlands in Berger, A.R. and Iams, W.J., Geoindicators: Assessing rapid environmental changes in earth systems:A.A. Balkema, Rotterdam, p. 235-246.

Warner, B.G., Kubiw, H.J. and Hanf, K.I., 1989, An anthropogenic cause for quaking mire formation in southwestern Ontario: Nature, v. 340, p. 380-384.

G. M. Bhat
Department of Geology
University of Jammu, Jammu
bhatgm@jugaa.com; bhatgm1@rediffmail.com

JOURNAL INDIAN ASSOCIATION OF SEDIMENTOLOGISTS ISSN NO 2582 – 2020
Vol. 39, Issue 2, 2022, pp. 3-9
DOI: https://doi.org/10.51710/jias.v39iII.238

Microtextures on quartz grains in the Estuary sediments of Gurupura River, Dakshina Kannada district, Karnataka State, West coast, India.

Darshan, M. S., Shivanna, K. Siddaraju and P. Madesh*

Department of Marine Geology, Mangalore University. 574199
*Department of studies in Earth Science. University of Mysore.570006
E-mail: darshanmadeshshobha@gmail.com. siddarajukgeo@gmail.com

Abstract;

The present study focuses on the surface textures of the quartz grains derived from the granitic rocks in a fluvial regime on the west coast of India. The surface microtextures formed during transport due to their stable physical and chemical properties. The surface textures include information about source rock types, transporting force, sedimentary environment and evolution history of the sediment. For this purpose, eight samples were collected and investigated from the Gurupura River estuary of Dakshina Kannada District of Karnataka state west coast in India. The quartz grains show distinct surface textures with unique mechanical, chemical and morphological features. The mechanical features such as conchoidal fractures with arcuate steps indicate that the sand grains were derived from crystalline source rock (i.e., granite) and transported in a high-energy condition. The silica globule, overgrowth, and precipitation marks on the grain surfaces suggest action of chemical processes in a saturated silica environment, which is evident in the upper reaches of the Gurupura River. Surface textures of the quartz grains along the lower reaches of the Gurupura River display an array of mechanical features like a conchoidal fracture, V-shaped marks and impact pits, indicating the impact of mechanical processes. The overall pattern of the surface textures present on the quartz grains suggests moderate to high energy conditions in the Gurupura River.

Keywords: Microtextures, Estuary Sediments, Gurupura, SEM, West coast.

Introduction

The study of surface textures of quartz grains with the help of scanning electron microscopy (SEM) is considered a powerful tool in sedimentary petrology for interpreting sedimentary environments and the provenance of the detrital sediments (Madhavaraju et al., 2006; Armstrong et al., 2014). Furthermore, the surface textures provide useful information regarding the various processes acting on the grains during transportation (Chakroun et al., 2009). Different impact features and the abrasion marks on the quartz grains are formed during transport in various dynamic environments, and they generally record those processes. Based on the variety of surface textures observed on the quartz grains it is possible to distinguish the particular depositional environment such as marine, fluvial, aeolian and glacial (Madhavaraju et al., 2006). The purpose of the present study is to study the surface textures present on quartz grains in the Gurupura River sediments exclusively derived from peninsular gneiss on the west coast of India.

Investigated Area

Dakshina Kannada is a three coastal district located in the southern and coastal part of Karnataka adjoining the Arabian Sea. The geographically entire district spreads over 4770 sq. km. The study area lies between lat. 12˚ 50’00’’& 12˚55’00’’N and long. 74˚ 50’ 00’’& 75˚00’00’’ East.

The Geological map of the area (Map.2) indicates that the N–G River basins are covered by Pliocene to Recent laterite capped plateaus and alluvium over the gneisses and continental type of sedimentary deposits with dolerite and norite dikes (Geological Survey of India 1981, Radhakrishna and Vaidyanadhan 1994). The Gurpura river is tectonically active due to a number of seismically active faults/ lineaments and its proximity to Mulki–Pulicat lake axis (a straight line close to 13^0 N connecting the west and east coasts of India). The slight deviation of the drainage divide from this fault can be ascribed to differential headward erosion of the north-easterly and south-easterly flowing rivers (Subrahmanya 1994). The N–G river channels consist of cobble–pebble–gravel at their upper reaches and coarse sand in their middle parts (for~ 50 km). The river basins consist of migmatites and, granodioritic to tonalitic gneisses of the Peninsular Gneissic Complex with enclaves of high-grade supracrustals (Geological Survey of India 1981, Nair 1990).

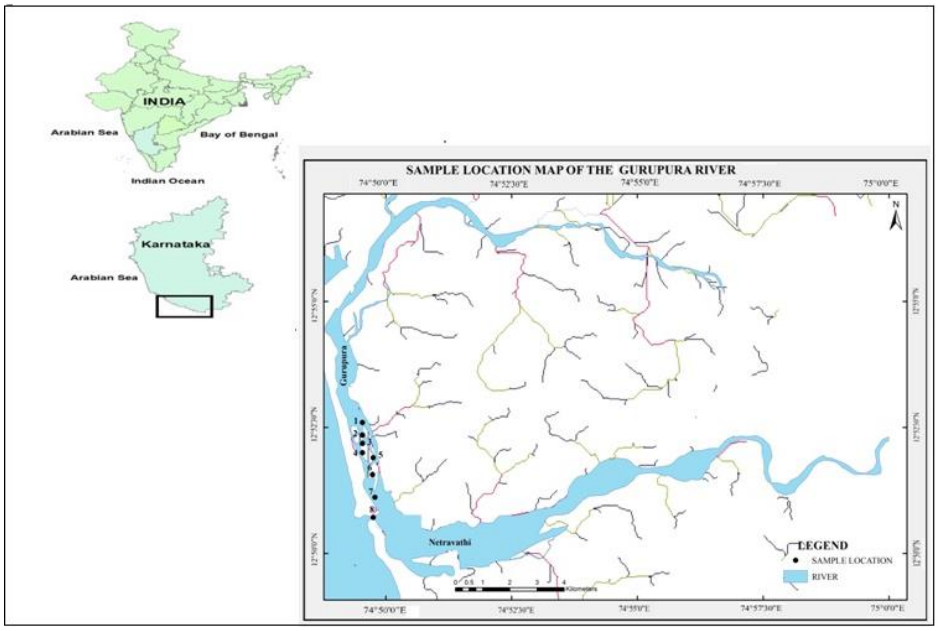

Map.1. Location and sample points of the study area, Geology of the Netravathi and Gurupura River Basin

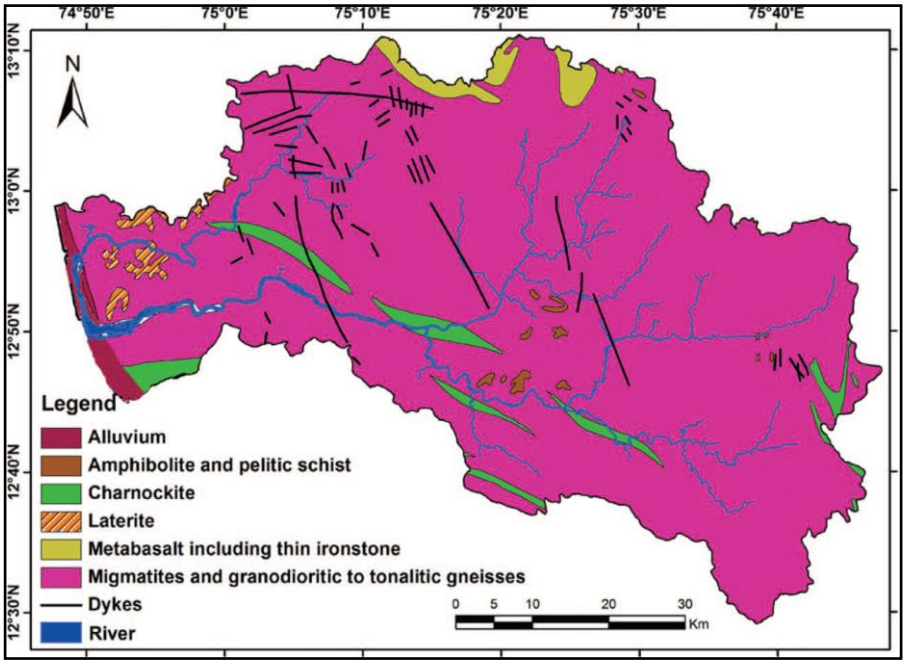

Map. 2 Geological Map of the Netravathi and Gurpura river basins (source: Geological Survey of India 1981).

Materials and Method

Sand samples were collected from the eight locations of the Gurupura River estuary. Samples were collected at 200-300 meters regular intervals along the 2-3 km length during the Post-monsoon season (Month of February 2020) (Map.1). For the microtextural study. Approximately 100g of each sample was socked with H_2O_2 and HCl to remove the organic matter and carbonate coatings from the quartz grains and then washed several times with distilled water (Krinsley and Doornkamp, 1973; Helland and Holmes, 1997). The treated samples were sieved to separate the sand-size fraction. The samples were sieved at 0.6-Ø interval by using the ASTM sieve setson Ro-tap mechanical sieve shaker. Sand grains of 120 ASTM size were used for the surface microtextural studies. Fot the study of variability present in the grains (Higgs 1979; Krinsley and Doornkamp, 1973), 3-4 selected quartz grains in each sample were selected. Quartz grains were examined for their surface microtextural features in *Hitachi S-3400N SEM at a magnification of ×5 to ×300,000* at the Department of Material science, Vijnana Bhavan, University of Mysore, Karnataka, India.

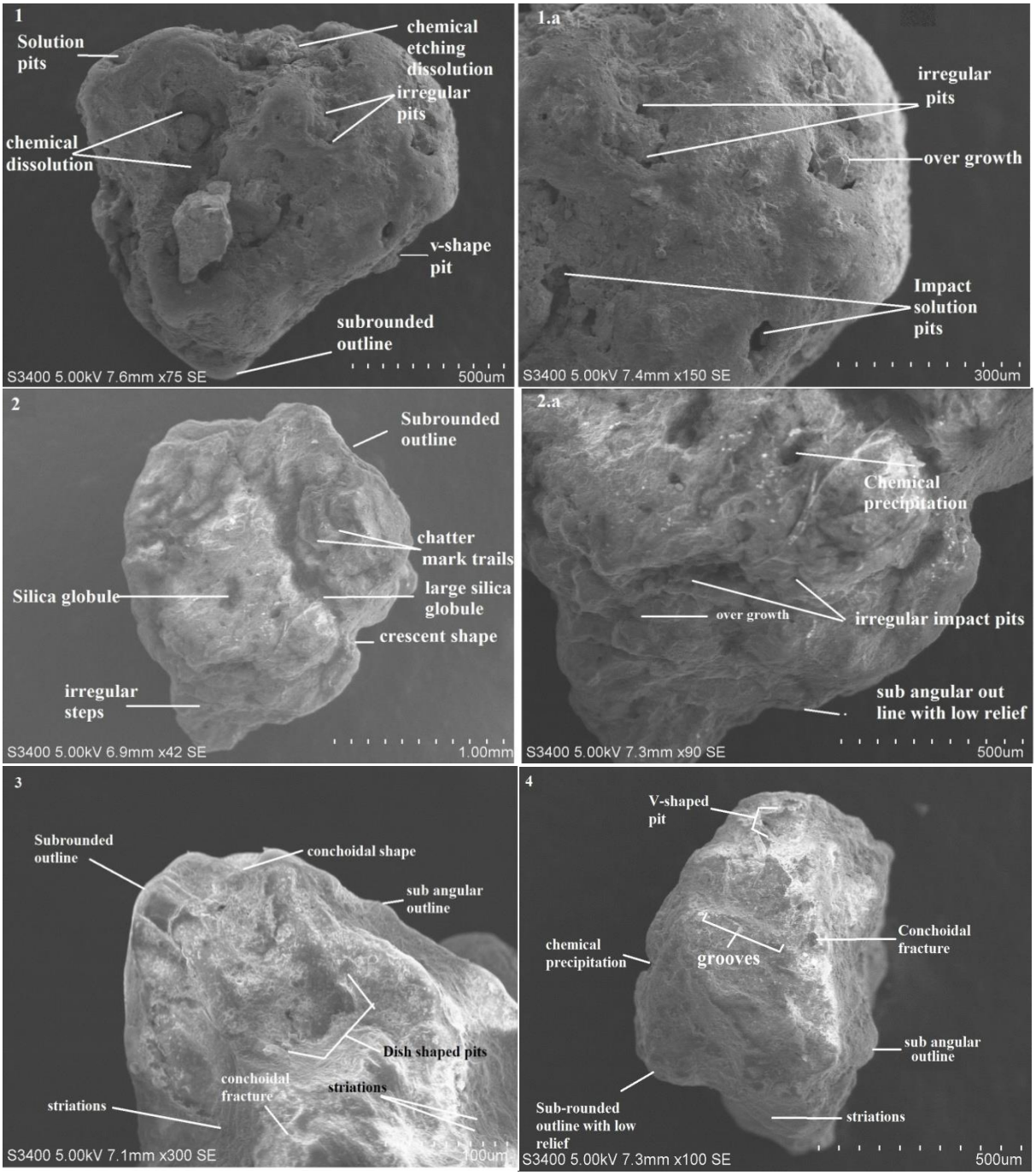

Plate-1 Microtextures observed on quartz grains form Gurupura estuary (Samples: 1–4) S-1: Quartz grain showing solution pit, chemical etching dissolution, irregular pits, V- shaped pit, sub rounded outline and chemical dissolution.S-1a: Irregular pits, over growth, impact solution pits.S-2: Sub rounded outline, chatter mark trails, silica globule, large silica globule, cresent shape, irregular steps. S-2a: Chemical precipitation, over growth, irregular impact pits, sub angular out line with low relief. S-3: Sub rounded outline, conchoidal fracture, dish shaped pits. S-4: V-shaped pit, chemical precipitation, grooves, conchoidal fracture, sub angular outline, striations, sub rounded out line with low relief.

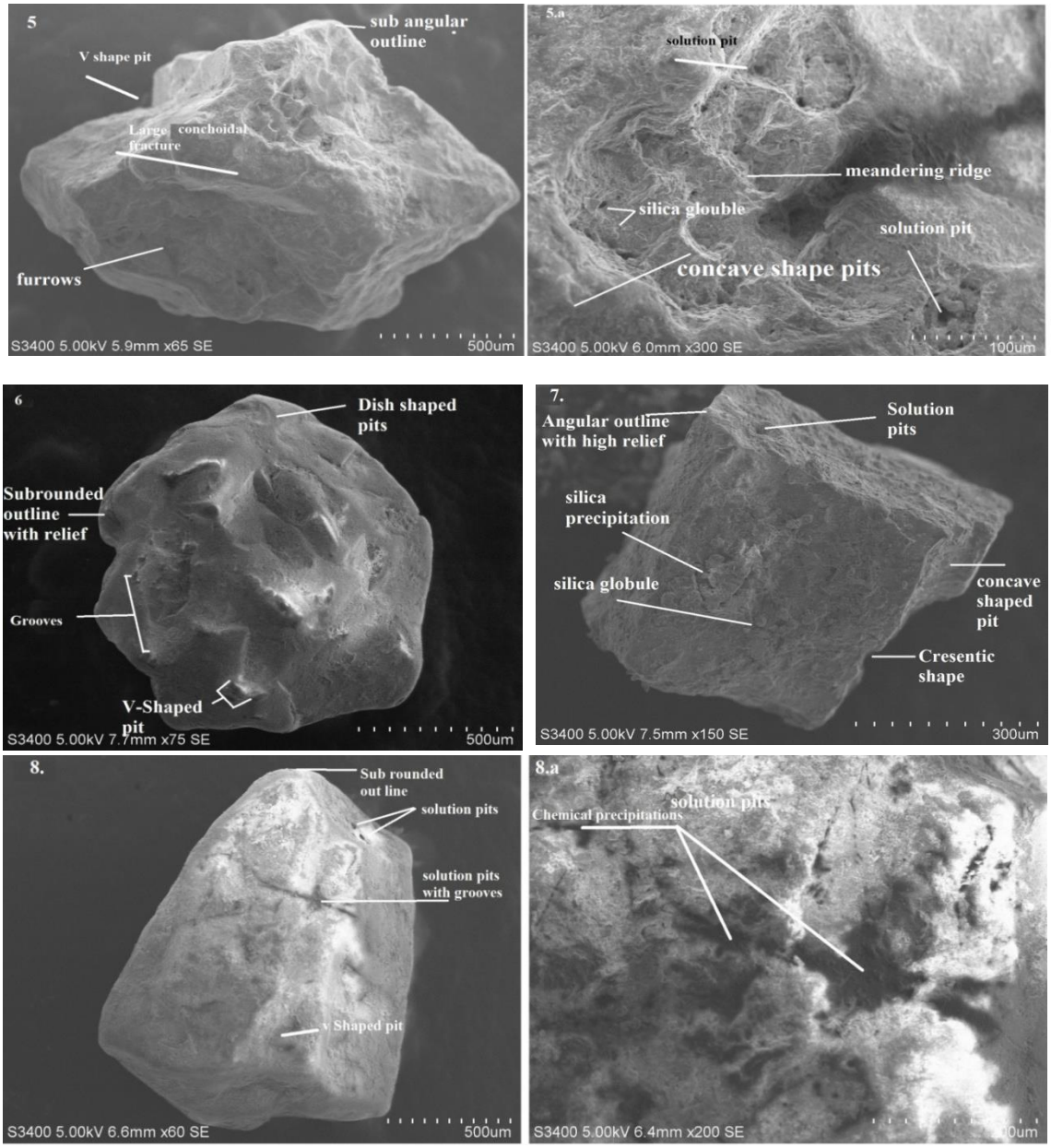

Plate-2 Microtextures observed on quartz grains form Gurupura estuary (Samples: 5-7) S-5: V-shaped pits, large conchoidal fracture, furrows, sub angular outline. S-5a: Solution pits meandering ridge, silica globule, concave shape pits steps. S-6: Dish shaped pits, sub rounded outline with low relief, Grooves, V- shaped pit. S-7: Angular outline with high relief, solution pits, silica precipitation, silica globule, concave shaped pits, cresentic shape S-8: Sub rounded outline, solution pits, solution pits with grooves, V- shaped pit. S-8a: Chemical precipitations, solution pits.

Fig.1 Number of Various types of Microtextures on Quartz grain

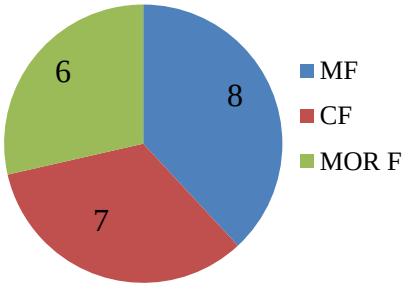

Fig.2 Mechanical microtexture features on quartz grain

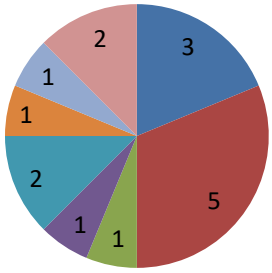

Table.1 Frequency of Quartz surface microtextural features in Gurupura River Estuary

Surface microtextural features	Sample numbers							
	1	2	3	4	5	6	7	8
Mechanical features								
Concoidal fracture	-	-	P	P	P	-	-	-
V-shaped pits	P	-	-	P	P	P		P
Meandering ridges	-	-	-	-	P	-		-
Dish shaped pit	-	-	-	-	-	P	-	-
Concave shaped pits	-	-	-	-	P	-	P	-
Irregular impacts	-	P	-	-	-	-	-	-
Curved striation	P	-	-	-	-	-	-	-
Irregular pits	P	P	-	-	-	-	-	-
Chemical features								
Silica Globules	-	P	-	-	P	-	P	-
Solution pits	P	-	-	-	P	-	P	P
Grooves	-	-	-	P	-	P	-	-
Over growth	P	P	-	-	-	-	-	-
Chemical precipitation, (dissolution)	P	P	-	P	-	-	-	P
Impact solution pits	P	P	-	-	-	-	-	-
Chatter marks trails	-	P	-	-	-	-	-	-
Morphological features								
Angular outline	-	-	-	-	-	-	P	-
Sub angular outline	-	-	P	P	P	-	-	-
Sub rounded outline	P	P	P	-	-	-	-	P
Angular sharp edge with high relief	-	-	-	-	-	-	P	-
Sub angular outline with low relief	-	P	-	-		P	-	-
Sub rounded out line with low relief	-	-	-	P	P	-	-	-

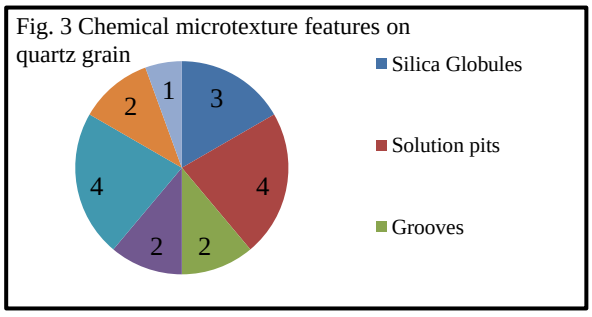

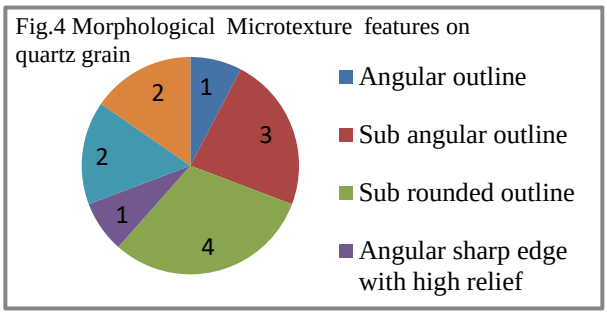

Result and Discussion

Mechanical features

The mechanical features like conchoidal fractures, V-shaped pits, meandering ridges, Dish shaped pits, concave-shaped pits, irregular impacts, curved striations and irregular pits are recognized on the quartz grains. These features are formed during the erosion or weathering process, grain to grain abrasion and collision during transportation of sediments commenced from their source. The mechanical features like conchoidal fracture are mainly observed in samples numbers of 3, 4 and 5 and V-shaped pits are identified in samples numbers 1,4,5,6 and 8 in the middle part of the river. Meandering are ridges observed only in sample number 5, and dish-shaped pits and concave-shaped pits are observed mainly in numbers 5, 6 and 7, and irregular impacts, curved striations and irregular pits are observed in samples number 2, 1, 1 and 2, respectively. Conchoidal

fractures, arcuate and straight steps marked on quartz grains are derived from the crystalline source rocks, i.e., granite. The linear striations are mainly produced in the high- energy environment (e. g. Krinsley and Marshall, 1987). The V-shaped features and parallel orientation are formed by grain-to-grain collision during transportation (e. g. Manickam and Barbarous, 1987). The abundance and size of the V-shaped pits on the grains indicate a long duration with high intensity of subaqueous agitation (e. g. Manickam and Barbarous, 1987). (Table.1 and Fig.2)

Chemical Features

The chemical features associated with silica globules and solution pits in the grains are formed by the precipitation of silica from chemical solution due to the long residence of the sediments in the depositional basin under a saturated silica environment (Udayaganeshan et al., 2011; Armstrong-Altrin and Natalhy-Pineda, 2014). Chemical features identified are silica globules, solution pits, grooves, overgrowth, chemical precipitation, impact solution pits and chatter mark trails (Table.1 and Fig.3). Based on the mode of origin, the chemical features are classified as chemical dissolution and precipitation. The solution pits formed by the chemical dissolution of sand grains are observed in samples numbers 1, 5, 7 and 8; silica globules are chemical precipitation origin noticed in samples numbers 2, 5 and 7 and are formed by the precipitation of silica from chemical solution due to the long residence of the sediments in the depositional basin (Udayaganeshan, et al. 2011) under silica saturated environment (Armstrong-Altrin and Natalhy-Pineda2013). Impact solution pits in sample locations 1and 2. The sands of variable grain size with circular and sub-circular (Krinsley and Doornkamp, 1973) shapes are attributed to the influence of contaminated seawater (Armstrong-Altrin and Natalhy-Pineda 2013). Chemical Precipitation features are mainly observed in sample numbers 1, 2, 4, and 8; Chetter marks trail are noticed in sample location 2. The grooves on the quartz grains are formed by a chemical process at reducing water velocity (e. g. Joshi, 2009). The low energy of the river during the low rainfall conditions is revealed by the high equency of chemical features on the quartz surface

Morphological(Mechanical/Chemical)features

The quartz grains of locations 1 to 8 showing more or less the sub angular to sub rounded outline of straight and arcuate steps suggesting that the sediments have undergone short transportation and rapid deposition. This result suggests angular outline has been gradually decreased by the action of downstream transportation and resulted in rounding of the quartz grains

River flow direction

Grab Sampler

Sample collection and packing

Sample collection from grab

Conclusion

Surface textures such as conchoidal fractures associated with arcuate step features suggest that the Gurupura River sediments were derived mainly from the crystalline source rocks. The v-shaped pits, and straight scratches indicate that the sand grains were transported in a high-energy fluvial environment during the high surface run-off conditions, especially during the monsoonal season. The surface textures such as striations and silica globules in the sediments represent the multicyclic character of varying transportation processes in the Gurupura River.

References

Armstrong-Altrin JS, Natalhy-Pineda O (2013) Microtextures of detritals and grains from the Tecolutla, Nautla, and Veracruz beaches,Western Gulf of Mexico. Mexico: implications for depositional environment and paleoclimate. Arabian Journal Geosciences. doi:10.1007/s12517-013-1088-x

Armstrong-Altrin J. S., Natalhy-Pineda O., 2014. Microtextures of detrital sand grains from the Tecolutla, Nautla, and Veracruz beaches, Western Gulf of Mexico. Mexico: implications for depositional environment and paleoclimate. Arabian Journal Geosciences 7, p. 4321M333

Chakroun A., Miskovsky J. C., Zaghbib-Turki D., 2009. Quartz grain surface features in environmental determination of Aeolian Quaternary deposits in northeastern Tunisia.Mineralogical Magazine 73 (4), p. 607-614.

Geological Survey of India, 1981. Geological and mineral map of Karnataka and Goa. Scale 1:5, 00,000

Helland, P.E., Holmes, M.A., 1997, Surface textural analysis of quartz sand grains from ODP Site 918 off the southeast coast of Greenland suggests glaciation of southern Greenland at 11 Ma: Palaeogeography, Palaeoclimatology, Palaeoecology, 135, 109-121.

Higgs, R., 1979, Quartz grain surface features of Mesozoic-Cenozoic sands from the Labrador and Western Greenland continental margins: Journal of Sedimentary Petrology, 49, 599-610.

Krinsley, D.H., Doornkamp, J.C., 1973, Atlas of quartz sand surface textures: Cambridge, England, Cambridge University Press, 91 p.

Krinsley, D.H. and Marshall, j.r. 1987. Sand grain textural analysis: an assessment. Clastic Particles. SEM and Shape Analysis of sedimentary and volcanic clasts (J.R. Marshall, editor). Van Nostrand-Reinhold, NewYork: 2-9.

Madhavaraju, J., Lee, YI., Armstrong-Altrin, J.S., Hussain, S.M., 2006, Microtextures on detrital quartz grains of upper Maastrichtian-Danian rocks of the Cauvery Basin, Southeastern India: implications for provenance and depositional environments: Geosciences Journal, 10, 23-34.

Manickam, s. and Barbaroux (1987) Variations in the surface texture of suspended quartz grains in the Loire River: ASEM Study. Sedim entology, v.34, pp.495-510.

Nair, M.M., 1990. Structural trend line patterns and lineaments of the Western Ghats, south of 130 latitude. Journal of Geological Society of India, 35, 99–105.

Radhakrishna, B.P. and Vaidyanadhan, R., 1994. Geology of Karnataka. Bangalore: Geological Society of India, 9–17.

Subrahmanya, K.R., 1994. Post-Gondwana tectonics of the Indian Peninsula. Current Science, 67, 527–530.

Udayaganeshan, et al. 2011 Surface Microtextures of Quartz Grains from the Central Coast of Tamil Nadu journal geological society of india Vol.77, January 2011, pp.26-34.

JOURNAL INDIAN ASSOCIATION OF SEDIMENTOLOGISTS ISSN NO 2582 – 2020
Vol. 39, Issue 2, 2022, pp. 10-16
DOI: **https://doi.org/10.51710/jias.v39iII.247**

Geochemistry of the Transitional beds between Disang and Barail Successions of the Imphal Valley, Indo-Myanmar Ranges

Salam Ranjeeta Devi
Department of Earth Sciences, Manipur University, Imphal-795003, India
Email: ranjeeta_27@rediffmail.com

Abstract

Major and trace element concentrations were studied from the tansitional beds between Disang and Barail Successions of the Imphal valley, Indo-Myanmar Ranges. Various major and trace element ratios and discrinant diagrams were used to descipher paleoclimate, paleo-redox condition and sedimentary depositional environment of the Disang-Barail Transitional beds. SiO_2 vs Al_2O_3+K_2O+ Na_2O diagram and Rb/Sr ratios indicates that paleoclimate during the deposition of the sediments changed from arid to semi-arid and humid climate. Ni/Co, V/Cr, V/(Ni+V), V/Sc ratios suggest that these sediments were deposited in oxic, suboxic to anoxic conditions. V/(Ni+V) vs V/Cr diagram suggests paleo-redox environment dominated by sub-reduction to oxidization during Disang –Barail Transitional deposition. The sediments were deposited in transitional to marine depositional environment.

Keywords: Disang-Barail, Transitional beds, Paleoclimate, Paleo-redox, Indo-Myanmar Ranges, sedimentary environment

Introduction

Geochemistry of siliciclastic rocks is commonly used for provenance interpretation compared to the petrographic approach used for sandstones (Taylor and McLennan, 1985; Culler, 2000; Armstrong-Altrin et al., 2017; Chaudhuri et al., 2020; Devi, 2021). The bulk geochemistry of shales preserves the near-original signatures of the provenance and more faithfully reflect the source-area weathering (Devi, 2022) and diagnostic process; geochemical indices are frequently used in the interpretation of depositional environments (Roaldest, 1970). Most important purpose of geochemistry of the sediments is to evaluate geological processes and determine the sedimentary environment. Sedimentary records provide a useful tool for paleoenvironmental studies because they preserve original lithological characteristics and record the climatic changes during their deposition (Ding et al. 2001; Shilling et al., 2020). Many recent studies have shown relationship between some chemical elements and change in the environments. Element abundance in sedimentary rocks is found to be influenced by many factors, including weathering, erosion, transportation and deposition of the sediments (Algeo and Maynard, 2004; Shurzynski et al., 2020).

The physicochemical properties of different elements are affected by external agents such as climate, biological activity, pH and tectonic setting during weathering and sedimentation (Gao et al., 2017; Quin et al, 2018). The distribution of elements in the rocks depends on the physicochemical properties of the elements and it is influenced by the paleoclimate and paleoenvironment. By selecting those elements or combinations of elements that are sensitive to water conditions and paleoclimate, the sedimentary environment can be studied either quantitatively or semi-quantitatively including paleoclimate and paleoredox condition. Several authors have used geochemical parameters to understand sediments paleo-oxygenation conditions (Jones and Manning, 1994; Nath et al., 1997; Cullers, 2002). The current study presents the geochemistry of the Disang-Barail transitional beds (DBTB) from the Imphal Valley. The samples were analysed for the major and trace elements as well as elemental ratios to determine environment of deposition. Geochemistry of the analysed sediments was used to identify the paleoclimate and paleo-redox conditions of sedimentary environment.

The Indo-Myanmar Ranges comprising of the Naga-Patkai hills, Manipur Hills, Mizo-Chin Hills and Arakan-Yoma Hills. The Indo-Myanmar Ranges (IMR) was formed due to subduction of Indian plate margin below the Eurasian plate. The Imphal Valley (Fig. 1), which is one of the largest valley of the Indo-Myanmar Ranges, was evolved in the later phase of the Indo Myanmar orogeny.

GEOLOGICAL SETTING

The Imphal valley and its adjoining areas are made up of the Disang Group (Late Cretaceous to Eocene), Disang-Barail transitional succession (Late Eocene- Early Oligocene) and Barail Group (Oligocene) with an overlying alluvium deposit. The Disang Group constitutes more or less the basement of the alluvium of the Imphal Valley. It consists of dark grey splintery shales with siltstone, sometimes giving rise to rhythmic character. The splintery nature of the shales is due to intense deformation, fracture and jointing. In the Imphal valley, Upper Disang is exposed in a vast area. The contact between the Disang and Barail Group runs nearly parallel to

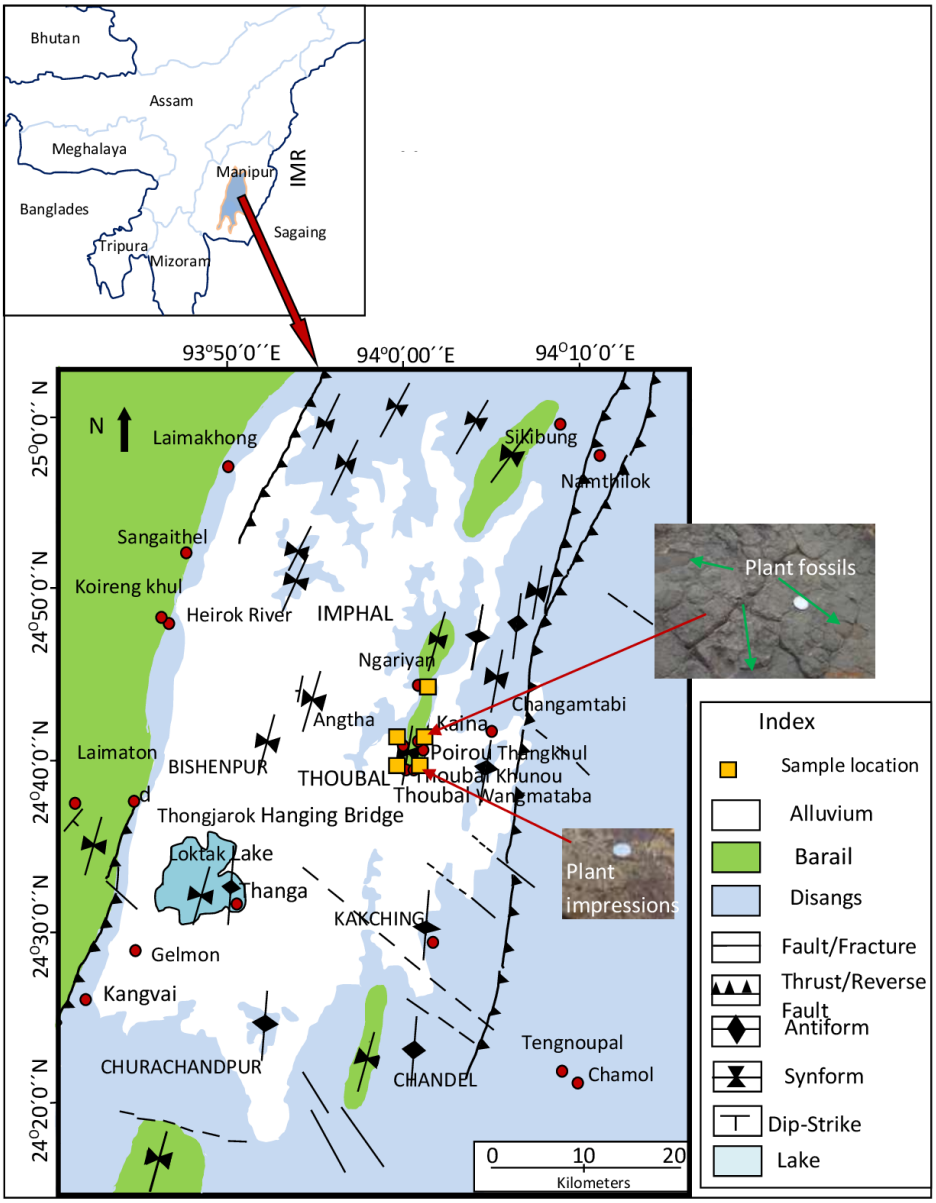

Fig. 1. Geological map of Imphal Valley, Indo-Myanmar Ranges showing the sample locations

the western margin of the Imphal valley and continue northerly towards the Naga Hills and Mizo-Hills of the IMR. This gradation at contact is related with a gradual change from dominantly argillaceous to arenaceous characteristics. The Barail and the Disang groups have transitional boundary, so the lower part of the Barail and upper part of the Disang-Barail transition have similar characteristics. The Disang-Barail transition beds of the Imphal Valley show numerous intercalation of thin, flaggy siltstone, fine-grained sandstone and sandy or silty shales (Fig. 2) Barail Group represents thick bedded sandstones interbedded with shale and thin bedded siltstone. They occur mainly in the western side of the Imphal valley. Alluvium covers a wide area

Figure 2. Photograph showing intercalation of shale, siltstone and sandstone from Imphal valley and as outliers in the eastern sides of the valley forming cappings of the Disangs.

of the valley. Stratigraphic Succession of the Imphal Valley of the Indo-Myanmar ranges is given in table 1.

Methodology

Samples of sandstone, siltstone and shale were collected from exposures of Disang-Barail Transitional beds from Imphal valley along the road cut and small quarries (Fig.2). Plant fossils are preserved in the siltstones of the Imphal valley (Fig,. 3a). Some weathered sandstones show plant impression (leaves, twig and bargs etc) (Fig. 3 b.).

For geochemical analysis, samples were thoroughly washed, dried and homogenized in an agate mortar by hand. Samples were powdered to 200 ASTM. Major element concentrations for sample TB-2K-1, TB-W-1 and Ng-3 were determined using a RIGAKU ZSX Primus II X-ray fluorescence spectrometer system and analyzed in pressed powder briquettes. The accuracy of major elements

Table 1. Stratigraphic Succession of the Imphal Valley (modified after Soibam, 1997).

Group	**Lithology**	**Age**
Alluviums	Dark grey to black clay, silt and sand deposits of fluvial-lacustrine origin. Flood plain deposits of the rivers and streams. Clay, sand, gravel and boulder deposits of the foothills and old river terraces. Possibly including lower deposits of the Imphal Valley.	(Quaternary: Holocene to Pleistocene (?) Older)
----------Stratigraphic Break----------		
Barails	Shale, sandy shale, massive siltstone, intercalation of bedded sandstone with shales showing turbidite character.	Oligocene
Disang-Barail Transition sequence (Gradational or local tectonic contact) consist of thick siltstone, fine-grained sandstone and sandy or silty shale (Late Eocene –Early Oligocene)		
Disangs	Dark grey splintery shale interbedded with thin siltstone and sandstones showing rhythmite nature.	Late Cretaceous to Late Eocene
~~ Unconformity ~		
Basement Complex	Unseen (?) Early Mesozoic/Paleozoic or Precambrian rocks	(?)Early Mesozoic/ Palaeozoic

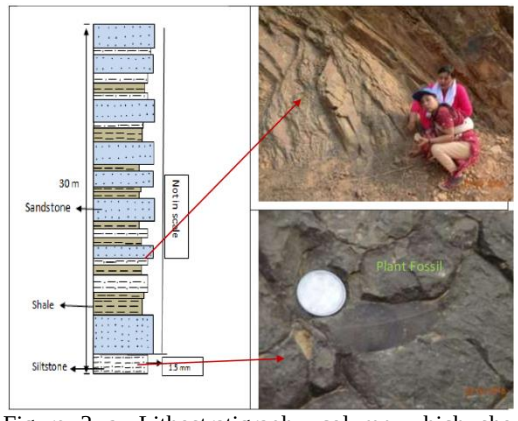

Figure 3 a. Lithostratigraphy column which shows plant fossil.

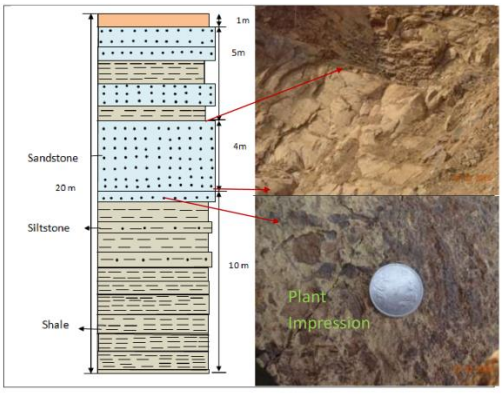

Figure 3 b. Lithostratigraphy column which shows plant impressions.

were evaluated using the rock standard Argillite whose values range from 102.6 to 93%, with the exception of Na_2O (70.0%), P_2O_5 (73.1%) and K_2O (89.3%).

For trace element analysis TB-2K-1, TB-W-1 and Ng-3, ~ 0.2 g of whole-rock powder of each sample was taken in 3 ml savillexR vials, supra pure acid mixture of $HF+HNO_3+HCl$ in 7:3:1 proportion was added, and heated for about 48 h on a hot plate at a temperature of 110°C with lids closed. The samples were repeatedly treated with HNO_3 + HCl until clear solutions were obtained. The solutions were dried, re-dissolved with 2% HNO_3 and diluted to 50 ml in polypropylene (PP) storage bottles. The stock solution was further diluted to ~7500 times with 2% HNO_3, and trace and REE concentrations were measured using Inductively Coupled Plasma-Quadrapole Mass Spectrometer (ICP-MS, Thermo X-Series) at the Department of Earth Sciences, Pondicherry University. USGS standards AGV-2, BCR-2, SCO-1 and multi-element standards were used for calibration, and 10 ppb Rhodium solution was used as an internal standard. To check the accuracy of data, USGS standard BHVO-2, AGV-2 were repeatedly analysed as unknown and the replicate analysis show precision of 2% for the REE, and better than 5% for other elements.

The major and trace elements of RNK3 and RTH1 were analysed by Wave Length Dispersive XRF system (Siemens SRS 3000) at Wadia Institute of Himalayan Geology, Dehra Dun. Analysis was carried out using pressed powder pellets glued with polyvinyl alcohol. Approximately 5-6 gms of the sample powder was mixed with 2-3 drops of polyvinyl alchohol solution and the mixture was pressed under the hydraulic pressure of 2000 kg/cm^2 to get a durable sample pellet and the resulted pellets were dried in a hot box maintained at 60-70 ^{o} C overnight to drive off excess water in the pellets. The accuracy and precision was ±1-3% for major oxides, and for trace ±5-10%.

Table 2. Major element oxides of the DBTB of Imphal Valley

	TB-2K-1	TB-W-1	Ng-3	RNK3	RTH1
SiO_2	72.239	70.903	69.046	64.67	56.61
TiO_2	0.708	0.691	0.707	0.70	0.81
Al_2O_3	11.437	10.485	11.559	14.71	19.49
Fe_2O_3t	4.971	4.93	5.245	6.93	7.61
MnO	0.06	0.113	0.078	0.04	0.05
MgO	2.627	2.87	3.24	3.59	2.77
CaO	0.783	1.643	1.505	0.41	0.48
Na_2O	2.531	2.252	2.916	1.35	0.66
K_2O	0.79	0.801	0.898	1.89	3.15
P_2O_5	0.134	0.121	0.135	0.15	0.12
P x C	3.51	4.84	4.5	6.27	9.42

Table 3. Trace element composition of the DBTB of Imphal Valley

	TB-2K-1	TB-W-1	Ng-3	RNK3	RTH1
Sc	7.76	12.52	11.90	13	16
V	47.0	92.0	91.4	114	155
Cr	201	548	526	277	194
Co	9.8	16.8	18.4	16	22
Ni	12	24	28	151	205
Cu	8.02	17.62	24.14	29	49
Zn	31	68	68	86	110
Ga	2.70	5.28	5.41	14	24
Rb	23.2	34.9	38.0	83	145
Sr	53	96	109	80	110
Y	9.4	17.2	18.9	26	34
Zr	38	115	96	207	151
Nb	3.52	7.76	7.31	10	12
Ba	52	89	93	154	258
Rb/Sr	0.44	0.36	0.35	1.04	1.32

Results

Major and Trace elements

SiO_2 values range from 56.61 to 72.23. Al_2O_3 has highest value of 19.49 and Fe_2O_3 ranges from 4.93 to 7.61. Major oxides of SiO_2, Al_2O_3, K_2O and Na_2O are used in study of paleoclimate. Major element oxides are shown in table 3. Trace elements, Rb values range from 23.2 to 145 and Sr values range from 52 to 258. Rb/Sr ratios were used as the main paleoclimate proxies. The highest value of Rb/Sr ratio is 1.32 in the samples with plant impression. The trace elements are presented in table 3.

Paleoclimate

In SiO_2 vs $Al_2O_3+K_2O+ Na_2O$ diagram (Suttner and Dutta ,1986, Fig. 4), the sediments were deposited in semi-arid condition.

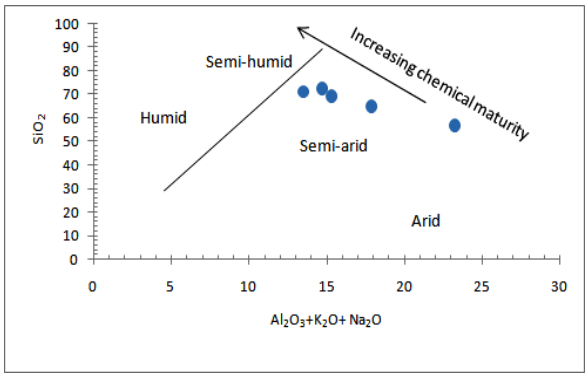

Figure 4. SiO_2 versus $Al_2O_3+K_2O+ Na_2O$ diagram indicates deposition mainly in semi-arid climate (modified after Suttner and Dutta ,1986).

The Rb/Sr ratio can reflect the chemical weathering process and also reveal the change of depositional environment and paleoclimate. High Rb/Sr ratio is generally indicative of warm and humid climates, in which Rb is relatively stable while Sr is often lost due to high precipitation and low Rb/Sr ratio indicates arid climate conditions, since little Sr is lost in the low precipitation environment (Jeong et al., 2006; Du et al., 2011; Chang et al., 2013). Based on existing research that uses the Rb/Sr ratio to reconstruct the paleoclimate, 0.45 is suggested as a threshold value, below which the climate is relatively dry and cold while above this value the climate is relatively wet and warm (Shen et al., 2006). In this study, the samples with plant impressions have higher values than 0.45 indicating deposited in the warm and humid climate, while other samples have ratios less 0.45 suggesting arid and hot climate (Table 3). Based on this, it can be inferred that the DBTB should have experienced humid and arid climate conditions. The flora in diverse form comprising of gymnospermous, monocotyledonous and dicotyledonous from the Imphal Valley also indicates tropical to subtropical climate (Singh et al., 2012).

Paleo-redox conditions

The paleo-redox environment has been mainly determined based on the analysis of elements that are sensitive to redox conditions such as V, Ni, Cr, Co, Fe, and Zn (Jones and Manning, 1994). In this study, Ni/Co, V/Cr, V/(V + Ni), and V/Sc ratios were used as proxies for the paleo-redox environment. In general, V is vulnerable to precipitation under reduction conditions and dissolution under oxidation conditions, and Ni is more stable than V in both conditions (Arthur and Sageman, 1994). The V/(V + Ni) ratio has been used as tool related to reducibility (Hatch and Leventhal, 1992; Jones and Manning, 1994), with a value range of 0.84 indicating water stratification in the anaerobic reduction environment. The DBTB is identified to be mainly formed in sub-reduction to oxidation environment (Fig. 5). The V/Cr ratio is another important proxy for the redox conditions (Jones and Manning, 1994; Scheffler et al., 2006), with a value of 4.25 indicating a reduction environment. As shown in Fig. 5 (Zou et al., 2021), the DBSB is identified to be mainly deposited in sub-reduction to an oxidation environment. These results of the redox condition are similar tp the values which indicate oxic to anoxic environment (Table 5).

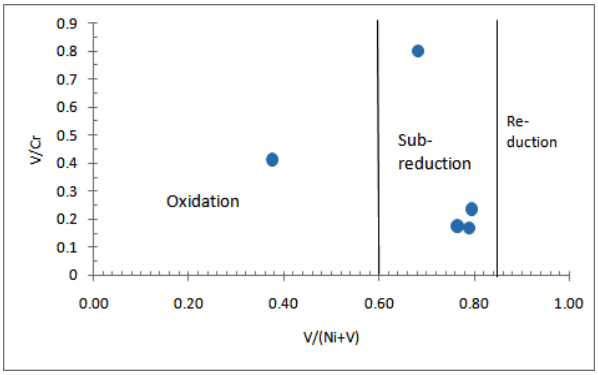

Figure 5. V/(V + Ni) versus V/Cr ratios plot to determine paleo-redox condition

Table 4.The average trace element values of the samples analysed in comparison to the standard parameters of paleo-redox conditions.

	Oxic	Dysoxic	Suboxic to anoxic	Euxinic	Average values of the samples from the study area
Ni/Co	<5	5 to 7	>7		3.64 -oxic
V/Cr	<2	2.4 to 4 .25	>4.25		0.36- Dyoxic
V/(Ni+V)	<0.46	0.46 to 0.60	0.54 to 0.82	>0.84	0.66- Suboxic to anoxic
V/Sc	<9.1				7.48- oxic

The change of paleo-redox environment is influenced by tectonic setting and depositional environment. Figure 6 (Zuo, 2020) shows that the samples with plant impressions indicate transitional depositional environment to the marine environment and samples without plant impressions indicate the marine environment. Singh et al. (2012) also suggest that the geological succession with diverse plant remains belong to the Upper Disang and Laisong formations of the Lower Barail Formation characterized by the rhythmic intercalations of dark grey splintery shale, siltstone and fine grained sandstone of shallow marine origin, while the latter has sandy shale and fine grained sandstones of shallow marine to fluvio-deltaic origin (Chandra and Kushwaha, 2008).

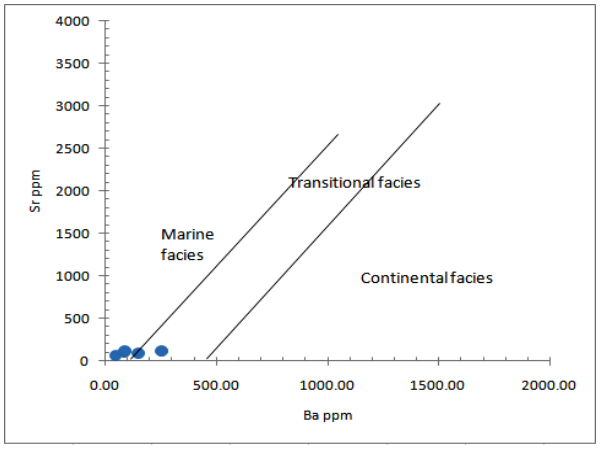

Figure 6. Sr versus Ba diagram of the sedimentary rock of the Imphal Valley

Conclusions

In this study, the paleoclimate, paleo-redox and sedimentary depositional environment of the Disang-Barail Transitional beds of the Imphal Valley, Indo-Myanmar Ranges was reconstructed based on geochemistry using the analysis of major and trace elements. Alternating semi-arid, arid and humid climates were suggested during deposition of DBTB by paleoclimate proxies. The palaeoredox environment during the DBTB deposition was dominated by sub-reduction, although there was a trend of oxidization, based on the V/(V + Ni) and V/Cr ratios. The DBTB is suggested to be deposited in the environment transitional to the shallow marine environment. Results of this study are expected to help better understand the paleoclimatic, paleo-redox and paleoenvironmental condition during DBTB deposit by furthering the research with more sample analyses.

Acknowledgements

The author thanks the Head, Department of Earth Sciences, Manipur University and Prof. Soibam Ibotombi of the department for providing necessary facilities and support. The author also sincerely thanks Nurul Absar, Department of Earth Sciences, Pondicherry University and John S. Armstrong-Altrin, Universidad Nacional Autónoma de México, Instituto de Ciencias del Mary Limnología, Unidad de Procesos Oceánicos y Costeros, Ciudad Universitaria, Ciudad de México for the geochemical analyses. Author acknowledges Department of Science and Technology, New Delhi for financial assistance under the DST project No: SR/WOS-A/EA31/2016 dated 06-01-2017.

References

Algeo T J and Maynard J B (2004). Trace-element behavior and redox facies in core shales of Upper Pennsylvanian Kansas-type cyclothems; Chemical Geology, 206(3) 289–318

Armstrong-Altrin, J.S., Lee, Y.I., Kasper-Zubillaga, J.J., Trejo-Ramirez, E. (2017). Mineralogy and geochemistry of sands along the Manzanillo and El Carrizal beach area, southern Mexico: implications for Paleoweathering, provenance and tectonic setting. Journal of Geology, 52, 559-582.

Arthur, M.A. and Sageman, B.B., (1994). Marine black shales: depositional mechanisms and environments of ancient deposits. Annu. Review Earth Planetary Sciences, 22 (1), 499–551.

Chandra Singh ,M., Kushwaha, R. A. S., Srivastava, G and Mehrotra, R. C., (2012). Plant Remains from the Laisong Formation of Manipur. Journal Geological Society Of India, 79, 2012, 287-294.

Chandra Singh, M. and Kushwaha, R.A.S. (2008). Ichnofossils from the Eocene- Oligocene deposits between Bijang and Tupul, Manipur, India. Journal of Indian Association of Sedimentologists, 27, 35-44.

Chang, H., An, Z.S., Wu, F., Jin, Z.D., Liu, W.G. and Song, Y.G., (2013). A Rb/Sr record of the weathering response to environmental changes in westerly winds across the Tarim Basin in the late Miocene to the early Pleistocene. Palaeogeography Palaeoclimatology Palaeoecology, 386 (6), 364–373.

Chaudhuri, A., Banerjee, S., and Chauhan, G. (2020). Compositional evolution of siliciclastic sediments recording the tectonic stability of a pericratonic rift: Mesozoic Kutch. Marine and Petroleum Geology, 111, p.476-495

Cullers, R. L., (2000). The geochemistry of shales, siltstones and sandstones of Pennsylvanian-Permian age, Colorado, USA: Implications for provenance and metamorphic studies; Lithos 51(3) 181–203

Cullers, R.L., (2002). Implications of elemental concentrations for provenance, redox conditions, and metamorphic studies of shales and limestones near Pueblo, CO, USA: Chemical Geology, 191(4): 305 - 327.

Devi, S. Ranjeeta. (2021). Geochemistry, depositional and tectonic Setting Of the Barail Group of the Indo-Myanmar Ranges. Journal Indian Association of Sedimentologists, 38 (1), 13-22.

Devi, S. Ranjeeta. (2022). Weathering and Source Rock Characteristics of the Upper Disang Sedimentary Rock of the Indo-Myanmar Ranges, NE India. Journal Indian Association Of Sedimentologists. 39 (1), 2022, 86-95.

Devi, S. Ranjeeta, Mondal, M.E.A. and Armstrong-Altrin, John S. (2017). Geochemistry and the Factors Controlling on the Weathering and Erosion of the Barail Group of Rocks, NW Manipur, India. Journal Indian Association of Sedimentologists, 34, p.9-16.

Ding, Z., Sun, J., Yang, S. and Liu, T., (2001). Geochemistry of the Pliocene red clay formation in the Chinese Loess Plateau and implications for its origin, source provenance and paleoclimate change. Geochimica et Cosmochimica. Acta 65, 901–913.

Du, S., Li, B., Niu, D., Zhang, D.D., Wen, X., Chen, D., Yang, Y. and Wang, F.N., (2011). Age of the MGS5 segment of the Milanggouwan stratigraphical section and evolution of the desert environment on a kiloyear scale during the Last Interglacial in China's Salawusu River Valley: Evidence from Rb and Sr contents and ratios. Chemie der Erde-Geochemistry-Interdisciplinary Journal Chemical Problems Geoscience Geoecology, 71 (1), 87–95.

Gao, G., Titi, A. and Yang, S.R., (2017). Geochemistry and depositional environment of fresh lacustrine source rock: a case study from the Triassic Baijiantan Formation shales in Junggar Basin, northwest China, Organic Geochemistry, 113, 75–89

Hatch, J.R. and Leventhal, J.S., (1992). Relationship between inferred redox potential of the depositional environment and geochemistry of the Upper Pennsylvanian (Missourian) Stark Shale Member of the Dennis Limestone, Wabaunsee County, Kansas, USA. Chemical Geology 99(1/2/3), 65-82.

Jeong, G.Y., Cheong, C.S., Kim, J., (2006). Rb-Sr and K-Ar systems of biotite in surface environments regulated by weathering processes with implications for isotopic dating and hydrological cycles of Sr isotopes. Geochimica et Cosmochimica. Acta 70 (18), 4734–4749.

Jones, B. and Manning, D.A.C., (1994). Comparison of geochemical indexes used for the interpretation of palaeoredox conditions in ancient mudstones, Chemical Geology, 111, 111–129.

Nath, BN; Bau, M, Ramalingeswara, RB; Rao, CM (1997). Trace and rare earth elemental variation in Arabian Sea sediments through a transect across the oxygen minimum zone: Geochimica et Cosmochimica Acta, 61(12), 2375 - 2388.

Qin, J.W., Wang, S.Q. and Sanei, H., (2018). Revelation of organic matter sources and sedimentary environment characteristics for shale gas formation by petrographic analysis of middle Jurassic Dameigou formation, northern Qaidam Basin, China, International Journal of Coal Geology, 195, 373–185.

Roaldest, 1970. Roaldest, E. (1978). Mineralogical and Chemical Changes during Weathering, Transportation, and Sedimentation in Different Environments with Particular References to the Distribution of Yttrium and Lanthanide Elements. Ph.D. Thesis, Geological Institute, the University of Oslo, Oslo.

Scheffler, K., Buehmann, D., Schwark, L., (2006). Analysis of late Palaeozoic glacial to postglacial sedimentary successions in South Africa by geochemical proxies-response to climate evolution and sedimentary environment. Palaeogeography Palaeoclimatology Palaeoecology 240 (1), 184–203.

Shen, H.Y., Jia, Y.L., Li, X.S., Wu, J.L., Wei, L., Wang, P.L., (2006). The composition of Rb, Sr and environmental changes of lake sediments of different sizes in Huangqihai, Inner Mongolia. Acta Geogr. Sin. 61 (11), 1208–1217 (in Chinese).

Shilling, A.M., Colcord, D.E., Karty, J., Hansen, A., Freeman, K.H., Njau, J.K., Stanistreet, I.G., Stollhofen, H., Schick, K.D., Toth, N. and Brassell, S.C., (2020). Biogeochemical evidence from OGCP Core 2A sediments for environmental changes preceding deposition of Tuff IB and climatic transitions in Upper Bed I of the Olduvai Basin. Palaeogeography Palaeoclimatology Palaeoecology, 555, 109824.

Skurzynski, J., Jary, Z., Kenis, P., Kubik, R., Moska, P., Raczyk, J. and Seul, C., (2020). Geochemistry and mineralogy of the Late Pleistocene loess-palaeosol sequence in Złota (near Sandomierz, Poland): Implications for weathering, sedimentary recycling and provenance: Implications for weathering, sedimentary recycling and provenance. Geoderma 375, 114459.

Taylor, S. R. and McLennan, S.M., (1985). The Continental Crust: Its Composition and evolution, London, Blackwell, 312pp.

Soibam,I. 1997. Structural control on ground water occurrence in shales: a case study of the Imphal valley. Indian journal Landscape Systems and Ecological Studies 20, 111-116.

Suttner, LJ and Dutta, PK (1986). Alluvial sandstones composition and paleoclimate, I. Framework mineralogy. Journal of Sedimentary Research, 56 (3), 329 - 345.

Zou, C , Mao, L, Tan, Z , Liang Zhou, L. and Liu, L. (2021). Geochemistry of major and trace elements in sediments from the Lubei Plain, China: Constraints for paleoclimate, paleosalinity, and paleoredox environment. Journal of Asian Earth Sciences: X 6 https://doi.org/10.1016/j.jaesx.2021.100071.

Zuo, X, Cunlei Li, C. , Zhang, J , Ma, G and Chen, P . (2020). Geochemical characteristics and depositional environment of the Shahejie Formation in the Binnan Oilfield, China. Journal of Geophysics and Engineering (2020) 0, 1–13.

JOURNAL INDIAN ASSOCIATION OF SEDIMENTOLOGISTS ISSN NO 2582 – 2020
Vol. 39, Issue 2, 2022, pp. 17-29
DOI: https://doi.org/10.51710/jias.v39iII.251

Geochemistry and clay mineral studies of Jurassic sedimentary rocks from the Spiti region, Himachal Pradesh, North India

Samar Sultana*, Shaik A. Rashid
Department of Geology, Aligarh Muslim University, Aligarh-202002, India
(Corresponding author*: samaramu.9@gmail.com)

Abstract

An attempt is made in the present study to unravel the provenance, paleoweathering and paleoclimatic conditions of the Jurassic (Spiti Formation) black shales and sandstones from the Spiti region, Tethys Himalaya, using multi proxy approach. The sandstones are subarkose in composition and texturally poorly sorted, subrounded to subangular in shape with moderate spheriocity. The range of the chemical index of alteration (CIA) is 55–90, recorded in the black shales strongly suggests moderate to strong chemical weathering conditions in the source area, which in turn reflect fluctuating climatic conditions prevailing during the deposition of these sediments in Jurassic period in the Spiti region. Geochemical studies reveal that shales are enriched in felsic elements (high SiO_2, Al_2O_3, K_2O) and depleted in mafic components (Fe_2O_3 and MgO).The various geochemical discriminant plots and elemental ratios (SiO_2/Al_2O_3, K_2O/Al_2O_3, Al_2O_3/TiO_2, K_2O/Na_2O, etc.) indicate the rocks to be the product of weathering of felsic rocks. The paleoclimate in the source area seems to be mostly semi-humid. The plot of the samples on the A-CN-K ternary diagram indicates a granitic weathering trend. The X-ray Diffraction studies show that the prominent clay minerals in the Spiti shales are illite, smectite, chlorite, kaolinite and vermiculite along with quartz, muscovite, alkali feldspar, calcite and phosphatic phase.When plotted on the tectonic discrimination diagram, the samples indicate passive margin tectonic setting.

Keywords: Black shales, Spiti region, Tethys Himalaya, Geochemistry, Paleo-climate, Paleo weathering.

Introduction

Due to a variety of factors, the Jurassic epoch in geological history has attained global prominence. Continental configuration, oceanic patterns, and biological systems all changed dramatically throughout the Jurassic period. The Jurassic of India can best be studied in the Spiti region because the Spiti basin records the complete and uninterrupted history of marine sedimentary rocks starting from Eocambrian to Paleogene which were deposited along the northern margin of India.The Spiti area is part of the Tethyan Himalayan mountain range and is located in the Lahaul-Spiti region of Himachal Pradesh in north India. The Tethys Himalayan mountain range has complex geological and geotechnical features and is one of the most seismically and tectonically active mountain ranges in the world. It presents an excellent prospect to comprehend provenance, paleoweathering, paleoclimatic conditions, and plate tectonic investigations throughout te earth history. The Spiti area is where black shales are best preserved. Black shales are common rocks that gained attention throughout the Phanerozoic period on a worldwide scale. The distorted remains of the Indian subcontinent's northern margin are represented by the sedimentary succession of the Tethys Himalaya. Understanding the sedimentary provenance, paleoclimatic state, crustal evolutionary history, and depositional environmental conditions of the sediments requires the fusion of geochemical and petrological approaches (Bhatia & Crook, 1986; Dickinson & Suczek, 1979). Siliciclastic sediments may contain mineralogical and chemical traces that monitor weathering severity in the source area as well as paleoclimate, source rock type, and sediment cyclicity (Nesbitt & Young, 1984; Nesbitt & Young, 1982; Taylor & McLennan, 1985). Geochemical studies of the sedimentary rocks in the Spiti region have received very little attention. However, the stratigraphy and palaeontology of the region have drawn yet more interest. Numerous recent studies have demonstrated that sedimentary geochemistry is a potent tool for identifying and predicting the processes and climate extremes that govern the degree of weathering of the source rocks. As a result, differences in paleo-climate can be determined (Garzanti et al., 2014). The major deciding factors in all of these aspects are the composition of the source rock, the weathering mechanism (Armstrong-Altrin et al., 2004; Taylor & McLennan, 1985) and the tectonic setting of the

sedimentary basin coupled with secondary processes (Wronkiewicz & Condie, 1987). By examining clastic rocks, it is possible to identify continental and oceanic source regions that underwent metamorphism during tectonic activity. This is possible because the source signature persists even after metamorphism (Condie, 1993; Cullers, 2000; McLennan et al., 1993; Nesbitt & Young, 1982). Because of their extremely fine-grained nature, shales take more time to petrographically examine than sandstone does (Blatt, 1985). However, because they are homogenised source representations, shales are preferred in the case of geochemical analysis. The present paper provides the detailed understanding of geochemical proxies and their implications for resolving the paleoweathering condition, provenance, geo-tectonic setting, and paleoclimatic conditions; we present new geochemical data from the Jurassic siliciclastic sequences from the Spiti region, NW Tethys Himalaya, Himachal Pradesh, north India.

Geological setting

The Indian Tethyan Himalayan zone, containing thick sequence of rocks which are predominantly fossiliferous and range in age from the late Precambrian to early Eocene, is developed in three important basins, viz.,Kumaun (Uttarakhand), Kinnaur-Spiti-Zanskar (Himachal Pradesh) and Kashmir (Jammu and Kashmir). These sequences which are best exposed in Spiti - Zanskar region and document depositional history of the Tethys sea over the north facing Indian Plate margin (Bhargava & Bassi, 1998).The Spiti basin along with Zanskar bain is the largest basin in the Indian Tethys Himalaya (Parcha, 2021).The Spiti region is located in the Lahual-Spiti district of Himachal Pradesh. It is flanked by Ladakh and Tibet in the north and northeast, Higher Himalaya in the south, and a nearly undisturbed Phanerozoic succession that spans in age from Eocambrian to Cretaceous with a thickness of more than 7 km (Bhargava, 2008). In the Indian subcontinent, prominent marine Mesozoic rock successions are confined to the Tethyan Himalaya.Based on a number of studies, a broad agreement is achieved to categorise the Jurassic sequences into formations and members of the Lagudarsi Group (Bhargava, 2008; Bhargava & Bassi, 1998).The three formations in ascending order—the Spiti, Giumal, and Chikkim formations make up the Lagudarsi Group in the Spiti region.The geology of Spiti region and sample locations are given in figure 1. Mesozoic rocks of the Spiti region are categorized as Lilang Supergroup, which is divided into five Groups viz. Tamba-kurkur Group, Sanglung Group, Nimoloksa Group, Kioto Group and Lagudarsi Group (Bhargava, 2008). Lagudarsi Group is further subdivided into Spiti, Giumal and Chikkim formations in ascending order (Table.1).The present work is mainly confined to the Spiti Formation of the Lagudarsi Group. Considerable efforts have been made to collect fresh samples from the type localities (along Lingti-Giumal road section) in the Spiti region where the Jurassic rocks are well exposed. The Spiti Formation rests with sharp contact over theTriassic Kioto Formation. It consist of dark Grey to black friable shale, minor chert flakes, local sandstone beds which are calcareous toward the top.In the upper part, the shales gradually become light in colour and have fine flakes of detrital mica.

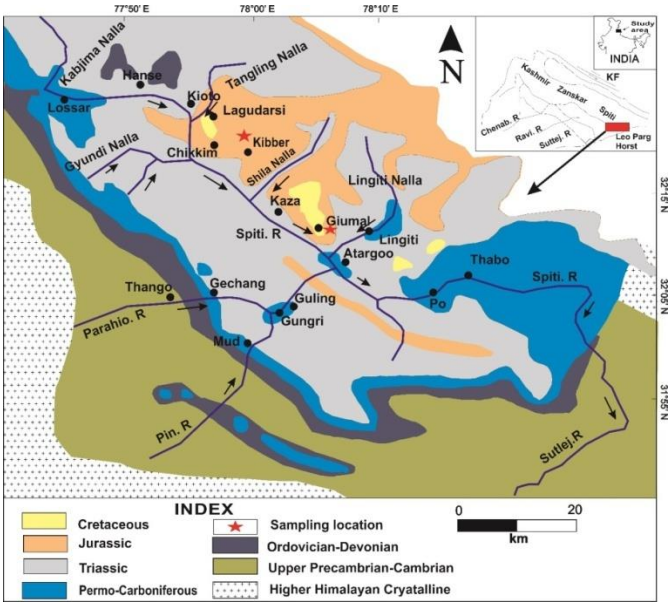

Fig.1.Geological Map of Spiti region (Bagati, 1990).

Table 1.General stratigraphy of the Spiti region (Bhargava, 2008)

Group	Formation	Main Lithology	Age
Lagudarsi	Chikkim	Limestone, Shale	Late Cretaceous
	Giumal	Sandstone, Shale	E-M Cretaceous
	Spiti	Shale	L-Jurassic to E-Cretaceous
Disconformity			
Kioto	Tagling	Limestone, Dolomite	M-Jurassic
	Para	Limestone, Dolomite	L-Triassic
Nimoloksa	Nunuluka	Sandstone, Siltstone, Limestone	L-Triassic
	Alaror	Shale, Sandstone, Limestone	L-Triassic
	Hangrang	Limestone, Dolomite	L-Triassic
	Rangrik	Shale, Sandstone, Limestone	L-Triassic
Sanglung	Rongtong	Dolomite, Limestone	L-Triassic
	Rama	Shale, Sandstone, Limestone	L-Triassic
Tamba- kurkur	Chomule	Limestone	M-L Triassic
	Kaga	Shale, Siltstone, Limestone	M-Triassic
	Mikin	Limestone	E-M Triassic
Disconformity			
Kuling	Gungri	Black Shale, Siltstone	Late Permain
	Gechang	Sandstone, Shale	Early Permain
Disconformity			
`Kanawar	Ganmachidam	Conglomarate, Shale,Sandstone	M-Carb. to E-Permain
	Po	Shale, Sandstone	E-Carb. to M-Carbon
	Lipak	Limestone, Sandstone, Shale	Early carboniferous
	Muth	Quartzite, Sandstone	Late Devonian
Disconformity			
Sanugba	Takche	Limestone, Sandstone, Shale	L-Ordov. L-Silurian
	Thango	Conglomerate	Early Ordovician
Disconformity			
Haimanta	Kunzam La	Sandstone, Shale, Limestone	Cambrian
	Batal	Sandstone, Siltstone, Shale	Precambrian

Note: E-Early, M-Middle, L-Late

Sampling and Analytical techniques

Twenty eight (28) representative samples of shales and six sandstone samples were collected from Giumal village. Agate milling was used to reduce representative samples to a powder with a grain size less than 200 mesh after they had been air dried and roughly crushed. Major oxides concentrations were determined using X-ray Fluorescence Spectrometry (Model name:Axios^{MAX}) at the Birbal Sahni Institute of Paleosciences, Lucknow. The analyses were carried out using pressed powder pellets for the principal components. Internal and international reference standards (such as MBH and SCo-1) were used for calibration. The data precision and accuracy is better than 5 percent and well within the bounds of international norms.The Gazzi-Dickinson method, which successfully reduces the effect of grain size, was used to count 500 points in each thin section for petrographic analyses. Scanning Electron Microscopy (SEM) studies were carried out for the identification of clay minerals in the samples at the University Sophisticated Instrument Laboratory (USIF) at Aligarh Muslim university (AMU), Aligarh, India in order to diagnose and understand the microstructures and diagenetic relationships among the main constituents and the matrix of the studied sediments particularly black shales and different phases. Identification of different phases was done by Bulk powder X-ray diffraction (XRD) analysis of five samples at the Department of Chemistry, AMU, Aligarh.

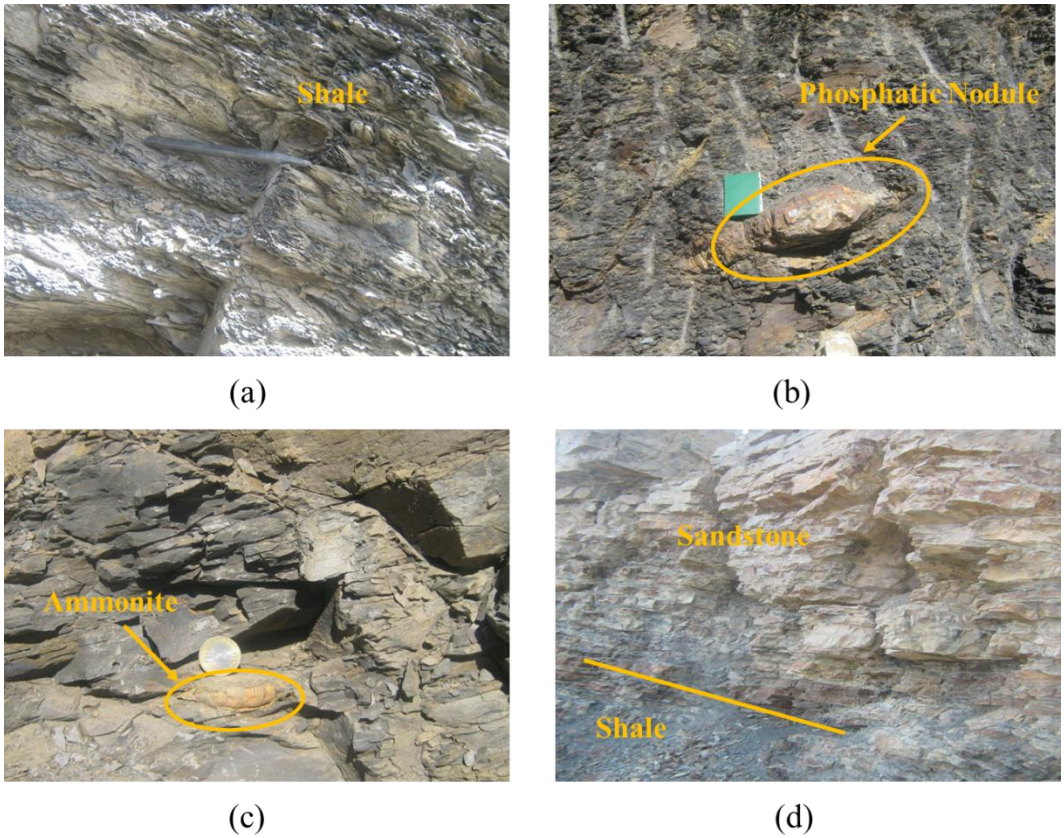

Fig. 2. Field photographs of Spiti Formation (a) Typical Spiti shales near Giumal village section. (b) Spiti black shales showing phosphatic nodules near Giumal village. (c) Photograph showing ammonite bearing Spiti black shales along Giumal village. (d) Spiti sandstone associated with black shales along Giumal village section.

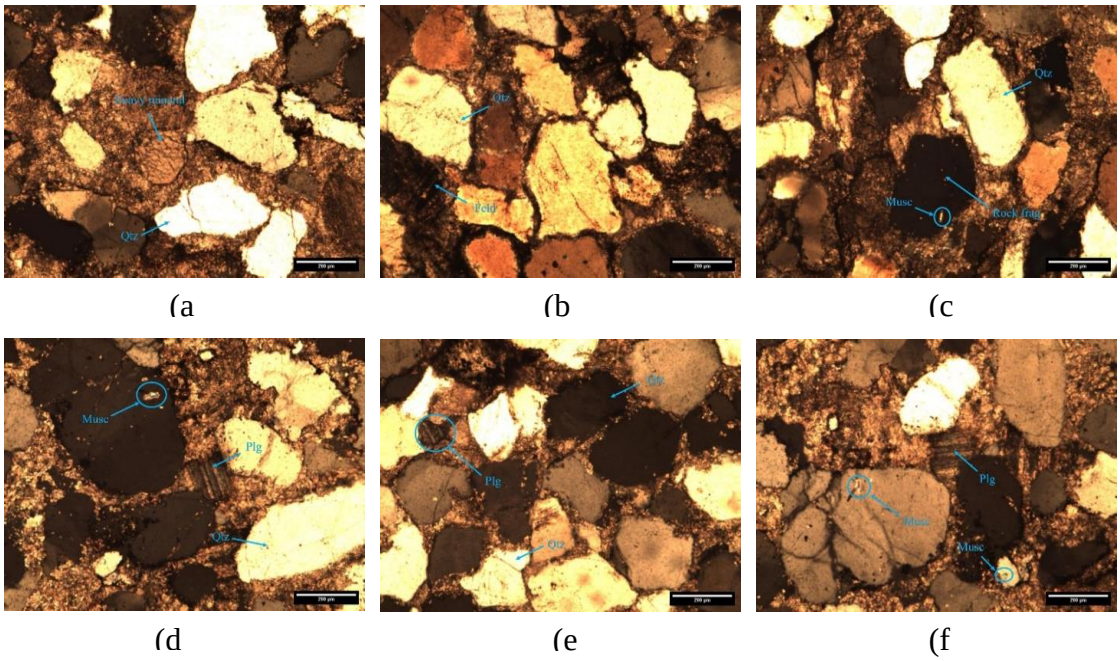

Fig.3.Photomicrograph showing predominantlydetrital monocrystalline quartz and other minerals (plagioclase, K-feldspar, muscovite, heavy minerals) and rock fragments

Results

Thin section analysis

Studying sandstone petrography can help better understand the grain texture, framework, and diagenetic history of sedimentary rocks and depositional history, like the processes involved in transit, deposition, and diagenesis (Lindsey, 1999). Petrographic analysis of Jurassic sandstones of Spiti region reveals that the sandstones are poorly sorted and rounded to subrounded with quartz (80%), feldspar (10%), and clayey matrix. The grain size of the sandstones ranges from fine to coarse. Quartz is predominately monocrystalline with undulose extinction and fractured edges.

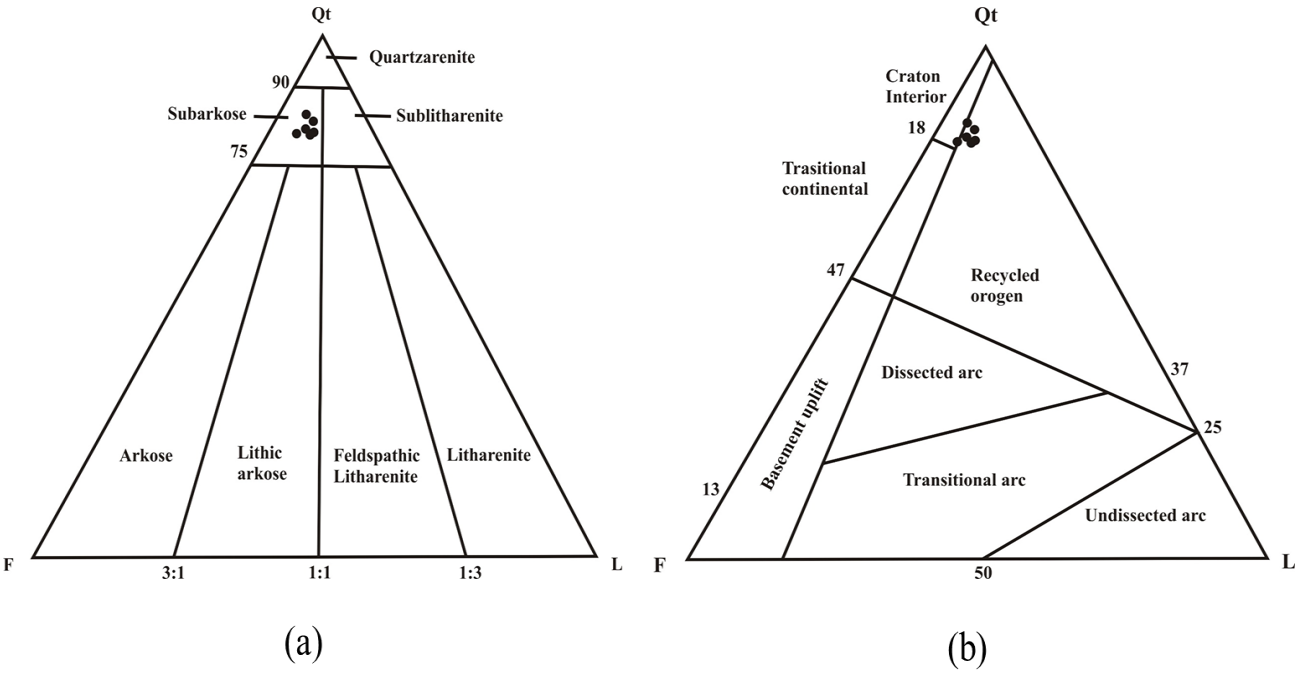

Fig.4. Triangular Qt-F-L plot for (a) classification of Spiti sandstones (Dickinson, 1985) and (b) showing different provenance fields for Spiti sandstones (Dickinson et al.,1979)

Most of the K-feldspars identified in thin sections are microclines i.e., K –feldspar dominating over plagioclase indicating the plutonic rocks (granite) as a dominant source. These sandstones also show presence of mica in the form of muscovite and heavy minerals and rock fragments. For quantitative analysis, approximately 500 points per thin section were counted for determining the modal composition of the samples according to point counting method by Gazzi-Dickinson. The average quartz percentage is about 83, feldspar is 12, and lithic fragments is 6, according to the modal analysis and these sandstones are classified as sub-arkose (Fig.4a). The data of these samples plotted in the Qt-F-L (Qt= total quartz; F: feldspar; L= lithic fragments) provenance diagram (Fig.4b.) show three different types of tectonic regimes as "continental block, magmatic arc and recycled orogen field (Dickinson, 1985; Dickinson & Suczek, 1979), most of these samples plot near Qt apex and in the recycled orogen field indicating that the samples are mineralogically mature and may have been derived from recycled orogen provenance (Fig.4b).

4.2. Clay mineralogy

The clay fraction derived from Spiti shales was subjected to bulk X-ray diffraction analysis, the results show that all of the studied samples mostly contain illite, smectite, kaolinite, vermiculite and chlorite. In addition to these minerals, calcite and phosphates are also identified within the shale rocks. Semi-quantitative analysis indicates that the quartz is the most abundant non-clay mineral, followed by illite, smectite, kaolinite, chlorite and vermiculite clay minerals and the bulk powder XRD patterns of these shales are shown in figure 5. The distribution of clay minerals at different levels of the sequence suggests moderate to intensive chemical weathering of feldspar.

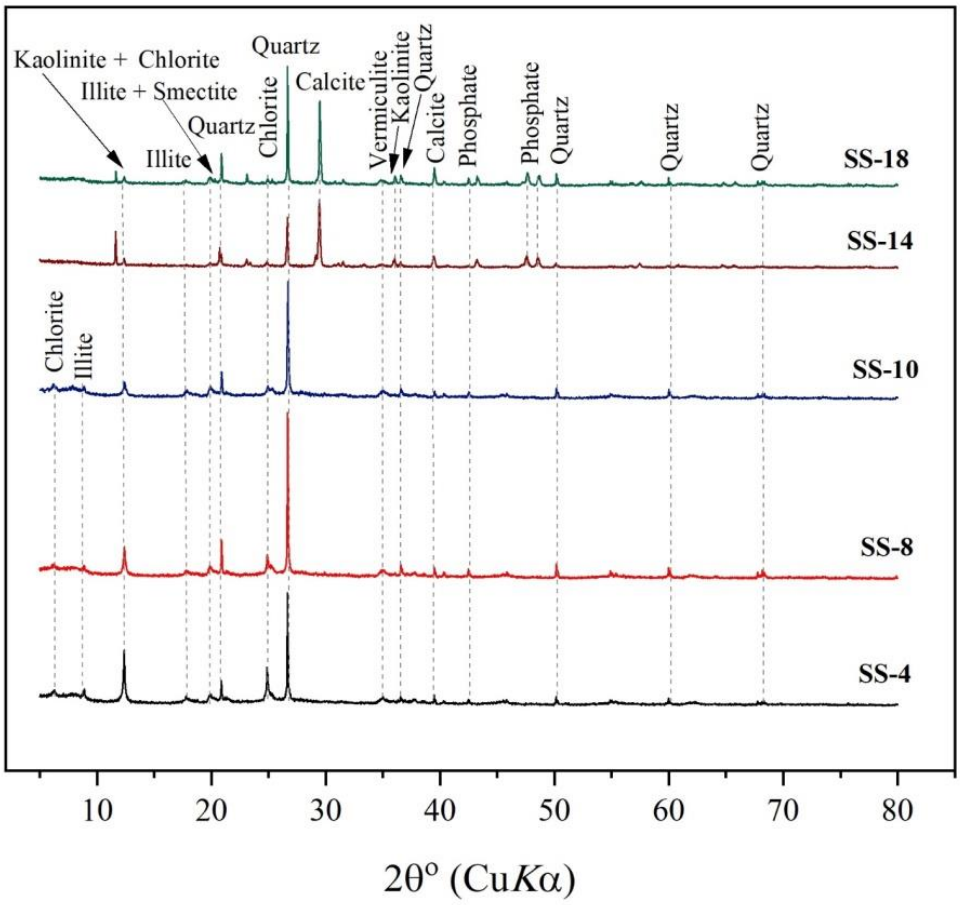

.

Fig.5. The bulk powder X-ray diffraction (XRD) patterns of spiti shales (Cl-chlorite; Q-quartz; I- illite; Ve-vermiculite ; Sm – smectite ; K- kaolinite; P - phosphate and C- calcite).

Geochemistry

The major elemental concentrations and their ratios of the sandstones and shales of present study are given in table 2. The sandstones exhibit high SiO_2 abundance (78-84 wt %) while shales have low range of values (46-65 wt %). The high concentration of SiO_2 in sandstones is due to the high percentage of quartz. Shales possess higher Al_2O_3 (18-28 wt.%), K_2O (1.2 to 5.4wt.%) and Fe_2O_3 (0.4 to 5.8 wt.%). In particular, the Na_2O concentration is less in sandstones (Table 2) as compared to K_2O which indicates the presence of K–rich minerals as compared to Na-rich minerals. This is confirmed by the petrographical study which shows more dominance of K-feldspar than the plagioclase in the sandstones.The apparent control of associated dolomitic limestones may be shown by the noticeably increased quantity of CaO and MgO in some samples, suggesting that CaO is largely absorbed into the calcite or dolomite rather than plagioclase. When compared to upper continental crust (UCC), the studied sandstones show depleted pattern except for SiO_2 and K_2O (Fig. 6). The Spiti shale sample plots on PAAS (post-Archean shales from Australia) diagram show similar values (Fig.7). However, the large enrichment in SiO_2 and Al_2O_3 is noticed indicating the presence of more clay fraction in the samples.

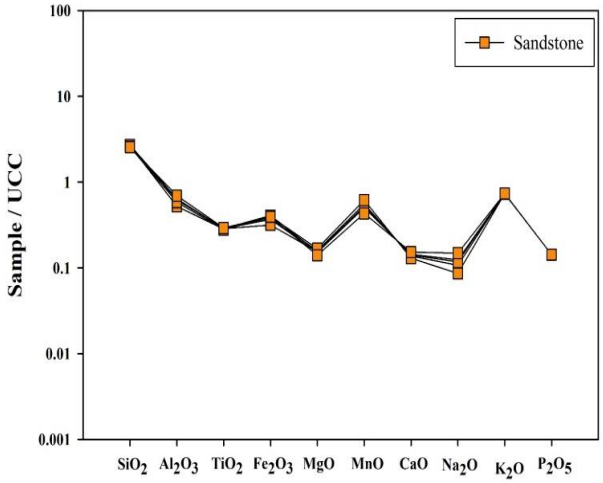

Fig.6. UCC normalized major element pattern of Spiti sandstones (UCC values after Mc Lennan, 2001).

Table 2. Major element concentrations (wt. %) of Spiti shales and sandstones from Spiti region

	Shales																												Sandstones					
	SS1	SS2	SS3	SS4	SS5	SS6	SS7	SS8	SS9	SS10	SS11	SS12	SS13	SS14	SS15	SS16	SS17	SS18	SS19	SS20	SS21	SS22	SS23	SS24	SS25	SS26	SS27	SS28	SPT1	SPT2	SPT3	SPT4	SPT5	SPT6
SiO_2	49.02	49.02	51.19	46.31	49.70	49.32	50.08	50.46	51.10	51.33	53.51	53.89	58.80	58.52	55.42	54.83	52.47	52.62	64.77	65.42	63.89	62.31	61.25	58.72	61.58	60.36	58.33	56.49	79.61	79.09	81.39	82.12	80.87	83.92
Al_2O_3	26.52	28.52	26.63	28.82	27.34	27.65	27.17	27.14	27.15	27.30	25.85	25.72	22.72	22.70	24.35	24.68	26.29	26.59	18.11	18.70	20.18	23.90	24.00	21.74	18.97	21.89	23.29	20.26	4.70	5.61	5.16	4.20	4.99	5.16
TiO_2	1.18	1.18	1.43	1.35	1.13	1.32	1.43	1.31	1.37	1.24	1.31	1.26	0.74	0.78	1.05	0.89	1.00	0.95	0.70	0.73	0.70	1.08	0.97	0.79	0.59	0.86	0.66	0.58	0.12	0.12	0.12	0.12	0.12	0.12
Fe_2O_3	5.39	5.39	5.80	5.66	5.97	5.88	5.75	5.77	5.31	5.17	4.88	4.73	3.75	3.73	4.71	4.72	5.40	5.27	3.01	3.07	1.96	3.06	4.32	3.81	0.42	1.01	1.70	1.46	1.39	1.38	1.43	1.32	1.29	1.11
MgO	1.58	1.58	1.42	1.40	1.58	1.61	1.59	1.61	1.57	1.55	1.50	1.53	0.72	0.71	1.58	1.50	1.33	1.33	1.03	2.02	0.92	0.85	0.82	1.37	1.88	3.07	2.40	3.75	0.22	0.19	0.21	0.21	0.20	0.21
MnO	0.01	0.01	0.00	0.00	0.01	0.01	0.01	0.00	0.01	0.01	0.00	0.01	0.00	0.00	0.01	0.01	0.00	0.01	0.05	1.40	0.72	0.61	0.89	0.47	0.29	0.03	1.02	0.21	0.37	0.26	0.32	0.33	0.30	0.32
CaO	0.30	0.30	0.25	0.22	0.40	0.48	0.51	0.42	0.34	0.31	0.40	0.44	0.60	0.77	0.46	0.70	0.71	0.15	0.26	0.41	0.16	0.16	0.79	0.62	0.52	0.24	0.12	0.39	0.39	0.46	0.42	0.41	0.43	0.42
Na_2O	0.52	0.52	0.54	0.54	0.51	0.52	0.52	0.46	0.82	0.77	0.60	0.63	0.24	0.22	0.24	0.25	0.25	0.28	0.45	0.47	0.27	0.46	0.25	0.18	0.21	0.47	0.29	0.25	0.25	0.43	0.34	0.31	0.36	0.34
K_2O	1.74	1.74	1.71	1.88	1.93	1.88	1.79	1.69	1.85	1.98	1.90	1.84	2.66	2.62	1.13	4.11	3.41	5.40	2.17	2.13	3.67	1.97	2.02	4.99	1.88	5.44	3.33	5.41	2.05	2.07	2.06	2.06	2.06	2.06
P_2O_5	0.08	0.08	0.11	0.11	0.09	0.12	0.18	0.15	0.08	0.08	0.07	0.05	0.32	0.31	0.07	0.09	0.06	0.10	0.14	0.17	0.07	0.04	0.09	0.05	0.15	0.20	0.33	0.19	0.01	0.01	0.01	0.01	0.01	0.01
Total	86.32	88.32	89.09	86.28	88.66	88.78	89.01	89.02	89.60	89.75	90.00	90.10	90.56	90.37	89.01	91.77	90.93	92.71	90.68	94.51	92.53	94.43	95.39	92.74	86.49	93.57	91.47	88.99	89.10	89.62	91.45	91.09	90.63	93.66
CIA	89.31	89.68	89.30	89.66	88.22	88.02	87.97	89.00	87.24	87.28	87.30	87.04	83.88	83.15	90.87	80.08	82.95	80.16	83.54	83.02	81.14	88.28	85.66	76.11	85.06	75.53	84.44	74.38	58.46	59.74	59.15	54.64	58.02	59.15
CIW	96.20	95.31	95.20	95.72	94.58	94.12	93.85	94.67	93.23	93.70	93.80	93.33	93.86	92.80	95.20	93.59	93.88	97.32	93.71	92.50	96.56	95.81	92.90	93.84	93.60	94.78	97.13	94.75	80.75	78.45	79.48	76.91	78.36	79.48
PIA	90.96	91.65	91.48	91.67	89.99	89.81	89.80	90.71	90.55	90.29	89.57	89.47	83.33	82.43	91.85	77.95	81.92	77.23	84.78	84.30	79.20	89.99	85.80	71.46	85.04	71.67	83.74	68.69	45.86	52.30	49.36	39.87	47.74	49.36
WIP	23.43	24.04	24.16	25.46	26.24	26.08	25.25	23.69	27.82	28.33	26.06	25.83	28.96	28.86	16.20	42.29	36.87	52.55	25.35	25.61	35.37	23.44	24.40	48.26	19.56	51.82	32.41	50.27	21.67	23.68	22.71	22.29	22.83	22.48

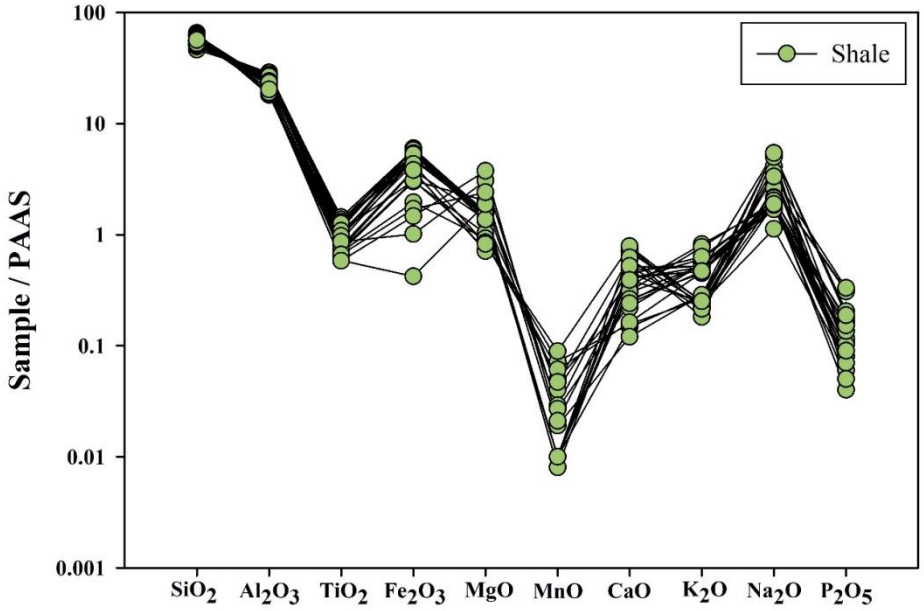

Fig.7. PAAS normalized major element patterns of Spiti shales from Spiti region (PAAS values after Taylor & McLennan, 1985).

Table 3. Correlation matrix of Spiti Shale

	SiO_2	Al_2O_3	TiO_2	Fe_2O_3	MgO	MnO	CaO	Na_2O	K_2O	P_2O_5
SiO_2	1.00									
Al_2O_3	-0.92	1.00								
TiO_2	-0.78	0.87	1.00							
Fe_2O_3	-0.79	0.85	0.83	1.00						
MgO	-0.05	-0.17	-0.20	-0.41	1.00					
MnO	0.65	-0.53	-0.48	-0.49	0.06	1.00				
CaO	0.06	-0.06	-0.11	0.14	-0.25	-0.09	1.00			
Na_2O	-0.49	0.53	0.74	0.46	0.04	-0.28	-0.40	1.00		
K_2O	0.27	-0.35	-0.55	-0.45	0.43	0.09	-0.04	-0.48	1.00	
P_2O_5	0.25	-0.32	-0.44	-0.41	0.22	0.14	0.08	-0.32	0.18	1.00

Table 4. Correlation matrix of Spiti Sandstone

	SiO_2	Al_2O_3	TiO_2	Fe_2O_3	MgO	MnO	CaO	Na_2O	K_2O
SiO_2	1.00								
Al_2O_3	-0.26	1.00							
TiO_2	-0.16	0.75	1.00						
Fe_2O_3	-0.78	0.01	-0.02	1.00					
MgO	0.16	-0.75	-1.00	0.02	1.00				
MnO	0.16	-0.75	-1.00	0.02	1.00	1.00			
CaO	-0.16	0.75	1.00	-0.02	-1.00	-1.00	1.00		
Na_2O	-0.16	0.75	1.00	-0.02	-1.00	-1.00	1.00	1.00	
K_2O	-0.16	0.75	1.00	-0.02	-1.00	-1.00	1.00	1.00	1.00

Because TiO2 is typically dispersed within the clays as separate minerals, such as rutile and anatase, the considerable positive association between TiO_2 and Al_2O_3 (r^2=0.75) suggests that Ti is mostly associated with clays and therefore reflecting its terrigenous origin (Wintsch & Kvale, 1994). It may be clear from the strong positive correlation (Table 4) between CaO and Al_2O_3 (r^2=0.75) that the majority of CaO is not derived from carbonates (von Eynatten et al., 2003).The Spiti sandstones show variable degree of negative correlation for SiO2 vs. Al_2O_3 (r^2= -0.26), TiO_2 (r^2= -0.16), Fe_2O_3 (r^2= -0.78), Na_2O (r^2= -0.16) and K_2O (r^2= -0.16), clearly reflecting a decrease in unstable components (e.g. feldspars and rock fragments) with an increase in mineralogical maturity (Tables 3&4) which may be due to quartz dilution effect. Because the concentrations of Al_2O_3 and SiO_2 are constrained by aluminous clay and quartz contents, respectively, in sedimentary rocks, SiO_2 has a high negative correlation with Al_2O_3 (r^2 = -0.26, Fig.8 a).

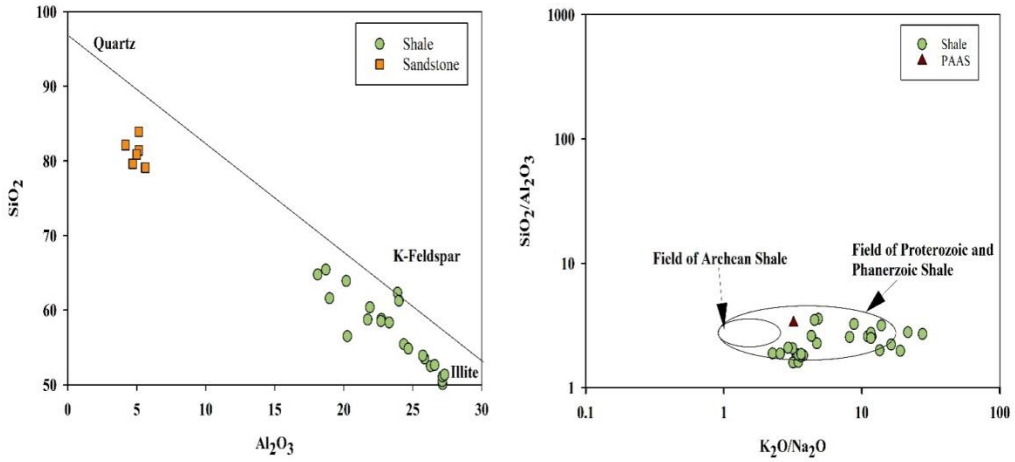

Fig.8. (a) Al_2O_3 –SiO_2 plot for shales and sandstones of Spiti Formation. Note the samples lie near the smooth line and so the sediments can be considered as the product of mixing of two ends (quartz and illite). (b) SiO_2 /Al_2O_3 vs. K_2O/Na_2O plot (Wronkiewicz & Condie, 1987) for Spiti shales and sandstones.

The SiO_2 /Al_2O_3 ratio of the shales lies in between 1.60 to 3.58. On the SiO_2 /Al_2O_3 versus K_2O/Na_2O bivariate diagram (Fig. 8b) the shales, as expected, plot in the field of Proterozoic-Phanerozoic shales (Fig. 8b). At a given K_2O/Na_2O ratio, the related sandstones have greater SiO_2 /Al_2O_3 ratios than the shales, indicating a quartz dilution effect. According to Cox et al., (1995) major element composition of shales is controlled mainly by clay minerals rather than the non-clay silicate phases. K_2O/Al_2O_3 ratio suggests how much alkali feldspar against plagioclase and clay minerals may have been associated with the original shales. The K_2O/Al_2O_3 ratio of minerals, from high to low values are represented by alkali feldspars (0.4 – 1), illite (0.3), other clay minerals (0) (Cox et al., 1995). Sediments with K_2O/Al_2O_3 larger than 0.5 indicates that there was a substantial amount of alkali feldspar in the original samples compared to other minerals; while those with K_2O/Al_2O_3 less than 0.4 indicates that there was minimal alkali feldspar in the original samples (Cox et al., 1995). The Spiti shales and sandstones have an average K_2O/Al_2O_3 = 0.17(range, 0.05 – 0.49). The overall low K_2O/Al_2O_3 ratios of the Spiti Formation suggest minimal involvement of alkali feldspar relative to other minerals in the original samples and strongly support the fact that K_2O addition to the shales has not taken place. The K_2O/Na_2O ratio of Spiti shales ranges from 2.25 to 27.6, which is higher than the value of different post-Archean shale standards (3.1–3.5, (Condie, 1993). The P_2O_5 and SiO_2 concentrations, on the other hand, range from 0.05 to 0.33 wt % and 46 to 65 wt %, respectively.

Discussion

Classification

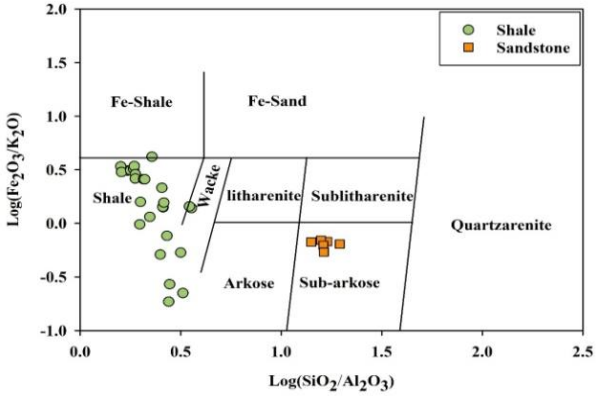

Fig.9 (a).Chemical classification diagram of the Spiti samples (Herron, 1988)

The chemical composition of the classes quartz arenite, graywacke, and arkose can be characterized using the ratios (silica, alumina, alkali oxides, magnesium and iron oxides), which can be represented using two-dimensional diagrams with varying degrees of success (Lindsey, 1999). A fourth sandstone class, lithic arenite, is compositionally diverse; several classifications with modest success, but lithic-arenites can not be identified with great reliance by chemical composition alone. Based on the geochemical studies, sandstones are classified as subarkose (Fig. 9 a) according to Herron (1988) classification. While it is also clear from the chemical classification diagram (Pettijohn et al., 1972), i.e., log (SiO_2/ $A1_2O_3$) vs. log (Na_2O/K_2O) diagram that the sandstones are classified as subarkose in nature (Fig. 9 b).

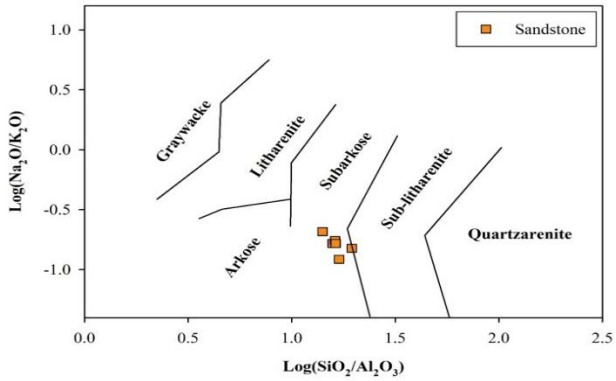

Fig. 9(b). Chemical classification diagram of Spiti sandstones (Pettijohn et al., 1972).

Paleoweathering

The intensity and duration of weathering in clastic sedimentary rocks can be estimated by examining the association between alkali and alkaline elements (Nesbitt et al., 1996). The Chemical Index of Alteration (CIA) (Nesbitt & Young, 1982) is a well-established way of assessing the degree of source rock weathering among the known indices of weathering. The Plagioclase Index of Alteration (PIA) (Fedo et al., 1995), Chemical Index of Weathering (CIW) (Harnois 1988), and Weathering Index of Parker (WIP) (Parker, 1970) can all be used to analyse source rock weathering and elemental redistribution during diagenesis.

CIA = {Al_2O_3 / (Al_2O_3+ CaO* + Na_2O + K_2O)} x 100

PIA = {(Al_2O_3 – K_2O) / (Al_2O_3 – K_2O + CaO*+ Na_2O)} x 100

CIW = {Al_2O_3 / (Al_2O_3 + CaO* + Na_2O)} x 100

WIP = {(2Na_2O / 0.35) + (MgO / 0.9) + (2K_2O / 0.25) + (CaO* / 0.7)} x 100

The major oxides are represented in molar proportions in the above equations, and CaO* represents the quantity of CaO integrated in the silicate fraction only. According to the WIP definition, the smaller WIP values indicate stronger chemical weathering, which is opposite to CIA values (Hamdan & Bumham, 1996). CIA, PIA, WIP and CIW values of Spiti samples were calculated and presented in table 2. The calculated CIA values are 55 -60 (avg. 58) and 74- 91 (avg. 85) for the Spiti sandstones and black shales, respectively suggesting that the source rocks underwent moderate to intense chemical weathering. Whereas, PIA values for the Spiti sandstones and shales are 40-52 and 69-92 (avg. 47and 85), respectively indicating moderate to intense chemical weathering. Similarly, CIW and WIP values also indicate moderate to intense degree of chemical weathering in the source area. The CIA values are also shown in Al_2O_3-(CaO+Na_2O)-K_2O ternary plot (Fedo et al., 1995; Nesbitt & Young, 1984) commonly known as the 'A–CN–K' diagram (Fig. 10) to classify the composition of the provenance and weathering trends. This diagram is used to understand the rate of weathering of K –feldspar and plagioclase (Ca–Na feldspar). As a result, CaO and Na_2O are preferentially leached during weathering compared to K_2O, allowing the weathering trend to follow the A–CN join.Weathering removes CaO, Na_2O, and K_2O from source rock, making the trend parallel to the A–K junction. The A–CN–K ternary diagram is used to plot the Spiti samples,with the majority of the samples placed above the feldspar tie line. It has been observed that the studied samples had undergone moderate to intense chemical weathering based on their weathering patterns.

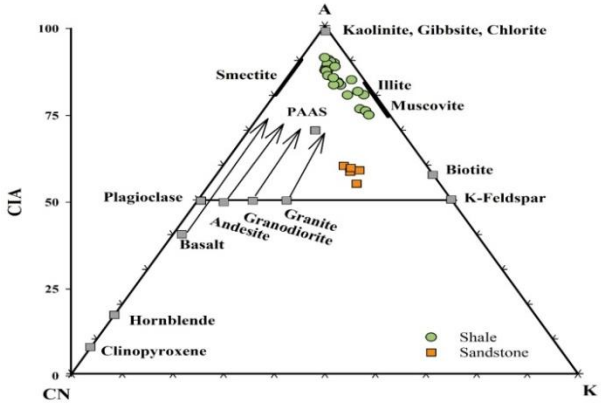

Fig.10. A–CN-K diagram (after Nesbitt & Young, 1984) of Spiti sediments. Arrows showing the weathering trends of basalt, andesite, granodiorite and granite.

Provenance characteristics

The objective of provenance study is to evaluate the evolution and the nature of source rocks. The chemical composition of siliciclastic sedimentary rocks is based on the chemical composition of their provenance, and this principle has been used to describe the source rocks from which the studied sedimentary

rocks were formed (Cullers, 2000; Taylor & McLennan, 1985; Kanhaiya et al., 2018; Verma et al., 2012). Thus, geochemical markers of clastic sediments were used to determine provenance attributes. Diagenesis, weathering and hydraulic sorting all have a consequence on the geochemical composition of the sediments. However, major oxides such as Al_2O_3 and TiO_2 (as well as their ratios i.e., Al_2O_3 /TiO_2), are significant immobile elements that provide significant indications about the source region (Taylor and McLennan 1985; Hayashi et al., 1997). For mafic rocks, the Al_2O_3 /TiO_2 ratio ranges from 3-8, for intermediate rocks from 8-21, and for felsic rocks from 21-70 (Hayashi et al., 1997). High Al_2O_3 /TiO2 values in the analyzed samples (18.5–35.3) for Spiti shales and (36-47) for Spiti sandstone show that the Spiti sediments were derived from intermediate and felsic igneous provenances. Knowing the importance of Al and Ti in provenance studies, (Mc Lennan et al., 1993) devised a bivariate discrimination diagram for Al_2O_3 vs.TiO_2 to determine the provenance of siliciclastic rocks. The Spitui shales data got plotted along the granodiorite to 3granite+ 1basalt trend line in the diagram (Fig. 11).

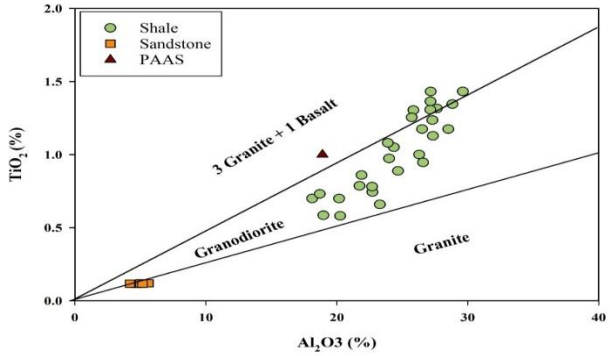

Fig.11. TiO_2 (wt%) vs. Al_2O_3 (wt%) bivariate diagram (Mc Lennan et al., 1993) for Spiti silliciclastic sedimentary rocks. The "granite line" and "3 granite + 1basalt line" (Schieber, 1992).

Overall major element geochemical characteristics of the Spiti sediments shows high SiO_2, Al_2O_3, K_2O contents and having low MgO, Fe_2O_3, CaO and Na_2O concentrations suggesting a dominant felsic source with minor mafic input.

5.4. Tectonic setting

Many studies reveal that the chemical composition of the siliciclastic rocks are influenced by the plate tectonic setting of their source regions and thus siliciclastic rocks from distinct tectonic settings have terrain specific geochemical signatures (Bhatia & Crook, 1986; Roser & Korsch, 1986). As a result, sediments from various tectonic settings show a wide range of geochemical features.

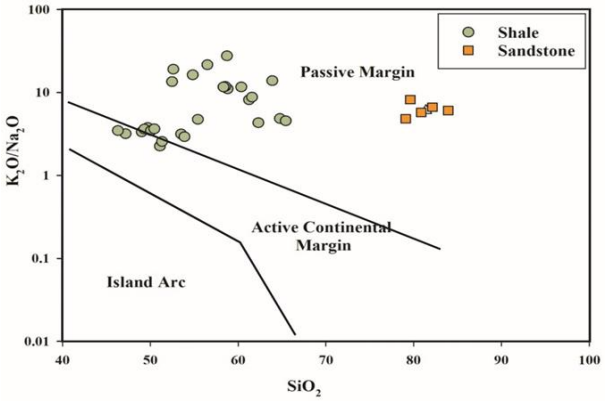

Fig.12. Tectonic setting diagram of Spiti shales and sandstones (Roser & Korsch, 1986)

By using log (K_2O/Na_2O) vs SiO_2, Roser & Korsch (1986) suggested major element based discrimination diagrams to create the tectonic setting of older sedimentary basins. The Spiti shales and sandstones are plotted in the passive margin tectonic setting while few samples lies in the active continental margin setting (Fig. 12). According to Roser & Korsch (1986) passive margin sediments are largely quartz-rich derived from plate interiors or stable continental areas and deposited on passive continental margins or in intracratonic basins .

Paleoclimatic conditions

To desipher the paleoclimatic condition of siliciclastic rocks, Suttner & Dutta (1986) presented a binary diagram SiO_2wt. % vs (Al_2O_3 +K_2O+Na_2O) wt. %. In the (Fig.13), the Spiti sandstones lie in a semi-humid climatic region.

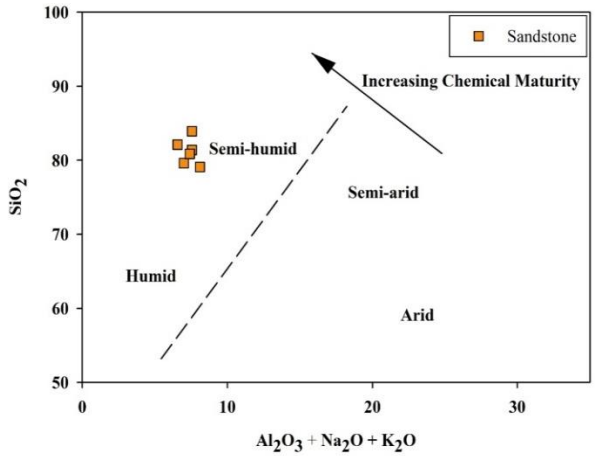

Fig.13. SiO_2Vs (Al_2O_3 +K_2O+Na_2O) palaeoclimate discrimination diagram (after Suttner & Dutta, 1986) of the Spiti sandstones.

Conclusions

A Jurassic siliciclastic sedimentary sequence from the Spiti Formation comprising of shales and sandstones were studied in the present study..On the basis of petrographical and geochemical studies, the sandstones are classified into sub-arkose type.

The bulk powder XRD (X-ray diffraction) studies of the black shales of the Spiti Formation show the dominance of illite, smectite, kaolinite, chlorite and vermiculite as clay minerals suite with silica and phosphatic phases.

The chemical weathering indices (CIA, PIA, CIW, and WIP) and the ACNK ternary diagrams reveal moderate to intense chemical weathering in the source area of Spiti Formation.

The Spiti rocks lie mainly in the passive tectonic setting and indicate semi humid paleoclimate conditions in the Spiti region during Jurassic period.

Discriminant function diagrams and Qt-F-L ternary diagram suggest dominantly felsic (including quartzose sedimentary and granitic rocks) provenance for the Spiti sedimentary sequence.

Acknowledgment:

The authors sincerely thank the chairperson Department of Geology, A.M.U., Aligarh for providing necessary facilities and continuous support. We also thank Dr. Indra Sen, IIT Kanpur and Dr. Anupam Sharma, BSIP, Lucknow for extending the analytical facilities.

References

Armstrong-Altrin, J. S., Lee, Y. I., Verma, S. P., & Ramasamy, S. (2004). Geochemistry of Sandstones from the Upper Miocene Kudankulam Formation, Southern India: Implications for Provenance, Weathering, and Tectonic Setting. *Journal of Sedimentary Research*, *74*(2), 285–297. https://doi.org/10.1306/082803740285

Bagati, T. N. (1990). Lithostratigraphy and facies variation in the Spiti basin (Tethys), Himachal Pradesh, India. *Journal of Himalayan Geology*, *1*(1), 35–47.

Bhargava, O. N. (2008). An updated introduction to the Spiti geology. *Journal of the Palaeontological Society of India*, *53*(2), 113–128.

Bhargava, O. N., & Bassi, U. K. (1998). *Geology of Spiti-Kinnaur Himachal Himalaya* (Vol. 124). Geological Survey of India.

Bhatia, M. R., & Crook, K. A. W. (1986). Trace element characteristics of graywackes and tectonic setting discrimination of sedimentary basins. *Contributions to Mineralogy and Petrology*, *92*(2), 181–193. https://doi.org/10.1007/BF00375292

Blatt, H. (1985). Provenance studies and mudrocks. *Journal of Sedimentary Research*, *55*(1), 69–75.

Condie, K. C. (1993). Chemical composition and evolution of the upper continental crust: Contrasting results from surface samples and shales. *Chemical Geology*, *104*(1–4), 1–37.

Cox, R., Lowe, D. R., & Cullers, R. L. (1995). The influence of sediment recycling and basement composition on evolution of mudrock chemistry in the southwestern United States. *Geochimica et Cosmochimica Acta*, *59*(14), 2919–2940. https://doi.org/10.1016/0016-7037(95)00185-9

Cullers, R. L. (2000). The geochemistry of shales, siltstones and sandstones of Pennsylvanian–Permian age, Colorado, USA: Implications for provenance and metamorphic studies. *Lithos*, *51*(3), 181–203.

Dickinson, W. R. (1985). Interpreting provenance relations from detrital modes of sandstones. In *Provenance of arenites* (pp. 333–361). Springer.

Dickinson, W. R., & Suczek, C. A. (1979). Plate Tectonics and Sandstone Compositions1. *AAPG Bulletin*, *63*(12), 2164–2182. https://doi.org/10.1306/2F9188FB-16CE-11D7-8645000102C1865D

Fedo, C. M., Wayne Nesbitt, H., & Young, G. M. (1995). Unraveling the effects of potassium metasomatism in sedimentary rocks and paleosols, with implications for paleoweathering conditions and provenance. *Geology*, *23*(10), 921–924.

Garzanti, E., Vermeesch, P., Padoan, M., Resentini, A., Vezzoli, G., & Andò, S. (2014). Provenance of passive-margin sand (Southern Africa). *The Journal of Geology*, *122*(1), 17–42.

Hamdan, J., & Bumham, C. P. (1996). The contribution of nutrients from parent material in three deeply weathered soils of Peninsular Malaysia. *Geoderma*, *74*(3–4), 219–233.

Hayashi, K.-I., Fujisawa, H., Holland, H. D., & Ohmoto, H. (1997). Geochemistry of 1.9 Ga sedimentary rocks from northeastern Labrador, Canada. *Geochimica et Cosmochimica Acta*, *61*(19), 4115–4137.

Herron, M. M. (1988). Geochemical classification of terrigenous sands and shales from core or log data. *Journal of Sedimentary Research*, *58*(5), 820–829.

Kanhaiya, S., Singh, B. P., & Singh, S. (2018). Mineralogical and geochemical behavior of sediments solely derived from Bundelkhand granitic complex, central India: Implications to provenance and source rock weathering. *Geochemistry International*, *56*(12), 1245–1262.

Lindsey, D. A. (1999). *An evaluation of alternative chemical classifications of sandstones*. US Geological Survey.

McLennan, S. M. (2001). Relationships between the trace element composition of sedimentary rocks and upper continental crust. *Geochemistry, Geophysics, Geosystems*, *2*(4).

McLennan, S. M., Hemming, S., McDaniel, D. K., & Hanson, G. N. (1993). Geochemical approaches to sedimentation, provenance, and tectonics. In *Geological Society of America Special Papers* (Vol. 284, pp. 21–40). Geological Society of America. https://doi.org/10.1130/SPE284-p21

Nesbitt, H. W., & Young, G. M. (1984). Prediction of some weathering trends of plutonic and volcanic rocks based on thermodynamic and kinetic considerations. *Geochimica et Cosmochimica Acta*, *48*(7), 1523–1534.

Nesbitt, H. W., Young, G. M., McLennan, S. M., & Keays, R. R. (1996). Effects of chemical weathering and sorting on the petrogenesis of siliciclastic sediments, with implications for provenance studies. *The Journal of Geology*, *104*(5), 525–542.

Nesbitt, Hw., & Young, G. M. (1982). Early Proterozoic climates and plate motions inferred from major element chemistry of lutites. *Nature*, *299*(5885), 715–717.

Parcha, S. K. (2021). Stratigraphy and the Fossil record of the Palaeozoic and Mesozoic Tethyan sequences of North-western Himalaya. *Himalayan Geology*, *42*(1), 1–68.

Parker, A. (1970). An index of weathering for silicate rocks. *Geological Magazine*, *107*(6), 501–504.

Pettijohn, F. J., Potter, P. E., & Siever, R. (1972). Sand and Sandstone. Springer-Verlag, Berlin Heidelberg New York. In *Pp 618 Pitman WC*.

Roser, B. P., & Korsch, R. J. (1986). Determination of tectonic setting of sandstone-mudstone suites using SiO2 content and K2O/Na2O ratio. *The Journal of Geology*, *94*(5), 635–650.

Schieber, J. (1992). A combined petrographical—Geochemical provenance study of the Newland Formation, Mid-Proterozoic of Montana. *Geological Magazine*, *129*(2), 223–237.

Scholle, P. A. (1979). Constituents, Textures, Cements, and Porosities of Sandstones and Associated Rocks. *US Geological Survey, Published by the American Association of The American Association of Petroleum Geologists Foundation. Tulsa, Oklahoma, USA 193p*.

Suttner, L. J., & Dutta, P. K. (1986). Alluvial sandstone composition and paleoclimate; I, Framework mineralogy. *Journal of Sedimentary Research*, *56*(3), 329–345.

Taylor, S. R., & McLennan, S. M. (1985). *The continental crust: Its composition and evolution*.

Verma, M., Singh, B. P., Srivastava, A., & Mishra, M. (2012). Chemical behavior of suspended sediments in a small river draining out of the Himalaya, Tawi River, northern India: Implications on provenance and weathering. *Himal Geol*, *33*, 1–14.

Von Eynatten, H., Barcelo-Vidal, C., & Pawlowsky-Glahn, V. (2003). Composition and discrimination of sandstones: A statistical evaluation of different analytical methods. *Journal of Sedimentary Research*, *73*(1), 47–57.

Wintsch, R. P., & Kvale, C. M. (1994). Differential mobility of elements in burial diagenesis of siliciclastic rocks. *Journal of Sedimentary Research*, *64*(2a), 349–361.

Wronkiewicz, D. J., & Condie, K. C. (1987). Geochemistry of Archean shales from the Witwatersrand Supergroup, South Africa: Source-area weathering and provenance. *Geochimica et Cosmochimica Acta*, *51*(9), 2401–2416.

Zuffa, G. G. (1985). Optical analyses of arenites: Influence of methodology on compositional results. In *Provenance of arenites* (pp. 165–189). Springer.

JOURNAL INDIAN ASSOCIATION OF SEDIMENTOLOGISTS ISSN NO 2582 – 2020
Vol. 39, Issue 2, 2022, pp. 30-46
DOI: https://doi.org/10.51710/jias.v39iII.256

Geochemical Evolution of Dolomites in Thanagazi Formation of Mesoproterozoic Alwar Basin, Northwest India

R. Sajeev, Dinesh Pandit*and Mallickarjun Joshi

Department of Geology, Institute of Science, Banaras Hindu University, Varanasi - 221005, India
**Corresponding author:dpandit@hotmail.com*

Abstract

The geochemistry of dolomite in part of the Thanagazi Formation in the Mesoproterozoic Alwar Basin has been studied employing major and trace elements, including rare earth elements (REEs) to understand their provenance and paleoweathering conditions. In the current study, two distinct types of dolomites were identified viz. amorphous and crystalline. Various geochemical discriminants such as SiO_2 vs Al_2O_3 and CaO vs MgO indicate that the dolomites were originated from sedimentary sources with substantial metasomatic and biogenic contributions. Geochemical constraints from plots of Fe_2O_3/Al_2O_3 vs. $Al_2O_3/(Al_2O_3+Fe_2O_3)$ and rare earth element compositions for provenance signatures suggest likely deposition of dolomites in shallow marine sedimentary environment. Based on geothermometric estimates and base metal concentrations in dolomites, it is inferred that the mixing of sediments derived from two different sources (metasomatic and biogenic) were likely responsible for the dolomitization in the Thanagazi Formation of the Mesoproterozoic Alwar Basin.

Keywords*:* Alwar, Dolomite,Diagenesis, Geochemistry, Sedimentary Provenance

Introduction

Dolomite is a carbonate mineral in the ancient platforms and is mostly associated with hypersaline brines or schizohaline waters or the long-term circulation of seawater through platform sediments (Land, 1985; Hardie, 1987; Warren, 2000). Geochemical constraints (salinity, temperature, pressure, etc.) probably affect the nature of carbonate precipitation from the waters, whereas the variation in the relative amounts of magnesium and calcium is particularly important (Alderman and Borch, 1963; Baithwaite, 1991; Bouton et al., 2020). Dolomite is one of the thermodynamically stable carbonate phases in ocean water and an extremely common constituent of ancient terrestrial carbonate rocks (Baker and Kastner, 1981; Lee and Lindgren, 2015). Precambrian carbonates are characteristically dolomitic in composition and associated with prevalent secondary silicification (Eriksson and Warren, 1983). Widespread occurrences of Precambrian dolomite were precipitated from seawater during diagenesis (Tucker, 1982) or late-stage dolomitization by penetrating ground waters in burial diagenetic settings i.e., penecontemporaneous dolomites (Machel, 2004). Hydrothermal dolomites are commonly crystallized from hydrothermal fluids in a diagenetic stage (Boni et al., 2000; Eickmann et al., 2009; Zhang et al., 2020). Along the spreading centers, hydrothermal fluids from the deep oceanic crust can move upwards through faults and escape at the ocean floor, resulting in a black smoker (Charlou et al., 2002) or a white smoker vent fluids (Kelley et al., 2001) that favour precipitation of carbonates (Turchyn et al., 2021) and dolomites (Roberts et al., 2013). Experimental investigation suggests that dolomitization can take place in marine and the lacustrine environments under low dissolved sulphate concentrations and silica diagenesis (Baker and Kastner, 1981). Geological models for dolomitization depend on the physicochemical conditions that can be produced in a range of environments in both eogenetic and mesogenetic settings (Braithwaite, 1991).

Base metal sulphide (pyrite, chalcopyrite, sphalerite, galena and other ore minerals) mineralization is ubiquitous in sedimentary basins and is common in rocks ranging in age from Paleoproterozoic (Wheatley et al., 1986; Deb et al., 1989; Pirajno and Joubert, 1993; Kesler and Reich, 2006) to Cenozoic (Megaw et al., 1988; Leach et al., 2001; Zhang et al., 2020). Proterozoic orogenic belts of the Pan-African age located between Congo and Kalahari cratons at the Otavi Mountain Land (Namibia) metallogenic province hich covers an area of approximately 10000 km^2 (Pirajno and Joubert, 1993). There are more than 600 carbonate-hosted base metal deposits in the sedimentary platform of the Damara Orogen affected by carbonate alteration evidenced in dolomite and calcite veins along with epigenetic, hydrothermal, replacement, and open space filling deposits (Chetty and Frimmel, 2000). Economically viable concentrations of base-metal deposits in the Silver mines area (Ireland) are confined to the Carboniferous sequence of the Irish Midlands (Banks et al., 2002). Zinc-lead deposits belong to extensively dolomitised horizons within the limestones, whereas sulphide minerals occur as open space-fillings as well as fine-grained massive, and

disseminated mineralisation (Reed and Wallace, 2004). Precambrian dolomite of the Aravalli Supergroup commonly hosts base metal minerals while other accompanying rocks are phyllite, greywacke, quartzite and conglomerate (Sachan, 1993). Economic lead-zinc deposits associated with the Precambrian dolomite rocks of the Zawar mineral belt occur in mineable quantity. The Alwar district has attracted researchers who have focused mainly on the structural settings and style of mineralisation (Singh, 1984; Khan et al., 2014; Sajeev et al., 2019; Srivastava and Prakash, 2020; Sahoo et al., 2022). In this study, we discuss the geochemical evolution of dolomites from theThanagazi Formation of the Mesoproterozoic Alwar Basin in relation to the sedimentaary environment, provenance and base metal content.

Geological Settings

The study area is located in the northern part of the Delhi Fold Belt (Delhi Supergroup) in the Aravalli Craton in Peninsular India (Fig. 1a). The Alwar basin constitutes the central part of the North Delhi Fold Belt (NDFB), which occurs as a narrow linear belt in the south and central Rajasthan and fans out over a wider zone in the north-eastern Rajasthan (Fig. 1b). This basin formed one such depocenter which was separated from Bayan in the east and Khetri basin in the west by Pre-Delhi basement complex (Fig. 1b). The Alwar basin of the Delhi Supergroup (Table 1a) is nearly 6000m thick package of volcanic and sedimentary rocks that comprise three groups (Raialo, Alwar, and Ajabgarh). The Raialo Group consists of a lower calcareous and an upper arenaceous sequence (viz., the Dogeta and the Tehla Formation, respectively) with marble, phyllite and schist best exposed in the northeastern sector around Dogeta, Gola-Ka-Bas, Kharar, Jhiri, Tilwarhi, Todi and Kho-Dariba (GSI, 2019).

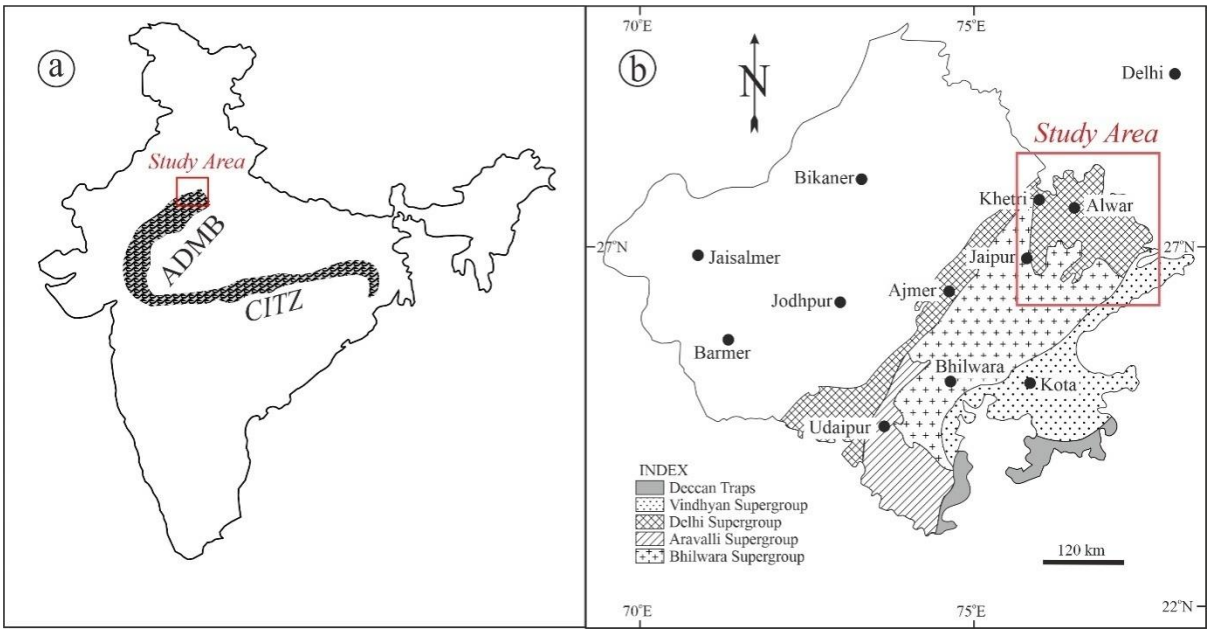

Fig. 1. (a) Location of the study area adjacent to the ADMB in the map of India; (b) outline of the geological map of Rajasthan shows the study area.

The Mesoproterozoic Alwar Group comprises metamorphosed arenaceous clastics with subordinate argillaceous and calcareous rocks interlayered with basic volcanics that rest unconformably over the Raialo Group (Table 1b). The generalized sequence of the Alwar Group is a basal conglomerate, arkose and quartzite followed by a sequence of argillaceous and impure calcareous rocks represented by pelitic schists which contain different mineral assemblages, impure marble and para-amphibolite which in turn is followed by a sequence of mainly arenaceous rocks with some amount of pelitic sediments (Fig. 1b). The rocks of the Mesoproterozoic Alwar Group have been classified into the Rajgarh, Kankawarhi, Pratapgarh, Nithar, Badalgarh, and Bayana Formation in northeastern Rajasthan and into the Srinagar and the Naulakha Formation in the Ajmer sector, respectively (GSI, 2001). The Mesoproterozoic Ajabgarh Group comprises of five formations (Table 1b). Metamorphosed argillites with intercalated arenites and subordinate carbonates have been included in the Kushalgarh and the Sariska formations. Carbonaceous phyllite, an interlayered sequence of quartzite, phyllite and schists containing chlorites, garnet, staurolite and andalusite are included under the Thanagazi, Bhakrol, and Arauli formations (GSI, 2019).

The Mundiyawas-Khera block located southwest of Thanagazi in the Mesoproterozoic Alwar Basin reveals a felsic volcanic-hosted thick copper and associated gold mineralization in the

Thanagazi Formation of Ajabgarh Group within the NDFB (Khan et al., 2014). The exposed rock types in the Mundiyawas-Khera area are meta-volcanosedimentary sequence, tremolite bearing dolomitic marble and carbonaceous phyllite (Fig. 2).

Table 1. (a) Stratigraphy of the Delhi Supergroup in the Alwar sub-basin (after Geological Survey of India, 2019).

Age	Supergroup	Group	Formation
Mezoproterozoic	Delhi Supergroup	Ajabgarh Group	Arauli Formation
			Bhakrol Formation
			Thanagazi Formation
			Seriska Formation
			Kushalgarh Formation
		Alwar Group	Pratapgarh Formation
			Kankwarhi Formation
			Rajgarh Formation
		Raialo Group	Tehla Formation
			Serrate Quartzite Formation
			Dogeta Formation

Table 1. (b) Lithostratigraphy of the Delhi Supergroup in the Alwar sub-basin (after Geological Survey of India, 2019).

Intrusives			Quartz vein and calcite vein
Delhi Supergroup (Mesoproterozoic)	Ajabgarh Group	Thanagazi Formation	Tremolite marble with quartzite
			Carbon phyllite
			Pyrite bearing biotite - quartzite
			Tremolite marble, biotite - marble
			Carbon phyllite/mica-schist/biotite marble
			Tremolite marble with quartzite
		Seriska Formation	Quartzite
		Kushalgarh Formation	Calcareous facies rocks – biotite – marble & dolomite – marble) hosting mineralization), calc. quartzite, calc. banded semipelite
	---------- Local Unconformity ----------		
	Alwar Group	Pratapgarh Formation	Tehal Formation
			Serrate Quartzite Formation
			Dogeta Formation
		Kankwarhi Formation	Conglomerate, mica schist, metavolcanics
	---------- Local Unconformity ----------		
	Raialo Group	Tehla Formation	Quartzite

Table 1. (c) Lithostratigraphy of Amra Ka Bas area in the Thanagazi Formation in the present study (after Geological Survey of India, 2019).

Meso-Proterozoic Age	Delhi Supergroup	Ajabgarh Group	Intrusive	Quartz vein
			Thanagazi Formation	Felsic metavolcanics
				Tremolite-bearing dolomitic marble
				Cherty quartzite
				Carbon phyllite

The felsic volcanics are represented by felsic tuff, lapilli tuff and agglomeratic tuff, which are rhyodacite in composition and occur as an interlayered sequence within the fine-grained quartzite, carbonaceous phyllite and dolomitic marble of Ajabgarh Group (Table 1c). The copper mineralization in Mundiyawas-Khera is hosted within the meta-volcanosedimentary sequence, dolomite, and tremolite-bearing dolomitic marble (Srivastava and Prakash, 2020). Sulphide ore minerals identified in this area as disseminations and stringers of pyrrhotite, pyrite and chalcopyrite which suggest base metal mineralization (Sajeev et al., 2019). Similar associations of sulphide ore minerals with volcanic rocks are also observed in various localities around Amra-Ka-Bas, Biharisar, Mejorh, Madri-Kishori, Bikrampura, etc.

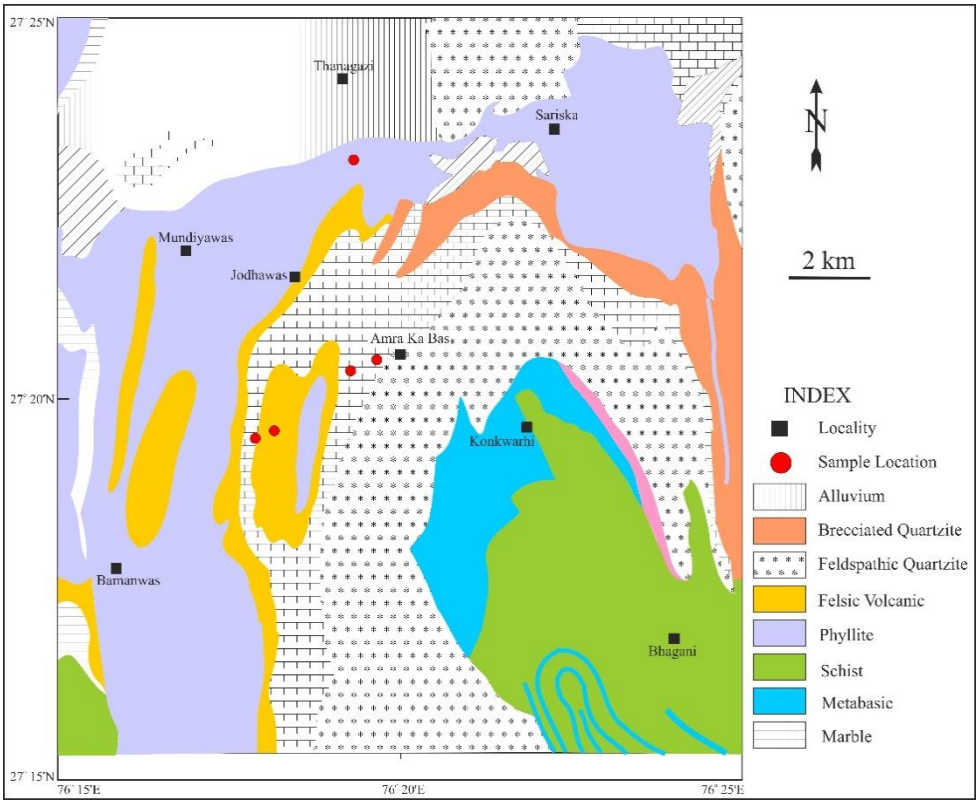

Fig. 2. Generalized local geological map of the Amra Ka Bas area in Thanagazi Formation with sample locations (Courtesy: Geological Survey of India).

Measured Litholog and Sampling Plan

Bulk dolomite samples are collected across the strike of the tremolitic marble interbanded with carbon phyllite. Litho-log of the study area around Amra Ka Bas and adjoining area is presented in the figure. Representative dolomite samples covering the stratigraphic lithosections were selected for bulk geochemical analysis using XRF and ICP-MS.

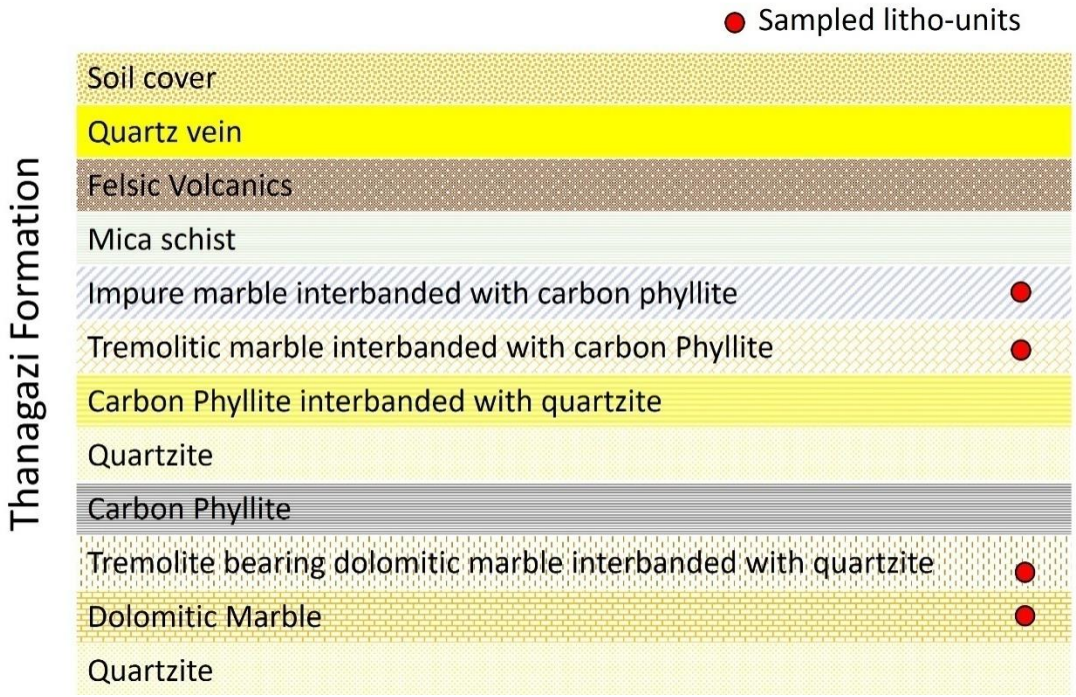

Figure: Detail lithological logs of Thanagazi Formation along Amra Ka Bas and adjoining area.

Lithological Associations

Dark grey coloured, very fine grained dolomite occurs along with dissolution cavities in the Amra Ka Bas area in association with volcano-sedimentary rocks (Fig. 3a). At some places, brown coloured carbonate matrix is also present in the dissolution cavities of dolomites. Micritic ferruginous dolomite occurs in few centimeters thick interbedded layers. Oxidation and ferruginisation of dolomite are also observed at several places around the Amra Ka Bas area (Fig. 3b). The buff grey coloured medium to fine grained crystalline dolomite shows profuse development of rosettes of tremolite. Occasional elephant skin weathering is observed on the surface of crystalline dolomite (Fig. 3c). The crystalline dolomite is brecciated due to silicification, shearing, grain rotation, and fragmentation. The crystalline dolomite is traversed by late-stage quartz veins which contain chalcopyrite and pyrrhotite grains along with malachite stains. The rotation of stretched and boudinaged quartz veins indicates simple shear stress in the dolomites of Amra Ka Bas area. It is intercalated with quartzite bands of variable thickness that range between 10-20 cm. Structural features like fold and boudinage are also present in the carbonate'smatrix at several places. White coloured material is coarsely crystalline calcite, which occurs as lining and partially fills small size cavities or vughs in dolomite (Fig. 3d). Tremolite occurs as broom shaped or slender type prismatic crystals of >5 cm size (Fig. 3e). In microphotograph, subhedral to euhedral prismatic crystals of tremolite shows distinct blue to green interference colours under cross polarized light (Fig. 3e, f). Most commonly, cracks and fissures are partially filled with calcite, quartz, and other secondary minerals in the dolomite are found in the Thanagazi Formation.

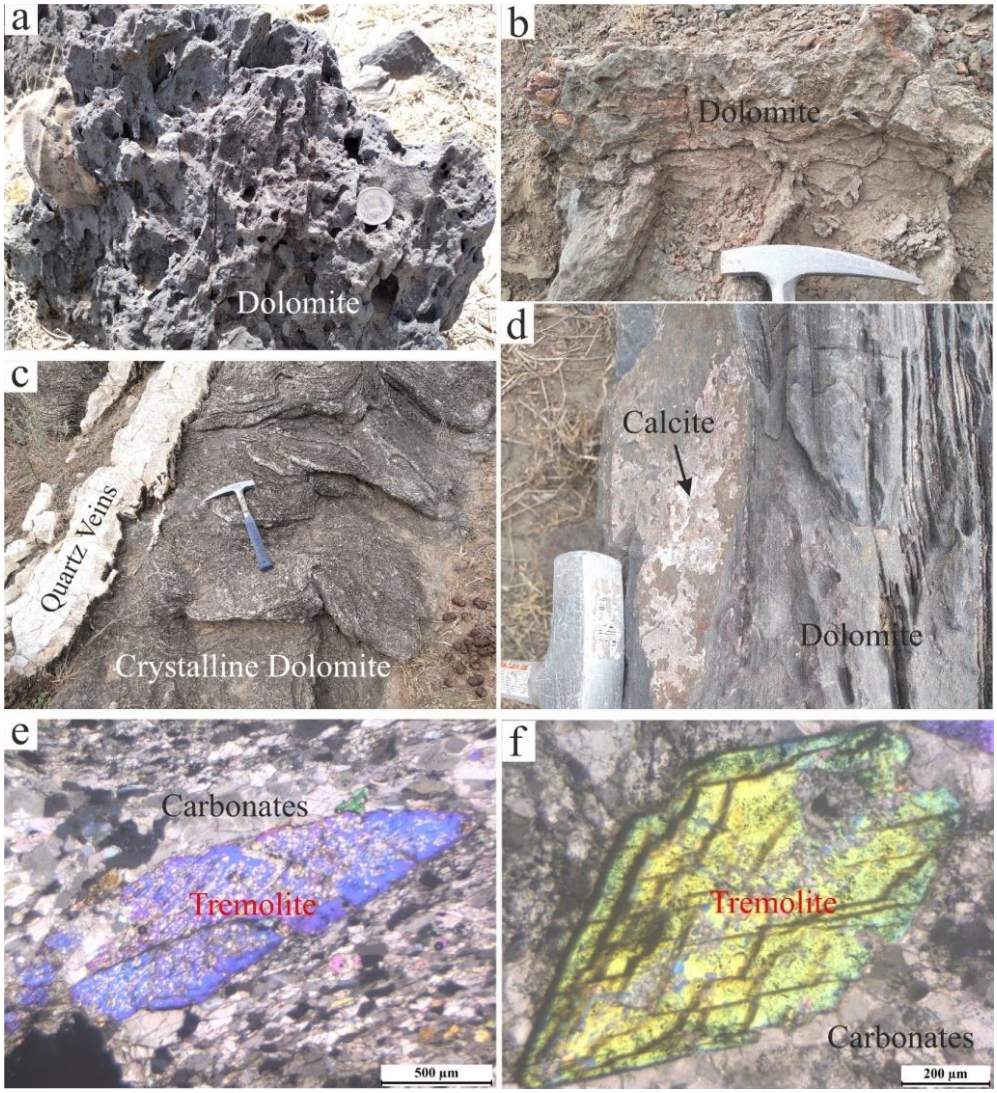

Fig.3. Field photographs of exposed dolomiteoutcrops near Amra Ka Bas area: (a) dissolution cavities and perforated surface of dolomite, (b) ferruginous intercalations with dolomite, (c) quartz veins in crystalline dolomite with elephant skin texture, and (d) bedded dolomite outcrop with calcite encrusts. Microphotographs of crystalline dolomite: (e) tremolite crystal in carbonate matrix and (f) euhedral tremolite grain with two sets of cleave planes in dolomite.

Analytical Methods

X-ray Fluorescence Spectrometer (XRF)

Representative rock samples, two kg each from dolomites were air-dried and fragmented to about 1 cm size and divided into 8 parts by coning and quartering. One part each (about 250 gm) was pulverized to -200 mesh size to a homogenous powder with the help of WC Planetary Mill. Care was taken at each stage of sample preparation such as crushing, coning-quartering, and pulverizing to avoid contamination. Six grams of each sample were powdered, thoroughly mixed with 0.6 gm of wax and poured into an aluminum cup. Homogenized samples were pressed at 40 tons using a hydraulic press to prepare pellets of 30 mm diameter and 5 mm thickness aluminum cup. These pellets were analyzed using a Bruker S8 Tiger wavelength dispersive X-ray fluorescence spectrometer (WD-XRF) having a 4 kW Rh anode X-ray target and operated at 30-50 KV and 50-100 mA. Several international rock, soil, and sediment standards (India, USGS, France, and China) were used for calibration (Singhal et al., 2019).

Inductively Coupled Plasma Mass Spectrometry (ICP-MS)

The homogenous powder rock samples were selected for the ICP-MS analysis in digested solution form, which essentially requires a very high quality, ultra-purified reagent, water and thoroughly cleaned crucibles and glassware. Millipore purified water (18 MΩ) was used in all investigations. PTFE Teflon beakers were used for open digestion of powdered rock samples where the teflon beakers and other glassware were cleaned with 1%HCl and millipore purified water. Analytical grade HF, analytical reagent (AR) grade $HClO_4$, distilled HNO_3 and HCl chemical reagents were used during the sample preparation. The sample preparation was done as follows: weight 0.05 g of -200 mesh size powdered rock sample with the help of electronic balance on butter paper, where the weighing is done up to four decimal points. For making the solution, 0.05 gm of each powdered rock sample was weighed, transferred weighed sample into ultra cleaned and thoroughly dried PTFE Teflon beakers and moistened with a few drops of ultra-pure water. 10 ml of an acid mixture of HF, HNO_3 and $HClO_4$ in the ratio of 7:3:1 were added to each sample in a Teflon beaker and swirled until the sample got completely moist. 1ml of 5 µg ml^{-1} of Rh solution was added to act as an internal standard in the beakers, it was covered with a lid and kept overnight for digestion. Next day, the beakers were heated on a hot plate at 200ºC after removing the lids in the fume hood chamber for about 1 hour, samples were allowed to evaporate until a crust or crystalline paste was obtained. The crust contents were dissolved in a beaker with 10 ml of 1:1 HNO_3 solution and kept on the hot plate for 10 minutes with moderate heat of ~70ºC. The sample was dissolved until all suspended particles came into the solution. The solution was made up to 250 ml volume with purified water in a cylindrical flask. The sample was kept in ultra-cleaned polythene sample bottles for analysis with proper labeling. All quantitative measurements were performed using instrument software Perkin Elmer SCIEX quantitative ELAN Version 3.4 software. Trace and rare earth element (REE) concentrations were analysed within accuracy ranges from 2 to 12% and precision varies between 3% to 8% by Inductively Coupled Plasma Mass spectrometry (ICP-MS, ELAN DRC-E, Perkin Elmer). ICP-MS instrumental parameters: RF power = 1100 W; Argon gas flow in (i) Nebuliser = 0.89 L/min, (ii) auxillary = 1.2 L/min, (iii) plasma 15 L/min; Lens voltage = 6V; sample uptake rate = 0.80 ml/min (Khanna et al., 2009). Acquisition parameters of ICP-MS: measuring mod – peak hopping; point per peak = 1; number of sweeps = 50; dwell time = 50 µs; integration time = 2500 ms; replicates = 3; internal standard = ^{103}Rh at an overall concentrations of 20 ng/ml. Japanese rock reference standards (JG-1a, JG-2) for granites were used to minimize the matrix effects. The acid-digested rock solutions were used in analyses where the sample introduction system in the instrument consists of a standard Meinhard nebulizer with a cyclonic spray chamber.

Geochemistry

The major and trace element composition of whole-rock samples are shown in tables 2 and 3. Sediment samples from the Amra Ka Bas were characterized by significant variations of the major component (Table 2). Major element geochemical composition of Amra Ka Bas samples plotted on the triangular diagram {$(Al, Fe)_2O_3.xH_2O$ – $(Ca,Mg)CO_3$ – SiO_2} of hydrated clays-carbonate-sand (Mason and Moore, 1982) are restricted to the dolomite field (Fig. 4a). At the same time, in the AKF {Al_2O_3 – (K_2O+Na_2O+CaO) – (Fe_2O_3+MgO)} ternary discrimination diagram (England and Jorgensen, 1973), these samples correspond to carbonaceous ferrite field (Fig. 4b).

Geochemistry of sediments normally reproduces the provenance of their source rocks (Roser and Korsch, 1986). The geochemical data of Amra Ka Bas sediments were compared with North American Shale Composite (NASC; data from Gromet et al., 1984) and Post Archean Australian Shale (PASS; data from Taylor and Mc Lennan, 1985). In the Al_2O_3 versus SiO_2 diagram (Barbera et al., 2006), they mainly resemble the trends of biogenic components whereas the detrital component is negligible (Fig. 5a). Binary discriminant diagram, MgO versus CaO (Siyi et al., 2019) displays mixed characteristics of the sedimentary and metasomatic line (Fig. 5b).

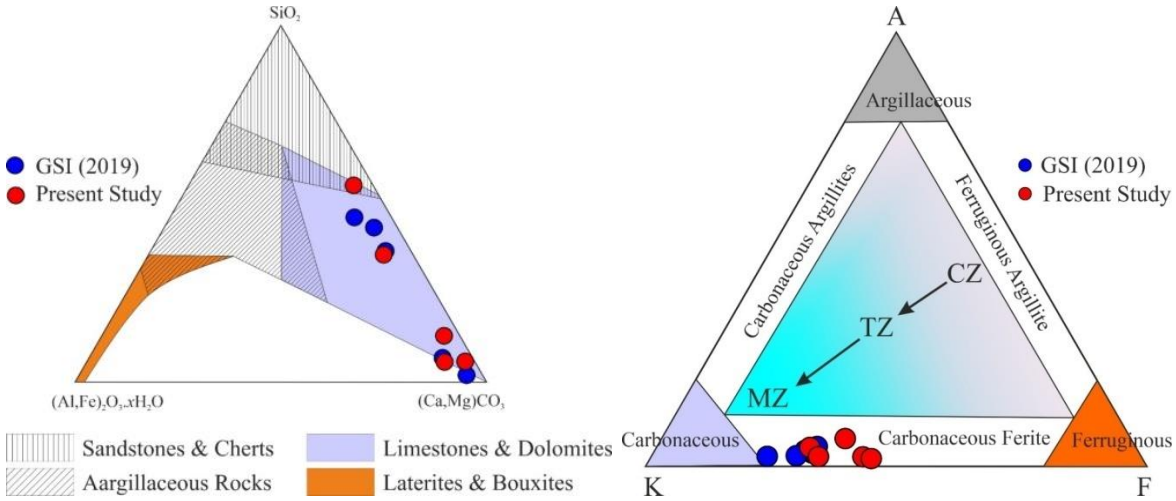

Fig.4. (a) Triangular diagram of hydrated clays [$(Al,Fe)_2O_3.xH_2O$] – carbonate [$(Ca,Mg)CO_3$] – Sand (SiO_2)displays the geochemical composition of sediments (afterMason and Moore, 1982), and (b) AKF Ternary discrimination diagram (after Englund and Jorgensen, 1973) of Al_2O_3 – (K_2O+Na_2O+CaO) – (Fe_2O_3+MgO) for representative samples of dolomites from Amra Ka Bas in Alwar basin.

Table 2. Bulk rock major oxides composition (wt%) of dolomite from Amra Ka Bas area in Alwar basin, Northwest India.

Rock Type	Crystalline Dolomite	Dolomite	Dolomite	Dolomite	Crystalline Dolomite
Sample No	59	64	AKB1	AKB24	31
SiO_2	27.67	42.27	3.15	3.06	7.16
Al_2O_3	1.59	1.83	0.56	0.54	0.31
TiO_2	0.1	0.1	0.045	0.042	0.042
Fe_2O_3	3.76	1.59	3.46	0.6	1.71
MnO	0.48	0.04	0.091	0.016	0.402
MgO	11.72	11.31	19.11	16.43	19.78
CaO	32.46	19.37	29.44	32.19	25.97
Na_2O	0.08	0.06	0.068	0.029	0.054
K_2O	0.25	0.61	0.14	0.54	0.34
P_2O_5	0.07	0.59	0.033	0.011	0.01
L.O.I.	21.78	20.51	42.76	42.38	47.07
Total	99.96	98.28	98.857	95.838	102.848
Ca/Mg	3.28	2.03	1.83	2.32	1.56
T(°C)	133	101	95	109	86

*Note: Temperature (T °C) of dolomite formation is estimated using the formulation of Rosenberg and Holland (1964).

For the recognition of the provenance sediments, it is important to depend on the least mobile geochemical elements during weathering, transport, diagenesis and metasomatism (Wronkiewicz and Condie, 1987). In the Fe_2O_3/Al_2O_3 vs $Al_2O_3/(Al_2O_3+Fe_2O_3)$ diagram (Murray, 1994; Girty et al., 1996), the Amra Ka Bas sediment samples plotted outside the area representing continental margin, pelagic, and ridge-proximals as well as old upper continental crust provenance subfields (Fig. 5c). All these depositional environments are independent of diagenetic modification intrinsic to dolomite chemistry (Murray, 1994). In the Fe_2O_3/TiO_2 vs $Al_2O_3/(Al_2O_3+Fe_2O_3+MnO)$ diagram (Bostrom, 1973), all sediment samples from Amra Ka Bas were plotted along the mixing curve of the two end-members of hydrothermal and argillite sources (Fig. 5d). On the whole, the mixed source for the dolomite precipitation around the Amra Ka Bas area is inferred from the geochemical investigations.

Table 3. Trace elements content (ppm) of dolomite from Amra Ka Bas area in Alwar basin, Northwest India.

Rock Type	Crystalline Dolomite	Dolomite	Dolomite	Dolomite	Crystalline Dolomite
Sample No	59	64	AKB1	AKB24	31
Ba	168.28	ND	30.04	61.04	15.07
Cr	ND	ND	ND	ND	ND
V	37.63	ND	5.7	17.91	19.3
Sc	2.15	0.8	1.53	1.47	2.58
Co	9.17	22.02	4.66	4.22	6.94
Ni	ND	ND	2.4	2.84	6.9
Cu	55.29	54.12	7.54	11.33	6.79
Zn	129.26	37.28	17.24	34.41	76.95
Ga	2.04	0.96	0.45	1.52	0.73
Pb	16.7	28.69	4.99	6.96	13.17
Th	1.38	1.62	0.8	0.98	0.69
Rb	3.58	11.8	3.12	10.43	9.58
U	1.53	1.6	1.47	0.66	1.01
Sr	33.52	33.57	53.12	55	53.41
Y	20.2	4.39	2.57	2.86	5.63
Zr	25.83	18.91	12.33	17.12	18
Nb	0.42	0.1	0.22	0.53	0.66

Rare Earth Elements Signature

Trace and rare earth element (REE) signatures of limestone and dolomites have been widely used to reconstruct the paleoenvironment of sedimentation (Frimmel, 2009; Franchi, 2018; Liu et al., 2019). It is also considred as reliable indicator of geochemical processes for the evolution of carbonate systems (Ozyurt et al., 2020). Redox-sensitive elements show diverse geochemical behaviour, which is mostly considered a natural proxy for revealing interaction processes between particles, solution, and redox reactions (Qing and Mountjoy, 1994; Li et al., 2019). These geochemical proxies are very supportive to rebuild early environmental settings (Sarangi et al., 2017; Mongelli et al., 2018). Geochemical analysis of REE in dolomite from the Amra Ka Bas area of Thanagazi Formation is presented in table 3.

The normalized pattern of the upper continental crust (UCC), spider diagram of dolomite samples from Amra Ka Bas shows Ba, U, P, and P enrichment, whereas, Th, Nb, and Ti show depletion trends (Fig. 6a). Enrichment of Ba is inversely related to the concentration of dissolved sulphate in the dolomitizing fluids (Di Bella et al., 2020). Inspite of this fact, it has been proposed that high salinity fluids yield high Sr content (1453 ppm; Lucia and Major, 1994; Hanor, 2004), whereas, mixing zone dolomites can be distinguished based on their low Sr content (Fouke and Reeder, 1992).

The normalized condition of the Post Archean Australian Shale (PAAS), dolomite samples from the Amra Ka Bas in Thanagazi Formation shows weakly depleted light rare earth elements (LREE) as compared to heavy rare earth elements (HREE) pattern (Fig. 6b). The abundance of Eu in the dolomite is related to the oxygen fugacity (fO_2), which means the reducing or oxidizing nature of the involved fluids (Di Bella et al., 2020). Geochemical stability of Eu^{3+} towards higher fO_2 and oxidation of Eu^{2+} under mildly acidic conditions improve to more oxidized environments (Bau, 1991; Kucera et al., 2009). Eu^{3+}/Eu^{2+} ratio is controlled by oxidation (Kamber and Webb, 2001; Zhang et al., 2014). According to Bau and Moller (1992), dolomite precipitation would involve Eu^{3+} ions, it would display a positive Eu anomaly due to the dispersion of the large Eu^{2+} ions from the dolomite crystal lattice.There is presence of a slightly positive anomaly of Eu displayed by some studied samples on the REE pattern (Fig. 6b) which suggests that environmental situations in which dolomite originated were to some extent oxidizing type.

Table 4. Rare earth elements content (ppm) of dolomite from Amra Ka Bas area in Alwar basin, Northwest India.

Rock Type	Crystalline Dolomite	Dolomite	Dolomite	Dolomite	Crystalline Dolomite
Sample No	59	64	AKB1	AKB24	31
La	5.396	3.635	3.328	2.327	2.442
Ce	10.847	7.018	6.208	4.358	5.32
Pr	1.971	0.973	0.711	0.54	0.722
Nd	6.412	3.701	3.579	2.816	4.642
Sm	2.178	0.864	0.494	0.359	0.895
Eu	0.484	0.234	0.087	0.202	0.335
Gd	2.875	0.867	0.459	0.332	0.796
Tb	0.51	0.125	0.07	0.049	0.135
Dy	3.17	0.684	0.456	0.353	0.886
Ho	0.642	0.131	0.106	0.089	0.214
Er	1.61	0.344	0.314	0.258	0.52
Tm	0.242	0.047	0.055	0.041	0.084
Yb	1.6	0.311	0.26	0.216	0.434
Lu	0.228	0.047	0.041	0.034	0.061

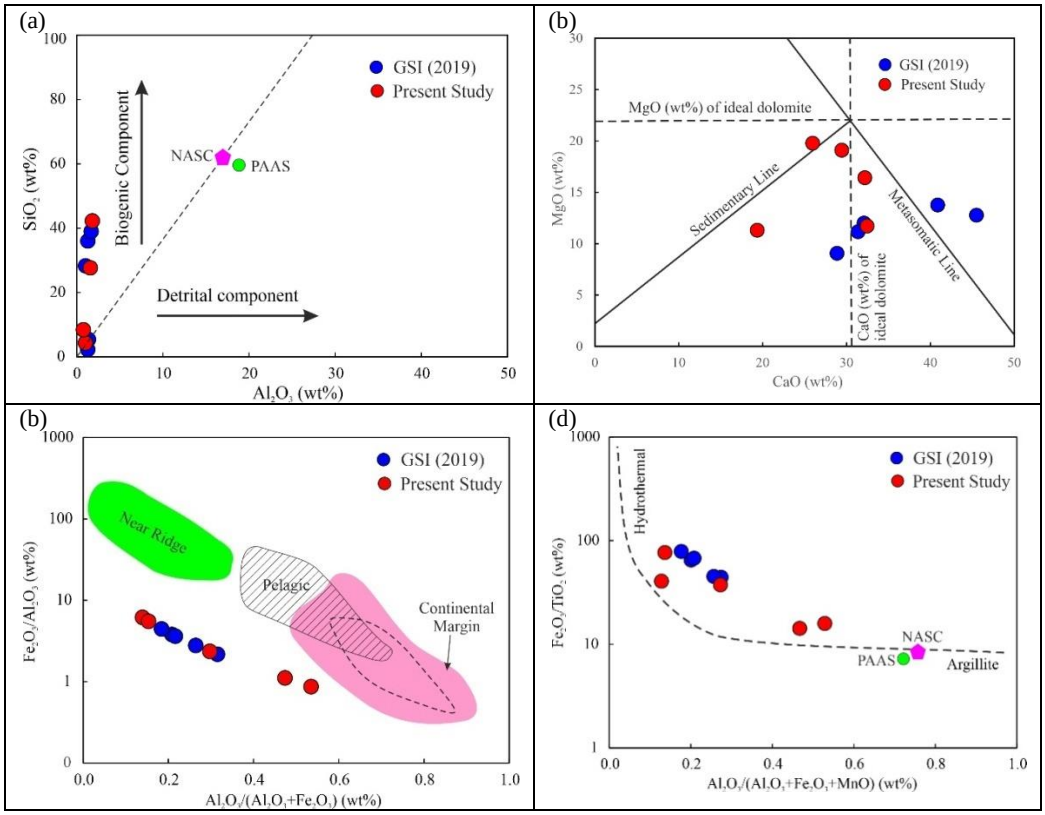

Fig.5. (a) Binary Al_2O_3 vs. SiO_2 diagram shows the presence of biogenic contribution in the present study, (b) Binary discrimination diagram MgO vs. CaO to distinguished dolomite forming processes (after Siyi et al., 2019), (c) Murray (1994) diagram displayed to discriminate depositional environment of sediments with old upper continental crust provenance subfield (dashed line-delimited area, after Girty et al., 1996), (d) Bostrom (1973) diagram shows end members mixing modelling curve of argillite and hydrothermal components with PAAS and NASC (data from Gromet et al., 1984; Taylor and McLennan, 1985), for representative samples of dolomites from Amra Ka Bas area in Alwar basin.

Base Metal Enrichment

The stability of dolomite in carbonate-rich hydrothermal solution indicates incongruent solubility towards low temperature whereas calcite field narrows towards higher temperature (Rosenberg and Holland, 1964). Dolomite precipitation in the sedimentary depositional environment is variable in composition within the temperature range between 25 to 200ºC (Arvidson and Mackenzie, 1999; Jiang et al., 2016; Banerjee, 2016). Experimental investigation demonstrated that the Ca/Mg ratio is directly proportional to the temperature of hydrothermal solutions up to 420ºC in the thermodynamic stability limit of calcite, dolomite and magnesite (Rosenberg et al., 1967). In the present study, the temperature of dolomite formation is calculated using the formulation of Rosenberg and Holland (1964). The calculated temperature of dolomite formation for the Amra Ka Bas samples ranges from 86-133ºC which is dependent on the Ca/Mg ratio (Table 2). Geochemical data reported by the Geological Survey of India (2019) has also been used to estimate the temperature of dolomite formation, which ranges from 130-152ºC.

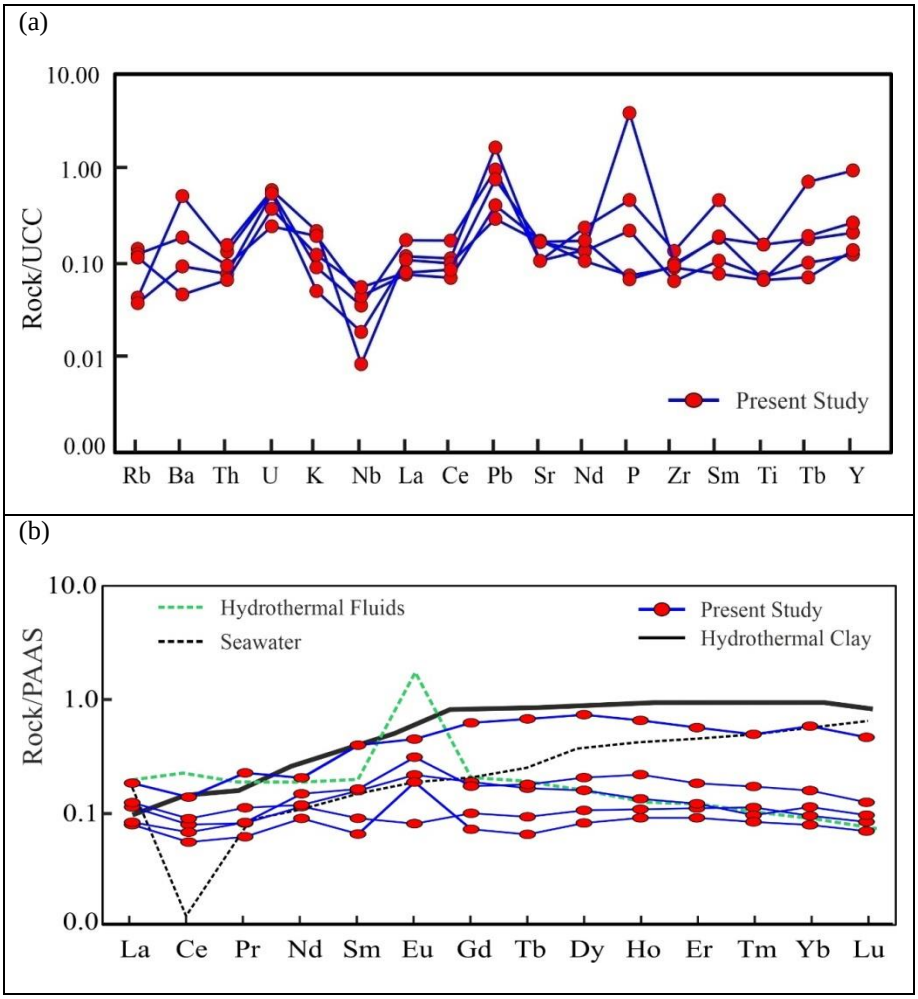

Fig.6. (a) Upper continental crust (UCC) normalized spider diagrams and (b) PAAS normalized REE patterns for representative samples of dolomites from Amra Ka Bas in Alwar basin. REE chemistry of seawater (Surya Prakash et al., 2012), hydrothermal fluids and clay (Severnmann et al., 2004), UCC(Rudnick and Gao (2003),and PAAS(Taylor and McLean, 1985) are taken from earlier studies.

Solubility of base metal in the hydrothermal fluid strongly depends on the temperature (Skinner, 1979; Pirajno, 1992; Zotov et al., 1994; Wood and Samson, 1998; Seward et al., 2014). Temperature versus copper concentration diagrams (Fig. 7a) indicate that hydrothermal fluids derived from different sources (black and white smokers) may have aplausible mechanism to enrich dolomite. Dissolved zinc concentration in hydrothermal fluids accelerates dolomite formation in shallow marine conditions (Vandeginste et al., 2019). Most of the marine hydrothermal vent fluids show high zinc concentration (<400 ppm) in the temperature range of 200 to 400ºC whereas zinc content in dolomite from Amra Ka Bas signifies a different scenario (Fig. 7b). Low temperature (100ºC) hydrothermal fluid associated with organic carbonate component related to the diagenetic processes in sedimentary basin

favour zinc enrichment in dolomite (Giordano, 2002).Thus, it could be inferred that there was a significant enrichment of zinc during the dolomite formation in the Amra Ka Bas possibly derived from a low-temperature hydrothermal fluid source during the diagenetic processes.

High-temperature hydrothermal vent fluids have been identified as the major source of base metal accumulation in the mid-ocean ridges, arc, and backarc spreading centers, mostly emitted from black and white smoker type plumes (Hannington et al., 2011; Edmond et al., 1995; Von Damm et al., 2003; Diehl and Bach, 2020). The chemical composition of seawater is quite different from the hydrothermal vent fluid that discharges from the ocean bottom at mid-ocean ridges and sea mounts (Corliss et al., 1979; Edmond et al., 1982). The composition of the dissolved material in the hydrothermal vent fluids is similar to the chemistry of hydrothermal particulate phases and appears to act as a significant source of dissolved base metals contents (German et al., 1991).

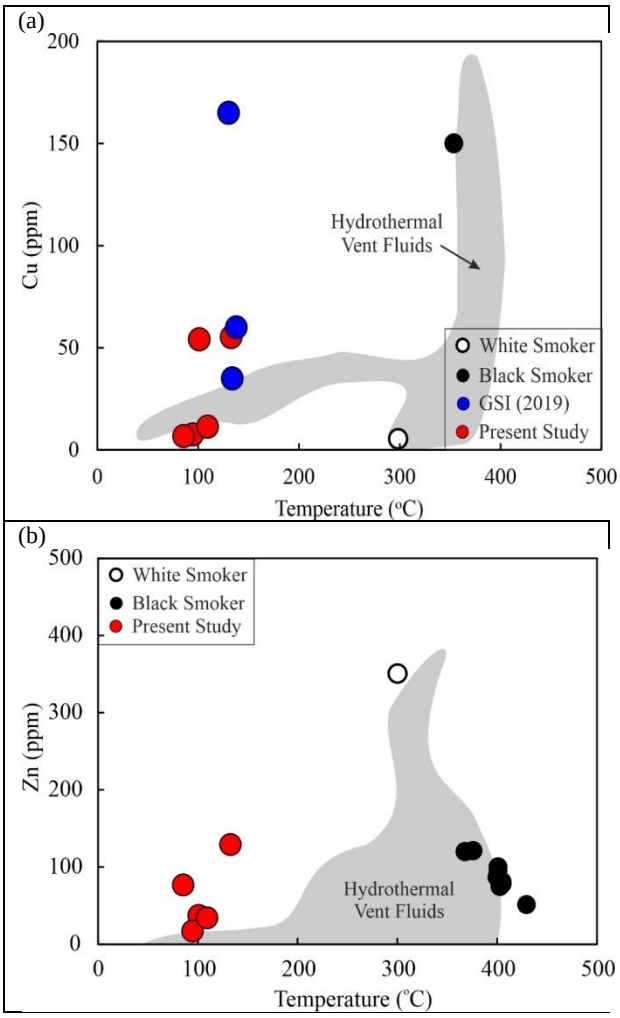

Fig.7. (a) Temperature versus copper solubility and (b) temperature versus zinc solubility in the hydrothermal system (after Rosenberg and Holland, 1964). Data for the composition of hydrothermal vent fluid (Diehl and Bach, 2020), black, and white smokers (Edmond et al., 1995; Von Damm et al., 2003) are taken from published literature.

A comparison of base metal concentrations (Cu and Zn) within the hydrothermal vent fluids and dolomite samples of the Amra Ka Bas area reveals their geochemical similarity, which may be derived from sources possibly of black smoker types (Fig 8a). In shallow subseafloor settings, thermal alteration of organic carbon and mudstones are considered to be the most significant factors for the enrichment of high concentrations of base metals (Pb, Zn) into the particulate phases of deposition (Magnall et al., 2016). The concentration of Pb in the dolomite samples is relatively low as compared to the chemistry of hydrothermal vent fluid (Fig. 8b) which indicates that the Pb scavenges were from other sources and contributed to the dolomitizing fluids in the area of investigation. Thus, it can be inferred that the mixing of hydrothermal fluids from two different sources possibly occurred during the dolomitization in the Amra Ka Bas area in the shallow subseafloor settings or marine conditions.

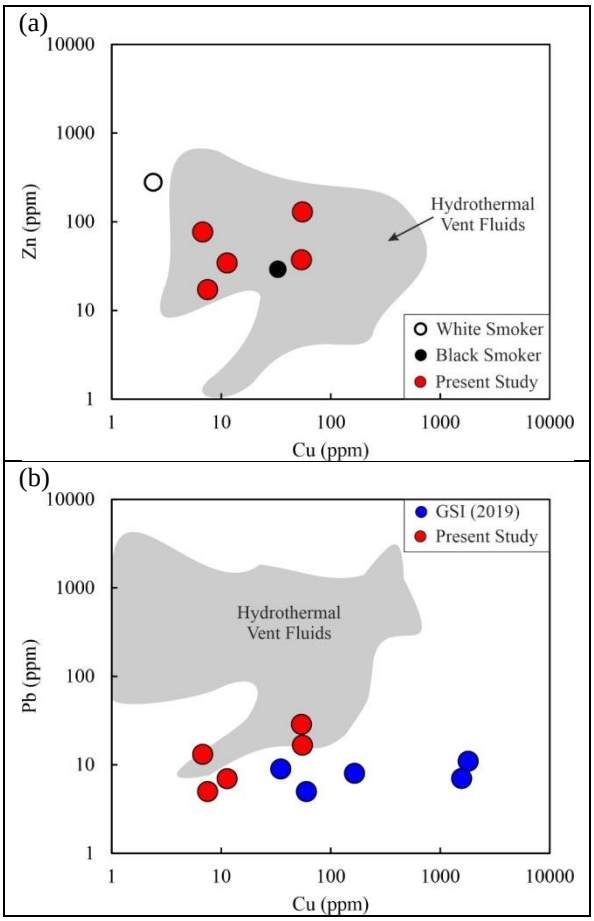

Fig.8.(a) Cu vs. Zn (ppm) and (b) Cu vs. Pb (ppm) content in the hydrothermal system. Data for the composition of hydrothermal vent fluid (Diehl and Bach, 2020), black, and white smokers (Edmond et al., 1995; Von Damm et al., 2003) are taken from published literature.

Discussions

Dolomite occurrences in the Amra Ka Bas area are supported by field observations of fine grained (amorphous) and coarse grained (crystalline)

dolomites. Generally, amorphous type dolomite is characterized by micritic-aphanitic textures, and laminated structures, and is a little porous (Fig 3a,b). Fine-grained dolomite precipitation may be connected to the synsedimentary hydrothermal fluid circulation in the sedimentary basin (Wen et al., 2007; Zhang et al., 2020). Crystalline dolomite (Fig. 3c) in the area shows coarse to very coarse grained clastic texture with shapes from sub-euhedral (xenotropic texture) to euhedral (idiotopic texture) with internal cavities along with pore-spaces (Gregg and Sibley, 1984). Interpretation of geochemical data of dolomite suggests a multistage evolution of dolomite in the area of investigation. The origin of crystalline dolomite can be attributed to the basin evolution, since dolomitization may take place at the diagenetic stages (Di Bella et al., 2020). Digenetic dolomitization coupled with the action of burial while the dolomitizing fluids transformed the slightly porous dolomites into nonporous mosaic dolomite (Montanez, 1997). The grain size of dolomite suggests the sedimentary environmental conditions in which the dolomitization occurs are evaporitic (Behrens and Land, 1972) or mixing water (Hanshaw et al., 1971) or marine type (Land, 1985). Evaporitic dolomite is associated with gypsum-anhydrite mineral and commonly occurs in a supra-tidal environment characterized by excessive evaporation under continental climatic conditions (Goldberg, 1967). Mixing water (seawater and freshwater) explains the formation of dolomite in the platform margin sections through the interaction of sea-level fluctuations, sedimentation, and subsidence (Badiozamani, 1973; Humphrey and Quinn, 1989). Marine solutions can be the only source of a large amount of Mg^{2+} ions needed for dolomitization of massive platform dolomite possibly formed directly from seawater (Varol and Magaritz, 1992). The formation temperature of the amorphous dolomite was higher than those of the crystalline dolomite in the Amra Ka Bas area of theThanagazi Formation.

Chemical and biochemical sedimentary rocks are dominated by components that have been transported as ions in solution and are very susceptible to changes in composition and mineralogy during the diagenesis (Bridge and Demicco, 2012). In the present study, the biogenic contribution is strongly influenced the dolomitization processes in the Amra Ka Bas area. Environmental conditions were probably responsible for the varying relative contribution of the material available in controlling the composition of the sediments (Lihou et al., 1996; Pandey et al., 2019).

Various factors contribute to explain the geochemical variations in the dolomite from the Amra Ka Bas area. Integrated approach of geochemistry (major, trace and rare earth elements) of dolomitic rocks gives support to reveal the source area composition. Weathering actions of sedimentary rocks may be appraised through investigation of the associations among alkali and alkaline earth elements (Nesbitt and Young, 1984). Chemical alteration largely involves calcium, sodium and potassium, which are preferentially mobilised, whereas aluminium remains immobile (Ding et al., 2016). The process of determining the provenance and origin of sedimentary rocks is very useful in understanding the past events of geological processes, which may describe the evolution of the sediment from source to the basin of deposition (Haughton et al., 1991). Dolomites of the Amra Ka Bas area are mainly plotted in the sedimentary provenance field. Investigations on sediment provenance concerning the origin, composition, transportation, and deposition are an important part of understanding the links between basinal sedimentation and tectonics (Smyth et al., 2014).

Experimental investigation demonstrated that dolomite formation is affected by the temperature of the mineralogical reaction as the Ca/Mg ratio of the solutions increases up to 420ºC (Rosenberg and Holland, 1964; Sibley et al., 1987). Dolomite formation can be facilitated by precipitation, diagenesis, hydrothermal processes and metamorphism under a variety of conditions in marine and lacustrine environments (Baker and Kastner, 1981). It may be produced from seawater, continental waters, mixing of basinal brines, mixing of hypersaline brine with seawater or mixing of seawater with meteoric water or hydrothermal vent fluids (Warren, 2000). Several studies have reported the precipitation of penecontemporaneous dolomite from normal seawater or pore water (Saller, 1984; Mitchell et al., 1987; Lumsden, 1988) in subtidal to deep-sea environmental settings. Dolomite formation during geothermal convections promotes calcium-rich and magnesium-poor fluids in the carbonate platforms in the temperature range of 25 to 200ºC (Pokrovsky and Schott, 2001; Wilson et al., 2001; Banerjee, 2016). In the present study, geothermometric estimates obtained for the composition of dolomites from Amra Ka Bas indicate low temperature (86-152ºC) stability conditions, which is suitable for thermochemical sulphate reduction and the precipitation of base metals. Hydrothermal fluids commonly precipitate base metal sulphides (chalcopyrite, sphalerite, galena, etc.) and associated carbonate minerals (calcite and dolomite) in the temperature range of 60 to 250ºC (Gregg, 2004). Copper and zinc content of the Amra Ka Bas dolomites is similar to that of high-temperature vent fluids. However, Pb content in the dolomite suggests its origin from a relatively low-temperature fluid. Therefore, it can be inferred that the mixing of hydrothermal fluids from two different sources possibly of variable composition and temperature were responsible for dolomitization in the Amra Ka Bas area of the Thanagazi Formation.

Conclusions

Integrated lithological, geochemical and geothermometric investigation of dolomites from the Amra Ka Bas area suggest the involvement of weathering, transport and diagenesis in ultimate rock composition and provide an understanding of the source rock composition. The abundance of major and trace elements is considered mainly related to the source rock composition, which was controled by a provenance of the shallow marine sedimentary environment. The source area for the studied dolomite is identifiable with the mixing of hydrothermal and argillite constituents and is dominated by biogenic processes during the digenesis. Digenetic processes control the formation of dolomite in the area of study with significant enrichment of base metal concentration during the precipitation in the temperature range of 86-152ºC. Base metal content and temperature of dolomite formation suggest two possible sources of low and high temperature sediments which contribute to the dolomitization processes in the Thanagazi Formation of the Mesoproterozoic Alwar Basin.

Acknowledgements

We thank to the Head, Department of Geology, Institute of Science, Banaras Hindu University and Additional Director General, Geological Survey of India, Western Region for providing all the necessary facilities. DP acknowledges financial support from BHU IoE SEED Grant No 21185 (Dev. Scheme No. 6031). Thanks are due to Dr. A. K. Singh for XRF and ICP-MS facilities at Wadia Institute of Himalayan Geology, Dehradun, India.

References

Alderman, A.R., and vonderBorch, C.C. (1963), A dolomite reaction series. Nature, v. 198, p. 466-467.

Arvidson, R.S., and Mackenzie, F.T. (1999), The dolomite problem: control of precipitation kinetics by temperature and saturation state. American Journal of Science, v. 299, p. 257-288.

Badiozamani, K. (1973), The Dorag dolomitization model – application to the middle Ordovician of Wisconsi. Journal of Sedimentary Petrology, v. 43, p. 965-984

Baithwaite, C.J.R. (1991), Dolomites, a review of origins, geometry and textures. Transactions of the Royal Society of Edinburgh: Earth Sciences, v. 82, p. 99 – 112.

Baker, P.A., and Kastner, M. (1981), Constraints on the formation of sedimentary dolomite. Science, v. 213, p. 214-216.

Banerjee, A. (2016), Estimation of dolomite formation: dolomite precipitation and dolomitization. Journal of Geological Society of India, v. 87, p. 561-572.

Banks, D.A., Boyce, A.J., and Samson, I.M. (2002), Constraints on the origins of fluids forming Irish Zn-Pb-Ba deposits: evidence from the composition of fluid inclusions. Economic Geology, v. 97, p. 471-480.

Barbera, G., Mazzoleni, P., Critelli, S., Pappalardo, A., Giudice, A.L., and Cirrincione, R. (2006), Provenance of shales and sedimentary history of the Monte Soro Unit, Sicily. Periodico di Mineralogia, v. 75, p. 313-330.

Bau, M. (1991), Rare-earth element mobility during hydrothermal and metamorphic fluid–rock interaction and the significance of the oxidation state of europium. Chemical Geology, v. 93, p. 219–230.

Bau, M., and Möller, P. (1992), Rare earth element fractionation in metamorphogenic hydrothermal calcite, magnesite and siderite. Mineralogy and Petrology, v. 45, p. 231–246.

Behrens, E.W., and Land, L.S. (1972), Subtidal Holocene dolomite, Baffin Bay, Texas. Journal of Sedimentary Petrology, v. 42, p. 155–161.

Boni, M., Parente, G., Bechstädt, T., De Vivo, B., and Iannace, A. (2000), Hydrothermal dolomites in SW Sardinia (Italy): evidence for a widespread late-Variscan fluid flow event. Sedimentary Geology, v. 131, p. 181–200. doi:10.1016/s0037-0738(99)00131-1.

Bostrom, K., (1973), The origin and fate of ferromanganoan active ridge sediments. Stockholm Contribution in Geology, v. 27, p. 149-243.

Bouton, A., Vennin, E., Amiotte-Suchet, P., Thomazo, C., Sizun, J.P., Virgone, A., Gaucher, E.C., and Visscher, P.T. (2020), Prediction of the calcium carbonate budget in a sedimentary basin: A "source-to-sink" approach applied to Great Salt Lake, Utah, USA. Basin Research, v. 32, p. 1005-1034. doi: 10.1111/bre.12412.

Bridge, J.S., and Demicco, R.V. (2012), Earth Surface Processes, Landforms and Sediment Deposits. Cambridge University Press, Cambridge, p. 1-883.

Charlou, J.J., Donval, J.P., Fouquet, Y., Jean-Baptiste, P., and Holm, N. (2002), Geochemistry of high H_2 and CH_4 vent fluids issuing from ultramafic rocks at the Rainbow hydrothermal field (36º14'N, MAR). Chemical Geology, v. 191, 345-359.

Chetty, D., and Frimmel, H.E., (2000), The role of evaporites in the genesis of base metal sulphide mineralisation in the Northern Platform of the Pan-African Damara Belt, Namibia: geochemical and fluid inclusion evidence from carbonate wall rock alteration. Mineralium Deposita, v. 35, p. 364-376.

Corliss, J.B., Dymond, J., Gordon, L.I., Edmond, J.M., von Herzen, R.P., Ballard, R.D., Green, K., Williams, D., Bainbridge, A., Crane, K., and van Andel, T.H. (1979), Submarine thermal springs on the Galapagos rift. Science, v. 203, p. 1073-1083.

Deb, M., Thorpe, R.I., Cumming, G., and Wegner, P.A. (1989), Age, source and stratigraphic implications of lead isotope data for conformable sediment-hosted base metal deposits in Proterozoic Aravalli–Delhi orogenic belt, NW India. Precambrian Research, v. 42, p. 1–22.

Di Bella, M., Italiano, F., Romano, D., Quartieri, S., Pino, P., Tripodo, A., and Sabatino, G. (2020), Massive dolomites in the Messinian evaporitic sequence (Sicily,

Italy): multi-analytical characterization and implication for the dolomitization processes. Carbonates and Evaporites, v. 35, 29. https://doi.org/10.1007/s13146-020-00559-8.

Diehl, A. and Bach, W. (2020), MARHYS (MARineHYdrothermal Solutions) Database: A global compilation of marine hydrothermal vent fluid, end member, and seawater compositions," Geochemistry, Geophysics, Geosystems, v. 21, e2020GC009385. https://doi.org/10.1029/2020GC009385

Ding, K., Seyfried Jr., W.E., Tivey, M.K., and Bradley, A. M. (2016), In situ measurement of dissolved H_2 and H_2S in high-temperature hydrothermal vent fluids at the Main Endeavour Field, Juan de Fuca Ridge. Earth and Planetary Science Letters, v. 186, p. 417-425.

Edmond, J.M., Campbell, A.C., Palmer, M.R., Klinkhammer, G.P., German, C.R., Edmonds, H.N., Elderfield, H., Thompson, G., and Rona, P. (1995), Time series studies of vent fluids from the TAG and MARK sites (1986, 1990) Mid-Atlantic Ridge: a new solution chemistry model and mechanism for Cu/Zn zonation in massive sulphide orebodies, Hydrothermal Vents and Processes. In: Parson, L.M., Walker, C.L., and Dixon, D.R. (ed.), Geological Society London Special Publication, v. 87, p. 77–86.

Edmond, J.M., Von Damm, K.L., McDuff, R.E., and Measures, C.I. (1982), Chemistry of hot springs on the East Pacific Rise and their effluent dispersal. Nature, v. 297, p. 197-191.

Eickmann, B., Bach, W., Rosner, M., and Peckmann, J. (2009), Geochemical constraints on the modes of carbonate precipitation in peridotites from the Logatchev Hydrothermal Vent Field and Gakkel Ridge. Chemical Geology, v. 268, p. 97-106.

Englund, J.O. and Jorgensen, P. (1973), A chemical classification system for argillaceous sediments and factors affecting their composition. GeologiskaFöreningeni Stockholm Förhandlingar, v. 95, p. 87-97.

Eriksson, K.A., and Warren, J.K. (1983), A paleohydrologic model for early Proterozoic dolomitization and silicification. Precambrian Research, v. 21, p. 299-321.

Fouke, B.W., and Reeder, R.J. (2018), Surface structural controls on dolomite composition: evidence from compositional sector zoning. Geochimica et Cosmochimica Acta, v. 56, p. 4015–4024.

Franchi, F. (2018), Petrographic and Geochemical Characterization of the Lower Transvaal Supergroup Stromatolitic Dolostones (Kanye Basin, Botswana). Precambrian Research, v. 310, p. 93-113.

Frimmel, H.E. (2009), Trace element distribution in Neoproterozoic carbonates as palaeoenvironmental indicator. Chemical Geology, v. 258, p. 338-353.

Geological Survey of India (2001) Geology and mineral resources of Rajasthan. Geological Survey of India, Miscellaneous Publication, v. 30(12), p. 1-113.

Geological Survey of India (2019), Copper-gold mineralization in Khera main block, Mundiyawas-Khera area, Alwar basin, Rajasthan: a prospective model for exploration. Bulletin Series A, v. 70, p. 1-160.

German, C.R., Campbell, A.C., and Edmond, J.M. (1991), Hydrothermal scavenging at the Mid-Atlantic Ridge: modification of the trace element dissolved fluxes. Earth and Planetary Science Letters, v. 107, p. 101-114.

Giordano, T.H. (2002), Transport of Pb and Zn by carboxylate complexes in basinal ore fluids and related petroleum-field brines at 100 ^oC: the influence of pH and oxygen fugacity. Geochemical Transactions, v. 3, p. 56-72.

Girty, G.H., Ridge, D.L., Knaack, C., Johnson, D., and Al-Riyami, R.K. (1996), Provenance and depositional setting of Paleozoic Chert and Argillite, Sierra Nevada, California. Journal of Sedimentary Research, v. 66, p. 107-118.

Goldberg, M. (1967), Supratidal dolomitization and dedolomitization in Jurassic rocks of HamakhteshHaqatan, Israel. Journal of Sedimentary Petrology, v. 37, p. 760-773.

Gregg, J.M. (2004), Basin fluid flow, base-metal sulphide mineralization and the development of dolomite petroleum reservoirs. Geological Society of London Special Publications, v. 235, p. 157-175.

Gregg, J.M., and Sibley, D.F. (1984), Epigenetic dolomitization and the origin of xenotopic dolomite texture. Journal of Sedimentary Petrology, v. 54, p. 908-931.

Gromet, L.P., Dymek, R.F., Haskin, L.A., and Korotev, R.L. (1984), The 'North American shale composite': its compilation, major and trace elements characteristics. Geochimica et Cosmochimica Acta, v. 48, p. 2469-2482.

Hannington, M., Jamieson, J., Monecke, T., Petersen, S., and Beaulieu, S. (2011), The abundance of seafloor massive sulfide deposits. Geology, v. 39, p. 1155-1158.

Hanor, J.S. (2004), A model for the origin of large carbonate- and evaporite-hosted celestine ($SrSO_4$) deposits. Journal of Sedimentary Research, v. 74, p. 168–175.

Hanshaw, B.B., Back, W., and Deike, R.G. (1971), A geochemical hypothesis for dolomitization by groundwater. Economic Geology, v. 66, p. 710–724.

Hardie, L.A. (1987), Dolomitization: a critical view of some current views. Journal of Sedimentary Petrology, v. 57, p. 166-183.

Haughton, P.D.W., Todd, S.P., and Morton, A.C., (1991), Development in sedimentary provenance studies. Geological Society London Special Publication, v. 57, p. 1-11.

Humphrey, J.D., and Quinn, T.M. (1989), Coastal mixing zone dolomite, forward modelling, and massive dolomitization of platform-margin carbonates. Journal of Sedimentary Petrology, v. 59, p. 438-454.

Jiang, L., Cai, C., Worden, R.H., Srowley, S.F., Jia, L., Zhang, K., and Duncan, I.J. (2016), Multiphase dolomitization of deeply buried Cambrian petroleum reservoirs, Tarim Basin, north-west China. Sedimentology, v. 63, p. 2130-2157.

Kamber, B.S., and Webb, G.E. (2001) The geochemistry of late Archaean microbial carbonate: Implications for ocean chemistry and continental erosion history. Geochimica et Cosmochimica Acta, v. 65, p. 2509–2525.

Kelley, D.S., Karson, J.A., Blackman, D.K., FruÈh-Green, G.L., Butterfield, D.A., Lilley, M.D., Olson, E.J., Schrenk, M.O., Roe, K.K., Lebon, G.T., and Rivizzigno, P. (2001), An off-axis hydrothermal vent field near the Mid-Atlantic Ridge at 30°N. Nature, v. 412, 145-149.

Kesler, S.E., and Reich, M.H. (2006), Precambrian Mississippi Valley-Type deposits; relation to changes in composition of the hydrosphere and atmosphere, In: Kesler S.E., and H. Ohmoto, H. (ed.), Evolution of early Earth's atmosphere, hydrosphere, and biosphere; constraints from ore deposits. Geological Society of America Memoirs, v. 198, p. 185–204.

Khan, I., Sahoo, P.R., and Rai, D.K. (2014), Proterozoic felsic volcanics in Alwar basin of North Delhi Fold Belt, Rajasthan: implication for copper mineralization. Current Science, v. 106, p. 27-28.

Khanna, P.P., Saini, N.K., Mukherjee, P.K., and Purohit, K.K. (2009), An appraisal of ICP-MS technique for determination of REEs: long term QC assessment of silicate rock analysis. Himalayan Geology, v. 30, p. 95-99.

Kucera, J., Cempirek, J., Dolnicek, Z., Muchez, P., and Prochaska, W. (2009) Rare earth elements and yttrium geochemistry of dolomite from post-Variscan vein-type mineralization of the NízkýJeseník and Upper Silesian Basins, Czech Republic. Journal of Geochemical Exploration, v. 103, p. 69–79.

Land, L.S. (1985), The origin of massive dolomite. Journal of Geoscience Education, v. 33, p. 112–125.

Leach, D.L., Taylor, R.D., Fey, D.L., Diehl, S.F., and R. W. Saltus, R.W. (2001), A deposit model for Mississippi Valley-Type lead-zinc ores. Scientific Investigations Report 2010-5070-A, U. S. Geological Survey, https://doi.org/10.3133/sir20105070A.

Lee, M.R., and Lindgren, P. (2015), 4.6-billion-year-old aragonite and its implications for understanding the geological record of Ca-carbonate. Carbonates and Evaporites, v. 30, p. 477–481.

Li, J., Redfern, S.A.T., and Giovannelli, D., (2019), Deep carbon cycle through five reactions. American Mineralogist, v. 104, p. 465–467.

Lihou, J.C., and Mange-Rajetzky, M.A. (1996), Provenance of the Sardona Flysch, eastern Swiss Alps: example of high-resolution heavy mineral analysis applied to an ultrastable assemblage. Sedimentary Geology, v. 105, p. 141-157.

Liu, J., Guo, H., Pourret, O., Wang, Z., Sun, Z., Zhang, W., and Liu, M. (2021), Distribution of rare earth elements in sediments of the North China Plain: A probe of sedimentation process. Applied Geochemistry, v. 134, 105089. https://doi.org/10.1016/j.apgeochem.2021.105089.

Liu, J., Song, J., Yuan, H., Li, X., Li, N., and Duan, L. (2019), Rare earth element and yttrium geochemistry in sinking particles and sediments of the Jiaozhou Bay, North China: potential proxy assessment for sediment resuspension. Marine Pollution Bulletin, v. 144, p. 79-91.

Lucia, F.J., and Major, R.P. (1994), Porosity Evolution through Hypersaline Reflux Dolomitization Ed. by B. Purser, M. Tucker, and D. Zenger (Dolomites). International Association of Sedimentologists Special Publication, v. 21, p. 345– 360.

Lumsden, D.N. (1988), Characteristics of deep-marine dolomite. Journal of Sedimentary Petrology, v. 58, p. 1023-1031.

Machel, H.G. (2004), Concepts and models of dolomitization: a critical reappraisal. In: Braithwaite, C.J.R., Rizzi, G., and Darke, G. (ed.), The Geometry and Petrogenesis of Dolomite Hydrocarbon Reservoirs. Geological Society of London Special Publication, v. 235, p. 7-63.

Magnall, J.M., Gleeson, S.A., Blamey, N.J.F., Paradis, S., and Luo, Y. (2016), The thermal and chemical evolution of hydrothermal vent fluids in shale hosted massive sulphide (SHMS) systems from the MacMillan Pass district (Yukon, Canada). Geochimica et Cosmochimica Acta, v. 193, p. 251-273.

Mason, B. and Moore, C.B. (1982), Principles of Geochemistry. John Wiley & Sons, Canada, p. 1-340.

McLennan, S.M., Hemming, S., McDaniel, D.K., and Hanson, G.H. (1993), Geochemical approaches to sedimentation provenance and tectonics. In: Johnsson M.J., and Basu, A. (ed.), Processes Controlling the Composition of Clastic Sediments. Special Paper of the Geological Society of America, v. 284, p. 21-40.

Megaw, P.K.M., Ruiz, J., and Titley, S.R. (1988), High-temperature, carbonate-hosted Ag-Pb-Zn(Cu) deposits of northern Mexico. Economic Geology, v. 83, p. 1856–1885.

Mitchell, J.T., Land, L.S., and Miser, D.E. (1987), Modern marine dolomite cement in a north Jamaican fringing reef. Geology, v. 15, p. 557-560.

Mongelli, G., Sinisi, R., and Paternoster, M., and Perri, F. (2018), REEs and U distribution in P-rich nodules from Gelasian Apulian Tethyan carbonate: A genetic record. Journal of Geochemical Exploration, v. 194, p. 19-28.

Montañez, I.P. (1997) Secondary porosity and late diagenetic cements of the upper Knox group, Central Tennessee region: a temporal and spatial history of fluid flow conduit development within the Knox regional aquifer. In: Montañez, I.P., Gregg, J.M., and Shelton, L.K. (ed.), Basin-Wide Diagenetic Patterns, v. 57, 101–117.

Murray, R.W. (1994), Chemical criteria to identify depositional environments of chert: general principles and applications. Sedimentary Geology, v. 90, p. 213-232.

Nesbitt, H.W., and Young, G.M. (1982), Early Proterozoic climate and plate motions inferred from major element chemistry of lutites. Nature, v. 299, p. 715-717.

Nesbitt, H.W., and Young, G.M. (1984), Formation and diagenesis of weathering profiles. Journal of Geology, v. 97, p. 129-147.

Ozyurt, M., Kirmaci, M.Z., Al-Aasm, I., Hollis, C., Tasli K., and R. Kandemir, R. (2020), REE Characteristics of Lower Cretaceous Limestone Succession in Gumushane, NE Turkey: Implications for ocean paleoredox conditions and diagenetic alteration. Minerals, v. 10, 683. doi:10.3390/min10080683.

Pandey, S., Parcha, S.K., and Srivastava, P.K. (2019), Petrography and geochemistry of the Neoproterozoic sedimentary rocks from the Batal Formation of Spiti Basin: implication on provenance. Arabian Journal of Geosciences, v. 12, 61. doi.org/10.1007/s12517-018-4189-8.

Pirajno, F. (1992), Hydrothermal Mineral Deposits. Springer-Verlag Berlin Heidelberg, p. 1-709.

Pirajno, F., and Joubert, B.D. (1993), An overview of carbonate-hosted mineral deposits in the Otavi Mountain Land, Namibia: implications for ore genesis. Journal of African Earth Sciences, v. 16, p. 265–272.

Pokrovsky, O.S., and Schott, J. (2001), Kinetics and Mechanism of Dolomite Dissolution in Neutral to Alkaline Solutions Revisited. American Journal of Science, v. 301, p. 597-626.

Qing, H., and Mountjoy, E.W. (1994), Rare earth element geochemistry of dolomites in the Middle Devonian Presqu'ile barrier, Western Canada Sedimentary Basin: implications for fluid-rock ratios during dolomitization. Sedimentology, v. 41, p. 787-804.

Reed, C.P., and Wallace, M.W. (2004), Zn-Pb mineralisation in the Silvermines district, Ireland: a product of burial diagenesis. Mineralium Deposita, v. 39, p. 87-102.

Roberts, J.A., Kenward, P.A., Fowle, D.A., Goldstein, R.H., Gonzalez, L.A., and Moore, D.S. (2013), Surface chemistry allows for abiotic precipitation of dolomite at low temperature. Proceedings of the National Academy of Sciences, 110(36), p. 14540-14545.

Rosenberg, P.E., and Holland, H.D. (1964), Calcite-dolomite-magnesite stability relations in solutions at elevated temperatures. Science, v. 145, p. 700-701.

Rosenberg, P.E., Burt, D.M., and Holland, H.D. (1967), Calcite-dolomite-magnesite stability relations in solutions: the effect of ionic strength. Geochimica et Cosmochimica Acta, v. 31, p. 391-396.

Roser, B.P., and Korsh, R.J. (1986), Determination of tectonic setting of sandstone-mudstone suites using SiO_2 content and K_2O/Na_2O ratio. Journal of Geology, v. 94, p. 635-650.

Roser, B.P., and Korsh, R.J. (1988), Provenance signatures of sandstone-mudstone suites determined using discriminant function analysis of major element data. Chemical Geology, v. 67, p. 119-139.

Rudnick, R.L., and Gao, S. (2003), The Composition of the Continental Crust. In: Holland, H.D. and Turekian, K.K. (ed.), Treatise on Geochemistry, Vol. 3, The Crust, Elsevier-Pergamon, Oxford, 1-64. http://dx.doi.org/10.1016/b0-08-043751-6/03016-4.

Sachan, H.K. (1993), Early-replacement dolomitization and deep-burial modification and stabilization: a case study from the Late Precambrian of the Zawar area, Rajasthan (India). Carbonates and Evaporites, v. 8, p. 191-198.

Sahoo, J., Sahoo, P.R., Khan, I., and A. S. Venkatesh, A.S. (2022), Insights into the Metallogenesis of the Felsic Volcanic Hosted Mundiyawas-Khera Cu Deposit, Alwar Basin, Western India. Minerals, v. 12(3), 370. https://doi.org/10.3390/min12030370.

Sajeev, R., Choudhary, S., Konwar, P., Kulshrestha, S.K., and Pandit, D. (2019), Identification of hydrothermal alteration zones for base metal exploration adjoining to Mundiyawas-Khera copper prospect, Rajasthan, India using ASTER data. Indian Journal of Geosciences, v. 73, p. 331-342.

Saller, A.H. (1984), Petrologie and geochemical constraints on the origin of subsurface dolomite, Enewetak Atoll: an example of dolomitization by normal seawater. Geology, v. 12, p. 217-220.

Sarangi, S., Mohanty, S.P., and Barik, A. (2017), Rare earth element characteristics of Paleoproterozoic cap carbonates pertaining to the Sausar Group, Central India: Implications for ocean paleoredox conditions. Journal of Asian Earth Sciences, v. 148, p. 31-50.

Severmann, S., Mills, R.A., Palmer, M.R., and Fallick, A.E. (2004), The origin of clay minerals in active and relict hydrothermal deposits. Geochimica et Cosmochimica Acta, v. 68, p. 73–88.

Seward, T.M., Williams-Jones, A.E., and Migdisov, A.A. (2014), The chemistry of metal transport and deposition by ore-forming hydrothermal fluids. In: Turekian, K., and Holland, H.D. (ed.), Treatise on Geochemistry, Elsevier Science, http://dx.doi.org/10.1016/B978-0-08-095975-7.01102-5.

Sibley, D.F., Dedoes, R.E., and Bartlett, T.R. (1987), Kinetics of dolomitization. Geology, v. 15, p. 1112-1114.

Singh, S.P. (1984), Fluvial sedimentation of the Proterozoic Alwar Group in the Lalgarh graben, northwestern India. Sedimentary Geology, v. 39, p. 95-119.

Singhal, S., Mukherjee, P.K., Saini, N.K., Dutt, S., and Kumar, R. (2019), Effect of carbon on major element analysis of carbonaceous silicate rocks by WD-XRF: An evaluation of error and its correction. Geochemistry: Exploration, Environment, Analysis, v. 19, p. 31-38. https://doi.org/10.1144/geochem2017-077.

Siyi, F., Chenggong, Z., Hondge, C., Anqing, C., Junxing, Z., Zhongtang, S., Shuai, Y., Guo, W., and Wentian, M. (2019), Characteristics, formation and evolution of pre-salt dolomite reservoirs in the fifth member of the Ordovician Majiagou Formation, mid-east Ordos Basin, NW China. Petroleum Exploration and Development, v. 46, p. 1153-1164.

Skinner, B.J. (1979), The many origins of hydrothermal mineral deposits. Ed. by H. L. Barnes Geochemistry of hydrothermal ore deposits, John Wiley & Sons, New York, pp 3–21.

Smyth, H.R., Morton, A., Richardson, N., and Scott, R.A. (2014), Sediment provenance studies in hydrocarbon exploration and production: an introduction. Geological

Society, London, Special Publications, v. 386, 1–6. http://dx.doi.org/10.1144/SP386.21.

Srivastava, V., and Prakash, D. (2020), Preliminary geological investigation for poly-metallic deposits in Khera North Block (Thanaghazi), Alwar district, Rajasthan. Journal of Scientific Research, v. 64, p. 58-65. doi: 10.37398/JSR.2020.640207.

Surya Prakash, L., Ray, D., Paropkari, A.L., Mudholkar, A.V., Satyanarayanan, M., Sreenivas, B., Chandrasekharam, Kota, D., Kamesh Raju, K.A., Kaisary, S., Balavam, V., and Gurav, T. (2012), Distribution of REEs and yttrium among major geochemical phases of marineFe–Mn-oxides: Comparative study between hydrogenous and hydrothermal deposits. Chemical Geology,v. 312-313, p. 127–137.

Taylor, S.R., and McLennan, S.M. (1985), The continental Crust: its Composition and Evolution. Blackwell Scientific Publications, Oxford, p. 1-312.

Tucker, M.E. (1982), Precambrian dolomites: petrographic and isotopic evidence that they differ from Phanerozoic dolomites. Geology, v. 10, p. 7-12.

Turchyn, A.V., Bradbury, H.J., Walker, K., and Sun, X. (2021), Controls on the Precipitation of Carbonate Minerals Within Marine Sediments. Frontiers in Earth Science, 9, 618311. doi: 10.3389/feart.2021.618311.

Vandeginste, V., Snell, O., Hall, M.R., Steer, E., and Vandeginste, A. (2019), Acceleration of dolomitization by zinc in saline waters. Nature Communications, v. 10, 1851. https://doi.org/10.1038/s41467-019-09870-y

Varol, B., and Magaritz, M. (1992), Dolomitization, time boundaries and unconformities: examples from the dolostone of the Taurus Mesozoic sequence, south-central Turkey. Sedimentary Geology, v. 76, p. 117–133.

Von Damma, K.L., Lilley, M.D., Shanks III, W.C., Brockington, M., Bray, A.M., O'Grady, K.M., Olson, E., Graham, A., Proskurowski, G. (2003), the SouEPR Science Party (2003), Extraordinary phase separation and segregation in vent fluids from the southern East Pacific Rise. Earth and Planetary Science Letters, v. 206, p. 365-378.

Warren, J. (2000), Dolomite: occurrence, evolution and economically important associations. Earth Science Reviews, v. 52, p. 1–81.

Wen, H., Zheng, R., Geng, W., Fan, M., and Wang, M. (2007), Characteristics of rare earth elements of lacustrine exhalative rock in the Xiagou formation of lower Cretaceous in Qingxi sag. Jiuxi basin. Frontiers of Earth Science in China, v. 1(3), p. 333-340. doi 10.1007/s11707-007-0040-3.

Wheatley, C.J.R., Friggens, P.J. and Dooge, F. (1986), The Bushy Park carbonate-hosted zinc-lead deposit Griqualand West. In: Anhaeusser, C.R., and Maske, S. (ed.), Mineral Deposits of Southern Africa, Geological Society of South Africa, Johannesburg, p. 891-900.

Wilson, A.M., Sanford, W., Whitaker, F., and Smart, P.

(2001), Spatial patterns of diagenesis during geothermal circulation in carbonate platforms. American Journal of Science, v. 301, p. 727-752.

Wood, S.A., and Samson, I.M. (1998), Solubility of ore minerals and complexation of ore metals in hydrothermal solutions. Eb. by J. P. Richards and P. B. Larson, Techniques in Hydrothermal Ore Deposits Geology, Reviews in Economic Geology, v. 10, p. 33-80.

Wronkiewicz, D.J., and Condie, K.C. (1987), Geochemistry of Archean shales from the Witwatersrand Supergroup, South Africa: Source-area weathering and provenance. Geochimica et Cosmochimica Acta, v. 51, p. 2401-2416.

Zhang, W., Guan, P., Jian, X., Feng, F., and Zou, C. (2014), In situ geochemistry of Lower Paleozoic dolomites in the northwesternTarim basin: Implications for the nature, origin, and evolution of diagenetic fluids. Geochemistry, Geophysics, Geosystems, v. 15, p. 2744–2764, doi:10.1002/2013GC005194.

Zhang., S., Liu, Y.-Q., Li, H., Jiao, X., and Zhou, D.-W. (2020), Hydrothermal-sedimentary dolomite – a case from the Middle Permian in eastern Junggar Basin, China. Journal of Palaeogeography, v. 9, 24. https://doi.org/10.1186/s42501-020-00070-0.

Zotov, A.V., Kudrin, A.V., Levin, K.A., Shikina, N.D., and Var'yash, L.N. (1994), Experimental studies of the solubility and complexing of selected ore elements (Au, Ag, Cu, Mo, As, Sb, Hg) in aqueous solutions. In: Shmulovich, K.I., Yardley, B.W.D., and Gonchar, G.G. (ed.), Fluids in the Crust, Chapman & Hall and Springer, Dordrecht, p. 95-137. https://doi.org/10.1007/978-94-011-1226-0_5.

JOURNAL INDIAN ASSOCIATION OF SEDIMENTOLOGISTS ISSN NO 2582 – 2020
Vol. 39, Issue 2, 2022, pp. 47-57
DOI: https://doi.org/10.51710/jias.v39iII.193

Thin-section Petrography and Heavy Mineral Study of sandstones of the Barail Group of rocks occuring around Sonapur area of Jaintia Hills, Meghalaya, India

Rupjyoti Hazarika*, Ranjan Kumar Sarmah, Jogendra Nath Sarma
Department of Applied Geology, Dibrugarh University, Dibrugarh, Assam- 786004
*Email ID of the corresponding author: hazarika.rupjyoti11@gmail.com

Abstract

The study area represents a part of the South Shillong Shelf, Meghalaya, where sandstones belonging to the Barail Group (Eocene-Oligocene) are well exposed. Thin section petrography and heavy mineral investigations have been undertaken to assess the geological significance of the sandstones. Framework grains of the Barail sediments comprise of quartz (56.98 to 71.91%), feldspar (1.87 to 7.35%), mica (1.07 to 9.72%), lithic fragments (2.20 to 8.41%) and matrix (9.20 to 20.43%). The detrital composition of the sandstones comprises primarily of quartz grains, angular to sub-rounded, fine to medium grained and moderately sorted in nature. The sandstones are classified as subarkose, feldspathic graywacke and lithic graywacke. Provenance discrimination triangular plots of QFL and Q_mFL_t reflect that the detritus were mostly derived from cratonic interior sources. The Diamond diagram indicates that the Barail sandstones were derived from middle and upper rank metamorphic source.

Heavy mineral study of these sandstones indicates the presence of zircon, tourmaline, rutile, sillimanite, kyanite, staurolite, garnet, epidote, sphene, hypersthene, hornblende, chlorite, chloritoid, andalusite, apatite and opaque minerals. The percentages of most stable heavy minerals zircon, tourmaline and rutile vary from 6.11to 21.61, 2.60 to 6.56 and 2.42 to 7.57 respectively. The ZTR maturity index varies from 15.15 to 34.37, which reflects that the sandstones are mineralogically immature. The petrographic and heavy mineral study of the sandstones suggest that the detritus was probably derived from Shillong Massif where Precambrian metamorphic rocks of pelitic and arenaceous composition with plutonic bodies were exposed around the shelf margin. As the Shillong Massif comprises of Precambrian metamorphic rocks of pelitic and semitic (arenaceous) composition with intrusive plutonic bodies.

Key words: feldspathic, heavy mineral assemblage and provenance, Oligocene Barail Group

Introduction

The present study area is an integral part of the South Shillong Basin which developed on the southern fringe of the Meghalaya Plateau. This basin evolved due to the subduction- collision tectonics between the Indian plate and Burmese (Myanmar) plate (Curray et al., 1979). The Tertiary sediments of the basin deposited over the Upper Cretaceous Mahadek Formation in the Precambrian rocks of Basement Complex in Meghalaya Plateau. Southern boundary of the basin is delineated by the Dauki fault (Johnson and Nur Alam, 1991; Dasgupta & Biswas, 2000). The sedimentation continued uninterruptedly during the Tertiary period in this peripheral foreland basin (Raju A.T.R., 1968; Ranga Rao, 1983; Dasgupta & Biswas, 2000 and Nandy, 2001). These sediments tend further to the east and NE in the contigurous parts of Karbi Anglong and North Cachar Hills of Assam and underneath of the Brahmaputra valley. Present study is confined fully to the Oligocene Barail Group of rocks which are well exposed in Lumshnong -Sonapur area along Jowai-Badarpur Road section, Jaintia Hills, Meghalaya (Fig. 1).

Pioneer geological works of Medlicot (1869) and Evans (1932, 1959) established the Tertiary stratigraphic succession of Assam and Meghalaya. Dasgupta et al. (1964) mapped the area along Jowai-Badarpur Road with a summarised description of various formations exposed along it. Subsequently, many workers like Sah and Dutta (1968), Saxena and Tripathi (1982) carried out geological investigations emphasising on palynostratigraphy. Das et al. (2001) studied the stratigraphic and sedimentation of the early Tertiary sediments from Sonapur-Lumshnong area, Jaintia Hills, Meghalaya. It is evident from the previous works that a data gap exist in the understanding the sedimentation history and provenance of the Eocene-Oligocene Barail Group of rocks of the region. The present study is an attempt to unreveal the provenance and tectonic settings based on petrography and heavy mineral analysis of the sandstones of the Barail Group.

Geological setting

The Meghalaya Plateau is presumably considered as the northeastern prolongation of the Indian Peninsular Shield. The Shield areas of the Plateau constitute of Palaeo-Proterozoic tonalite gneisses, meta-gabbronorites and amphibolites (Nandy, 2001; Ghosh et al., 2005; Yin et al., 2010). These rocks form the basement of the younger sediments of the South Shillong Basin and adjoining parts of Upper Assam Basin underneath the Brahmaputra valley. The basement rocks are

overlain by the Meso-Proterozoic metasedimentary cover rocks of the Shillong Group with metavolcanic Khasi Greenstone and volcaniclastics. Both the Basement rocks and Shillong Group of rocks were intruded by Neo-Proterozoic and early palaeozoic granites (Mitra and Mitra, 2001). After long period of quiescence during Permian time, Peninsular Lower Gondwana sediments deposited in the western margin of the Meghalaya Plateau in Garo Hills in Singrimari (25044/: 89044/) (Nandy, 2001). During Jurassic-early Cretaceous time, effusion of plateau basalt (Sylhet trap) took place along the southern margin of the plateau and closely associated with the Dauki Fault System (Nandy, 2001). The Sylhet trap at Therriaghat (25011/00//:91045/20//) section are in contact with the gneisses, granites or rocks of the Shillong Group at E-W trending Raibah Fault. The southern block along the Raibah fault subsided and the northern block uplifted. Soon after the cessation of the basaltic effusion the sinking of the southern block became intense, resulting into a marine transgression. In this downsinking basin Upper Cretaceous sediments represented by Mahadek Formation was deposited. Thereafter the rate of subsidence slowed down forming a stable platform with warm sea condition. The carbonate rocks of the Jaintia Group (Plaeocene- Eocene) were deposit (Nandy, 2001). All throughout the South Shillong Basin, the subsidence of the different blocks is not uniform over the southern fringe of the Meghalaya Plateau. The Garo Hills in the west and the Jaintia Hills in the East remain landmass till mid-Eocene and later it witnessed progressive subsidence. As a consequence, coal bearing sandstone followed by carbonate rocks equivalent to the upper Sylhet Limestone of the Khasi Hills were accumulated in these sectors of the basin. During late Eocene time, predominantly argillaceous lithofacies of the Kopili Formation were deposited under fluctuating shallow marine condition in the southern, southwestern and eastern margin of the Meghalaya Plateau. At the Oligocene-Miocene boundary due to terminal collision of the Indian plate with the Burmese plate, the Indo-Burmese Ranges (IBR) raised considerably forming high hills and ridges to the south and south of the south Shillong Basin. This resulted in the shallowing of the remnant sea and regressive deltaic to shallow marine deposition took place in the southern margin of the Shillong Plateau and in Upper Assam Basin. This lithosequence of platform facies has been variously named as Chokpotgiri Formation in the southern Khasi Hills, Simsang or Kherapara Formation in Garo Hills and as Barails in the East Khasi, Jaintia, North Cachar and Mikir Hills (Karbi Anglong) (Nandy, 2001). Stratigraphically a dual classification is followed for the Barail Group of rocks (Oligocene). In upper Assam and adjoining fold-thrust belt the Barails are subdivided into Nagaon, Baragolai and Tikak Parbat formations and their equivalents to the south of Naga Hills and in the south Shilling Basin are termed as Laisong, Jenam and Renji formations (Chakraborty, 1972; Ranga Rao, 1983; Nandy, 2001; Najman et al., 2019; Yin et al., 2010).

During Miocene, sedimentation continued uninterruptedly over the southern and western part of the Garo Hills and southern margin of the Khasi Hills. But the Jaintia Hills remained positive areas at that period. The major upliftment of the Meghalaya Plateau was at the end of Miocene resulting into the formation of continental fluvio-lacustrine basins along the southern margin of the Plateau. The Pliocene Dupi Tila sediments were deposited in these basins. The recent older and newer alluvium along the southern fringe of the Meghalaya Plateau represents fluvial deposits along old river valleys. The Tertiary stratigraphic succession of the south-eastern part of the Jaintia Hills (after Rangarao, 1983; Singh and Singh, 2000) is given in the Table 1.

Materials and Method

The Oligocene Barail sediments were collected systematically along Lubha River section, a part of Jowai-Badarpur Road in Sonapur village, Meghalaya. For thin-section petrographic investigations, ten numbers of representative sandstone samples of the Barail Group were taken from a continuous outcrop of larger and thicker major unit of sandstones. Modal analysis for detrital grains was done following the Gazzi–Dickinson method of point counting (Ingersoll et al., 1984). A total number of 400 framework grains were counted in each thin-section. The mineralogical classification of the sandstones was done following Dott (1964), while, the nature of the source rock was

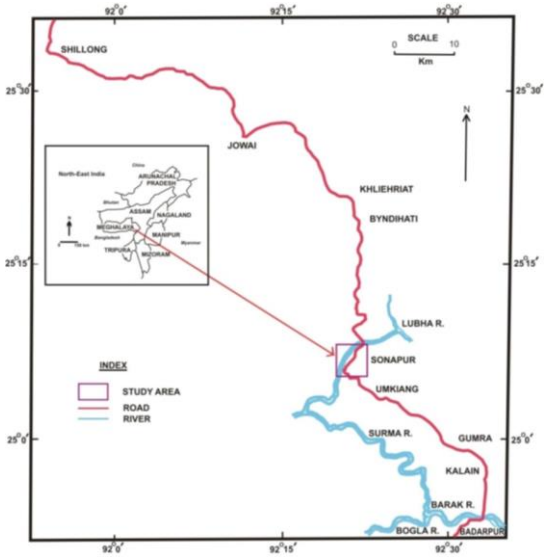

Fig. 1: Location map of the study area

determined following Basu et al. (1975). The tectonic set up of the source area was determined

from QmFLt and QFL triangular plots of Dickinson et al. (1983).

Table 1. Tertiary stratigraphic succession of the study area (after Rangarao, 1983; Singh and Singh, 2000).

Age	Group	Formation	Thickness (m)	Lithology
Pliocene to Pleistocene	Dupi Tila	Dupi Tila	1200	Massive to cross bedded sandstone at the lower part with increasing mud units toward the top.
Unconformity (?)				
Upper Miocene to Pliocene	Tipam	Girujan Clay Tipam Sandstone Sanstone	1900	Not exposed in this area Massive,thick-bedded sandstone
Lower Miocene	Surma	Boka Bil Bhuban	2500	Fine-grained, laminated sandstone and shale. Fine-grained, indurated sandstone alternating with shale.
Unconformity (?)				
Oligocene .	Barail	Renji Jenum Laisong	577 814 1658	Medium to fine-grained, hard massive sandstone. Argillaceous sandstone Medium to fine sandstone with subordinate shale and conglomerate
Eocene	Jaintia	Kopili Sylhet Limestone Therria	500 500 100	Alternating sandstone & black shale Bluish, massive to thinly bedded limestone. Coarse to medium grained sandstone with bands of sandy limestone. Gray to pinkish gray limestone, sandy limestone, and calcareous sandstone. One member, known as Lakadong Sandstone, is made up of medium– grained arkosic sandstone with carbonaceous shale and coal seams. Medium to coarse sandstone with thin bands of pyrite-rich siltstone

Heavy minerals rarely constitute more than 1% of the total volume of the sediments. They provide valuable information concerning provenance which describe the character of the source terrain. Heavy minerals were separated from the more abundant light minerals following the "Funnel Separation Method" of Milner (1962) with the help of heavy liquid Bromoform (specific gravity 2.89). The separated heavy minerals were mounted on a glass slide and examined under a petrological microscope.

Petrographic Study

Thin section studies of the sandstone samples and their modal analysis shows that the detrital constituents include different types of quartz followed by feldspar, mica, rock fragments, cement and matrix (Table 2). Among the various framework constituents, quartz is the most dominant constituent. The detrital grains are mostly fine to medium grained, angular to sub angular and moderately sorted in nature. The interlocking grain shows point, line and concavo-convex contact. Concavo-convex contact is most dominant. A brief description of the mineralogical constituents is as follows.

Quartz: Quartz is the most abundant detrital component of the sandstones. The grains are mostly angular to subrounded, fine to medium grained and moderately sorted in nature. Both monocrystalline and polycrystalline variety of quartz are present. In the monocrystalline type both undulose and non-undulose varieties are present. In case of polycrystalline quartz type both "2-3 crystal units per grain type" (Fig. 2a) and ">3 crystal units per

grain type" (Fig. 2b) are present. Different varieties of polycrystalline quartz are present like schistose metamorphic quartz, stretched metamorphic quartz and vein quartz. Among these the stretched metamorphic quartz is the dominant one. The total percentage of quartz in the sandstones varies from 56.98 to 71.92.

Feldspar: Feldspar is the second dominant mineral in the studied sandstones. Both K-feldspar and plagioclase feldspar are present in the sandstone of the Barail Group. Plagioclase grains are identified by its characteristic lamellar twinning. Orthoclase is identified by its characteristic carlsbad twinning whereas microcline is identified by its crosshatched twinning. Weathered feldspar grains (Fig. 2c) are also found in the sandstones. These grains are identified by its bending and displacement of twin lamellae within the broken grains, which may be due to the effect of deformation. The total percentage of feldspar in the sandstone varies from 1.87 to 7.35.

Mica: Both muscovite and biotite are present in the sandstone samples. They are also present in the argillaceous matrix as authigenic mica. Muscovite is dominant in comparison to biotite. Bending of mica (Fig. 2f) due to compaction has also been observed in the studied sandstone. The percentage of mica varies from 1.07 to 9.72 in the sandstone.

Lithic Fragments (Rock fragments): Rock fragments are very important in the study of provenance and tectonic setting of the source area as they are the disintegrated particles of source rocks. All the three types of rock fragments i.e. igneous, metamorphic and sedimentary (Fig. 2d) are present in studied samples. Metamorphic rock fragments show elongated and foliated minerals such as quartz and mica. Igneous rock fragments show intergrown crystal of quartz, feldspar and mica whereas sedimentary rock fragments show detrital texture and dull in appearance. The percentage of the rock fragments varies from 2.20 to 8.41.

Matrix: All the detrital grains which have 0.02 mm diameter or less in size are included in the group of matrix. Clayey matrix i.e. argillaceous matrix (Fig. 2d) is the most dominant one in the studied sandstones. The argillaceous matrix is identified by the presence of clay and recrystallized micas. The siliceous matrix is also present in the sandstones of the Barail Group. The percentage of matrix varies from 9.20 to 20.43 in the sandstone samples.

Cement: Siliceous, argillaceous and ferruginous cement are present in the intergranular spaces of the sandstone of the Barail Group under study. Argillaceous matrix when undergoes alteration to other clay and phyllosilicates minerals due to diagenetic processes can be treated as argillaceous

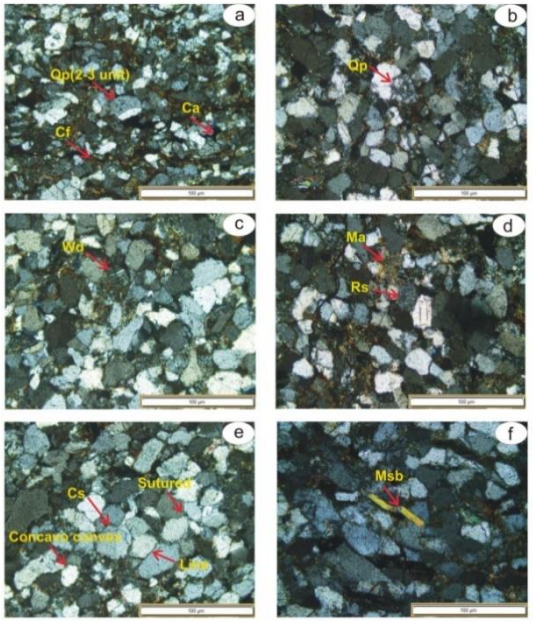

Fig. 2: Representative photomicrographs of the constituents of Barail sandstones of the study area showing (a) Qp(2-3 unit)- Polycrystalline quartz (2-3 unit), Ca- Argillaceous cement, Cf- Ferruginous cement (b) Qp- polycrystalline quartz (c) Wd- Weathered feldspar grain (d) Ma- Argillaceous matrix, Rs- Sedimentary rock fragment (e) Cs- Siliceous cement and diagenetic features like line, concavo-convex and sutured contact (d) Msb-bent muscovite flake.

cement (Fig. 2a). When grain margins of the quartz are cemented by secondary silica can be treated as siliceous cement (Fig. 2e) and ferruginous cement (Fig. 2a) are rich in iron oxide, deep brown to blackish in colour. The percentage of cement varies from 3.02 to 8.18 in the studied samples.

Sandstone Classification

The sandstones under study have been classified on the basis of Dott's (1964) scheme of classification. For this classification the percentage of Quartz (Q), Feldspar (F) and Rock fragments(R) (Table 2) of the studied sandstones are plotted on the QFR triangular plot (Fig.3). In this classification, two groups of sandstone are recognized i.e. arenite group having less than 15% matrix and wacke group having more than 15% matrix. The plot shows that the sandstones are mainly subarkose type. Few of them are classified as arkosic wacke and lithic graywacke. Subarkose sandstones are arenite sandstones having less than 25% feldspar. Arkosic wacke and lithic greywacke sandstones are wacke sandstones. Arkosic wacke sandstones have more feldspar than rock fragments as compared to lithic greywacke sandstones.

Provenance and Tectonic Setting

Sandstone petrography of the Barail sandstones has been used to constrained provenance

Table 2: Results of Modal Analysis of the sandstones of the Barail Group.

Sample No.	Qm		Qp		Qt	F	Lt	Mica	Chert	C	M
	Un	Non	2-3 unit	>3 unit							
S-1	27.66	24.67	1.87	12.15	66.35	1.87	8.41	1.87	1.87	3.74	15.89
S-2	6.86	31.86	6.86	19.60	65.18	7.35	4.9 0	1.23	2.48	5.39	13.47
S-3	10.06	28.17	11.07	15.09	64.32	5.03	4.02	3.42	5.03	3.02	15.09
S-4	10.75	26.88	6.45	12.90	56.98	3.23	7.52	1.07	3.23	7.53	20.43
S-5	15.34	42.94	3.07	10.22	71.57	4.50	4.08	4.11	1.02	5.52	9.20
S-6	6.12	50.00	2.04	8.16	66.32	6.12	3.07	2.04	3.06	4.08	15.31
S-7	8.64	30.24	9.72	12.96	61.56	3.24	3.23	9.72	2.16	6.05	14.04
S-8	11.32	23.58	11.33	18.86	65.09	5.66	3.77	8.49	0.94	2.83	13.21
S-9	14.85	24.75	7.92	17.82	65.34	3.96	3.97	4.94	0.00	6.93	14.86
S-10	11.06	50.88	2.23	7.74	71.91	4.42	2.20	1.11	2.22	8.18	9.95

Qm= Monocrystalline quartz; Un= Undulatory monocrystalline quartz; Non= Non-undulatory monocrystalline quartz; Qp= Polycrystalline quartz; Qt= Total quartz; F= Total feldspar; Lt= Total lithic fragments; C= Cement; M=Matrix.

and tectonic settings of study area. Information on the nature of the source of the sediments was derived through the use of the Diamond diagram of Basu et al. (1975). The plot indicates the sediments of the Barail Group of rocks to have been derived from iddle and upper rank metamorphic sources (Fig. 4). For determination of the tectonic setting of the area under study, the QFL and Q_mFL_t triangular plots of Dickinson et al. (1983), were considered. For these QFL and Q_mFL_t triangular plot the recalculated percentage values of total quartz, monocrystalline quartz, feldspar and lithic fragments are considered (Table 2 & 3). QFL triangular plot reflects that the Barail sediments were mostly derived from cratonic interior source and few samples showing recycled orogenic source (Fig. 5a). Q_mFL_t triangular plot also reflects that Barail sediments were mostly derived from cratonic interior source and few samples showing recycled orogenic source (Fig. 5b).

Heavy Mineral Study

Heavy minerals can be classified as opaques and non-opaques. The opaque iron minerals are most abundant in the studied sandstones of the Barail Group. The percentage of the opaque minerals vary from 45.46 to 72.73. The non-opaque minerals of the sandstones are zircon, tourmaline, rutile, sillimanite, kyanite, staurolite, garnet, epidote, sphene, hypersthenes, hornblende, chlorite, chloritoid, andalusite, and apatite (Table 4) (Fig.7). The characteristic salient features and percentage of heavy minerals are described below.

Zircon: Zircon is the most abundant heavy mineral present in the studied sandstones. Grains are colourless and occur as prismatic, euhedral slender and elongated in shape. Rounded grains (Fig. 6c) are also observed. Under cross nicols the grains show parallel extinction, strong birefringence, high refractive index and well defined zoning (Fig. 6a). Percentage of zircon in the sandstones of the Barail Group varies from 6.11 to 21.61.

Tourmaline: Tourmaline grains are pale brown to dark brown in colour. The grains display a variety of shapes such as irregular, prismatic, sub rounded and rounded (Fig. 6f). Tourmaline grains are strongly pleochroic and have no cleavage. They have strong birefringence and high-order interference colours. The percentage of tourmaline varies from 2.60 to 6.56.

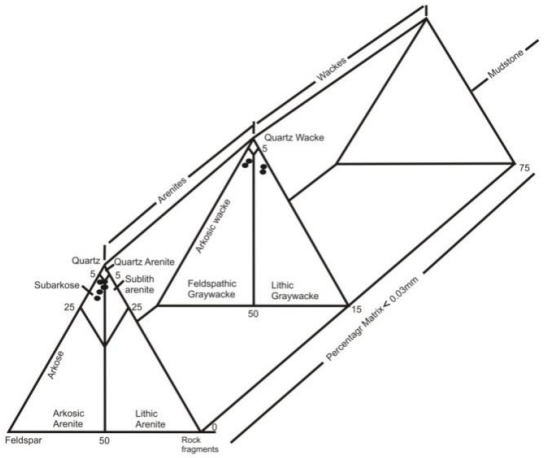

Fig. 3: Mineralogical Classification of the sandstones of Barail Group of the study area (after Dott, 1964).

Table 3: Recalculated percentage data for QFR triangular plot, Diamond diagram and QmFLt triangular plot.

Sample No.	QFR triangular plot			Data for Diamond diagram			Data for QmFLt triangular plot		
	Q	F	R(Lt)	Qp (>3 unit)	Qm (Un)	Qm (Non)	Qm	F	Lt
S-1	86.58	2.44	10.97	18.84	42.90	38.26	83.58	2.99	13.43
S-2	84.18	9.49	6.33	33.61	11.76	54.63	75.97	14.42	9.61
S-3	87.66	6.85	5.48	28.30	18.87	52.83	80.86	10.64	8.50
S-4	84.13	4.77	11.10	25.53	21.27	53.19	77.78	6.68	15.54
S-5	89.30	5.61	5.09	14.92	22.39	62.69	87.17	6.73	6.10
S-6	87.83	8.10	4.07	12.69	9.52	77.78	85.93	9.37	4.70
S-7	90.49	4.76	4.75	25.00	16.67	58.33	85.73	7.14	7.12
S-8	87.34	7.60	5.06	35.08	21.06	43.86	78.73	12.77	8.50
S-9	89.18	5.40	5.42	31.03	25.86	43.10	83.32	8.33	8.35
S-10	91.57	5.63	2.80	11.11	15.87	73.02	90.34	6.45	3.21

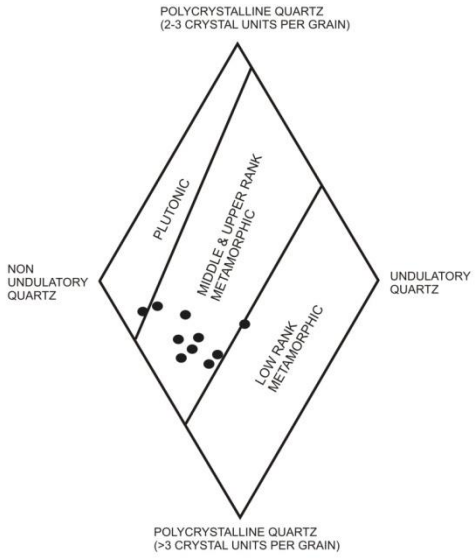

Fig. 4: Diamond diagram of sandstones of the Barail Group (after Basu et al., 1975).

Rutile: Rutile grains are identified by its characteristic blood red (Fig. 6b, d) and brownish red colour. Grains are rounded to sub rounded and prismatic in shape. They show slight pleochroism. Rutile grain shows the same colour under cross nicols as in ordinary light owing to its strong birefringence. They have extremely high refractive indices. The percentage of rutile varies from 2.42 to 9.20.

Sillimanite: Grains are mostly colourless and pale brown variety is also present. Grains occur in elongated prismatic and fibrous forms. The grains show parallel extinction, moderate to fairly strong birefringence. The percentage of sillimanite in the sandstones of the Barail Group varies from 3.09 to 7.36.

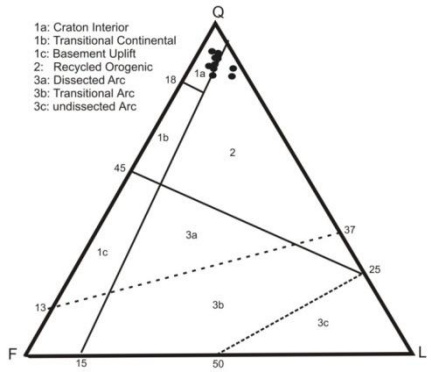

(a)

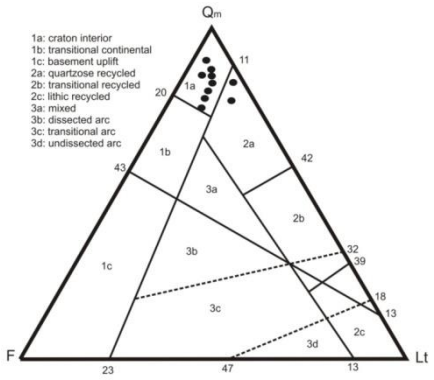

(b)

Fig.5: (a) QFL and (b) Q_mFL_t triangular plot of sandstones of the Barail Group (after Dickinson et al., 1983)

Kyanite: kyanite grains are dominantly colourless or rarely blue (Fig. 6g). Grains are elongated, bladed and angular. It exhibits weak pleochroism, perfect cleavage and show inclined extinction and a step like change in the order of interference colour. The percentage of kyanite varies from 0.78 to 3.12.

Staurolite: The grains are golden yellow in colour and occur as sub angular to irregular in forms. It shows marked pleochroism, moderate birefringence and exhibits conchoidal fractures. The percentage of staurolite varies from 1.71 to 4.68.

Garnet: Grains are mostly colourless. They are isotropic under cross nicols. Grains are occurs in the form of irregular fragments as well as subrounded to rounded grains which are bounded by conchoidal fracture surface (Fig. 6c). The Percentage of garnet varies from 0.00 to 2.93.

Epidote: grains are mostly pale greenish in colour (Fig. 6i). They are subrounded to rounded in form. It shows moderate birefringence, weak pleochroism and appears almost same under cross nicols as in ordinary light due to its high order interference colour. The percentage of epidote varies from 0.73 to 2.86.

Sphene: Sphene are colourless and sometimes green in colour. They are sub angular in shape and are marked by conchoidal fractures. Coloured grains exhibits weak pleochroism and show same colour under cross nicols as in ordinary light owing to its birefringence. The percentage of sphene in the

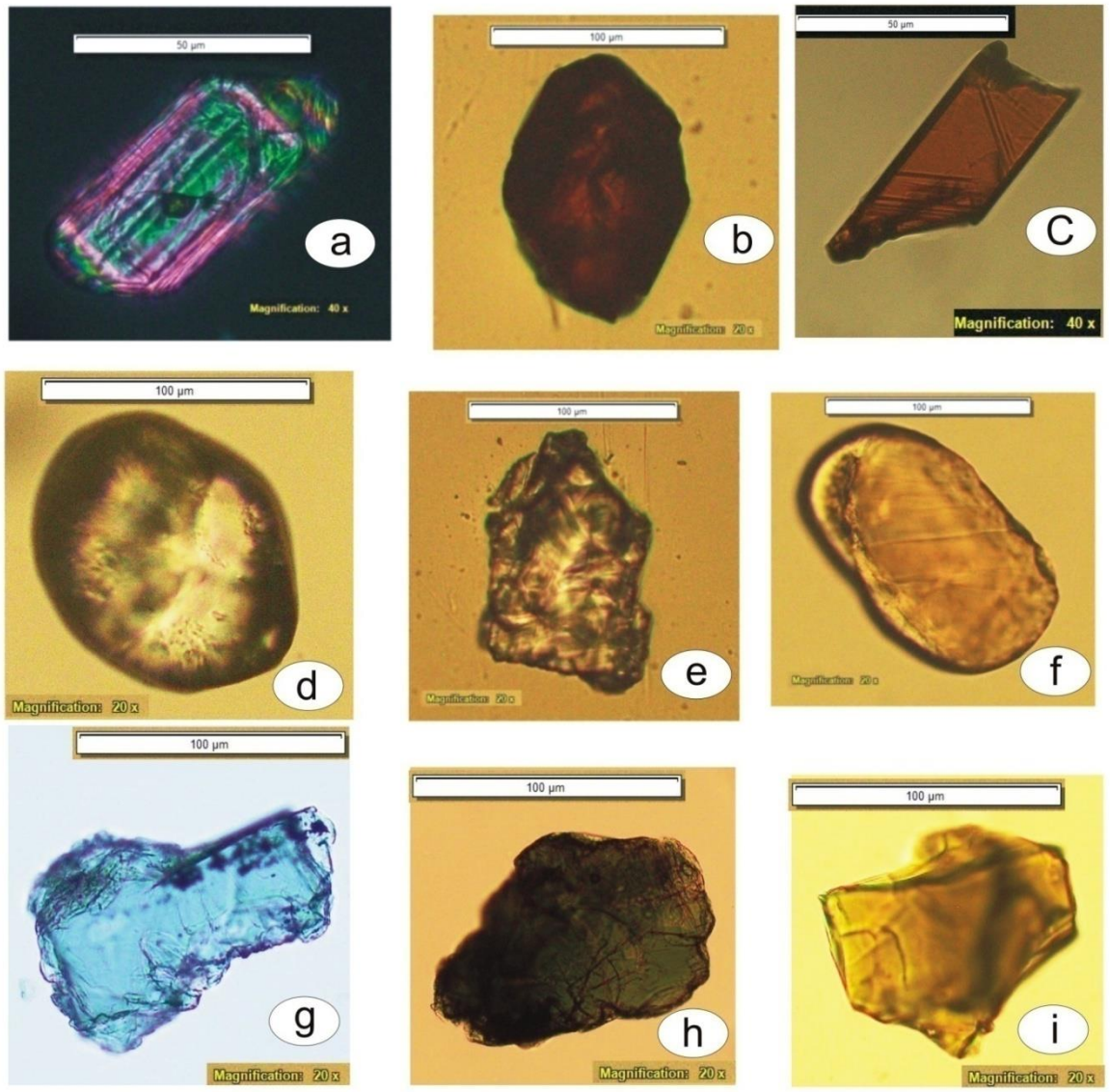

Fig. 6: Representative photomicrographs of Heavy minerals showing (a) a prismatic zircon grain (b) a rounded rutile grain (c) a prismatic rutile grain (d) a rounded zircon grain (e) garnet (f) oval shaped tourmaline (g) kyanite (h) chlorite and (i) epidote

sandstones of the Barail Group varies from 0.24 to 1.30.

Hypersthene: The grains exhibit various shades of pink and also found pale reddish brown, green in colour variety. The grains are prismatic, elongated and irregular in shape. They show distinct pleochroism and moderate to strong birefringence. Prismatic grains show parallel extinction. The percentage of hypersthene in the sandstones of the Barail Group varies from 0.00 to 0.52.

Hornblende: Hornblende grains are bluish green and brownish green in colour. The grains are prismatic, elongated and irregular in shape and also occur in the form of long thin flakes. They are strongly pleochroic, moderate to strong birefringence and show inclined extinction. Extinction angle measured in longitudinal sections varies from about 12^0 to about 30^0. The percentage of hornblende varies from 0.00 to 0.76.

Chlorite and Chloritoid: Chlorite grains exhibit various shades of green and occurred as flaky and rounded with irregular grain boundary (Fig. 6h). Pleochroism is not distinct in chlorite grains but deep coloured varieties are strongly pleochroic. Extinction is almost parallel in chlorite. Chloritoid grains are distinguished by its greyish blue or slightly greenish to yellowish blue colour. They show distinct pleochroism in shades of grey and blue. Birefringence is weak to moderate and extinction angle varies from almost parallel to 18^0. The percentage of chlorite varies from 0.26 to 1.76 and chloritoid varies from 0.00 to 3.03.

Andalusite: Andalusite grains are colourless and few of them have pinkish tinge. They are occurred as angular, irregular, occasionally prismatic, subrounded and rarely rounded. Some grains are non-pleochroic and others display a distinct pleochroism. Birefringence is weak in andalusite. The percentage of andalusite varies from 0.60 to 2.18.

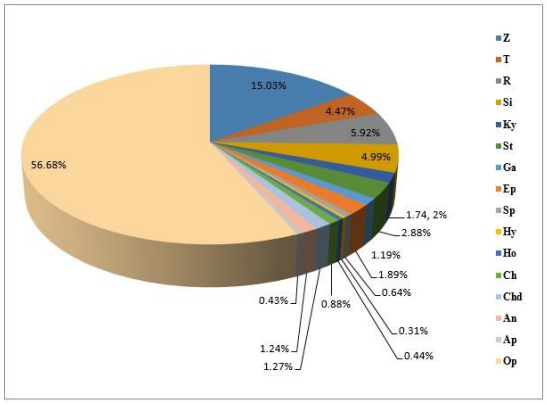

Fig. 7: Distribution of heavy minerals in the sandstones of the Barail Group.

Apatite: Grains are usually colourless and sometimes they show greyish-green colour. The grains are prismatic, subrounded to rounded form. They show weak to moderate birefringence. Prismatic grains show parallel extinction. The percentage of apatite varies from 0.00 to 0.92.

ZTR maturity index

ZTR index is the combined percentage value of zircon, tourmaline and rutile (Hubert, 1962) and is used to express the mineralogical maturity of sedimentary rock. The ZTR maturity index of the studied sandstone varies from 15.15 to 34.37. Low percentage value of ZTR index of the present sediments indicates that the sandstones are mineralogically immature. The recalculated percentage values of zircon, tourmaline and rulite (Table 5) are plotted in ZTR triangular plot and it shows that most of the samples fall in the A2 tier of field A (Fig.8) indicating Z>R>T.

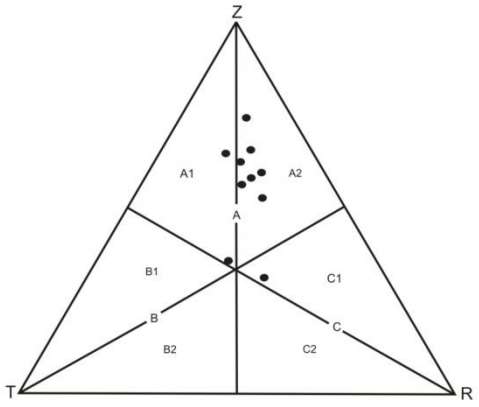

Fig. 8: ZTR triangular plot of the sandstones of the Barail Group.

Discussion and Conclusions

The petrographic study reveals that the studied Barail sandstones of the Barail Group comprises primarily of quartz grains which are angular to sub-rounded, fine to medium grained and moderately sorted in nature. According to Folk (1980), the textural maturity of sandstone is characterized by the decrease in clay matrix, improvement of sorting and increase in roundness value. So, the studied sandstones belong to sub-mature to immature classes of Folk (1980). High proportion of monocrystalline quartz indicates the plutonic source (Conolly, 1965). According to Basu et al. (1975), the presence of both unit and undulose monocrystalline quartzs gives an evidence for low rank metamorphic source. Presence of detrital mica minerals like muscovite and biotite gives an evidence for metamorphic source (Pettijohn, 1975) but some of the mica grains are of diagenetic origin. The sandstones are classified as subarkose, arkosic wacke and lithic graywacke type on the basis of mineralogical classification (after Dott, 1964).

Table 4: Heavy mineral distribution in sandstones of the Barail Group.

Sample no.	Z	T	R	Si	Ky	St	Ga	Ep	Sp	Hy	Ho	Ch	Chd	An	Ap	Op
S-1	14.67	4.40	6.36	3.91	1.22	1.71	2.93	0.73	0.24	0.49	0.49	1.71	1.71	0.98	0.49	57.95
S-3	18.43	6.56	7.57	5.05	1.51	3.04	1.78	1.77	0.76	0.51	0.50	1.76	3.03	2.02	0.25	45.46
S-4	15.25	3.63	6.78	6.05	2.18	3.39	0.73	2.66	0.74	0.24	0.48	1.21	1.69	2.18	0.24	52.54
S-5	15.86	5.29	9.20	7.36	1.38	3.91	0.92	2.53	0.46	0.45	0.47	0.91	0.68	1.38	0.92	48.27
S-6	6.11	5.86	5.34	6.10	2.80	2.03	1.03	1.27	0.51	0.25	0.76	0.50	0.77	1.02	0.26	65.39
S-7	9.70	3.03	2.42	4.54	1.82	2.12	0.00	1.51	0.61	0.30	0.31	0.30	0.00	0.60	0.00	72.73
S-8	19.22	2.60	4.15	5.45	3.12	2.86	1.04	2.34	0.26	0.52	0.00	0.26	1.82	1.30	0.52	54.54
S-9	21.61	5.99	6.77	3.38	0.78	4.68	1.82	2.86	1.30	0.00	0.53	0.78	1.32	0.79	0.52	46.87
S-10	14.38	2.88	4.65	3.09	0.87	2.21	0.46	1.33	0.89	0.00	0.43	0.45	0.44	0.88	0.66	66.37

Z= Zircon; T= Tourmaline; R= Rutile; Si= Sillimanite; Ky= Kyanite; St= Staurolite; Ga= Garnet; Ep= Epidote; Sp= Sphene; Hy= Hypersthene; Ho= Hornblende; Ch= Chlorite; Chd= Chloritoid; An= Andalusite; Ap= Apatite; Op= Opaque.

Table 5: Tabulated data for the determination of ZTR Maturity Index of sandstones of the Barail Group.

Sample No.	Actual ZTR percentage				Recalculated ZTR percentage			
	Z	T	R	ZTR Maturity Index	Z	T	R	Total
S-1	14.67	4.40	6.36	25.43	57.69	17.30	25.01	100
S-3	18.43	6.56	7.57	32.56	56.60	20.15	23.25	100
S-4	15.25	3.63	6.78	25.66	59.43	14.15	26.42	100
S-5	15.86	5.29	9.20	30.35	52.26	17.43	30.31	100
S-6	6.11	5.86	5.34	17.31	35.30	33.85	30.85	100
S-7	9.70	3.03	2.42	15.15	64.03	20.00	15.97	100
S-8	19.22	2.60	4.15	25.97	74.01	10.01	15.98	100
S-9	21.61	5.99	6.77	34.37	62.87	17.43	19.70	100
S-10	14.38	2.88	4.65	21.91	65.64	13.14	21.22	100

Diamond diagram (after Basu et al., 1975) shows that the sediments of the Barail Group were derived from the middle and upper rank metamorphic source. QFL and QmFLt triangular plot (after Dickinson et al., 1983) reflects that the sediments were mostly derived from the cratonic interior source and few of them showing recycled orogenic source. Progressive compaction and deep burial stage of diagenesis is indicated by the presence of concavo-convex and sutured grain contacts (Blatt, 1980). Quartz overgrowth may be formed from the pressure solution of quartz (Pettijohn et al., 1987).

The heavy mineral study of the sandstones shows that zircon is the most abundant heavy mineral. Occurrence of Prismatic and slender grains of zircon indicate their derivations from igneous source (Poldervarrt, 1950). The presence of prismatic rutile grains with sharp boundaries may be attributed to high grade metamorphic as well as acid igneous source (Force, 1980; Milner, 1962). Presence of rounded and sub-rounded grains of zircon and tourmaline indicate their derivation from reworked sediments while the occurrence of heavy minerals like sillimanite, kyanite, andalusite and staurolite indicates high rank metamorphic source (Pettijohn, 1975). Presence of pale brown tourmaline indicates the source of the sandstones is metamorphic (Blatt et al., 1980). Low percentage of ZTR maturity index (15.15 to 34.37) indicates that the sandstones of the Barail Group are mineralogically immature.

Thus, from the above petrographic and heavy mineral study it can be interpreted that the studied sandstones of the Barail Group were mainly derived from the plutonic and metamorphic sources and are mineralogically sub-mature to immature. The sediments show a mixed source of cratonic interior and recycled orogenic source. Najman et al. (2019) observed that the inner folded belt of the Indo-Burmese Ranges (IBR) became positive landmass and uplifted considerably at the end of the Oligocene period. There is also a positivity of contribution of detritus during Barail sedimentation from the uplifted parts of the IBR (Uddin and Lundberg, 1998). So, we can conclude that the sediments were probably derived from raised Shillong Massif where Precambrian metamorphic rocks of pelitic and arenaceous composition with plutonic bodies were exposed around the shelf margin and also from the uplifted parts of the Indo-Burmese Ranges.

Acknowledgement

The authors are thankful to the Department of Applied Geology, Dibrugarh University for assisting in laboratory work. We are also thankful to

anonymous reviewers for their constructive suggestion to improve our manuscript.

References

Basu, A., Young, W. S., Suttner, J. L., James, C. W., and Mack, H. G., 1975, Re – evaluation of the use of Undulatory Extinction and Polycrystallinity in Detrital Quartz for Provenance Interpretation, Journal of Sedimentary Petrology, Vol. 45(4), p. 873 – 882.

Blatt, H., Middleton, G. V. and Murray, R., 1980, Origin of sedimentary rocks; Englewood Cliffs, NJ, Prentice-Hall, p.782.

Chakraborty, A., 1972, On the rock stratigraphy and tectonics of the sedimentary belt in the southwest of the Shillong Plateau, Meghalaya, Oil Nat. Gas Comm. Bull., Vol. 9, p. 133 – 141

Conolly, J. R., 1965, The occurrence of polycrystallinity and undulatory extinction in quartz in sandstones, Jour. Sed. Petrol., Vol.35, p.116-135.

Curray, J. R., Moore, D. G., Lawver, L. A., Emmel, F. J., Taitt, R. W., Henry, M., and Kieckhefer, R., 1979, Tectonics of the Andaman Sea and Burma, in Watkins, J.S., Montadert, L., and Dickinson, P., eds., Geological and geophysical investigations of continental margins, American Association of Petroleum Geologists, Memoir 29, p. 189-198.

Das, P.K., Joychandra Singha, L. and Sharma, A., 2001, Stratigraphy and sedimentation of the Lower Tertiary sediments around Sonapur-Lumshnong area, Jaintia Hills, Meghalaya, India. Him. Geol., Vol. 22 (2), p. 55-60.

Dasgupta, A. B., Evans, P., Metre, W.B. and Viswanath, 1964, Excursion No. A17 and C14, 22nd Int. Geol. Congr., New-Delhi.

Dasgupta, A. B., Biswas, A. K., 2000, Geology of Assam, Geo. Soc. of India, p. 27-42.

Dickinson, W.R., Bread L.S., Brakenrideg, G.R., Erjavec, J.L., Ferguson, R.C., Inmam, K. F. Knepp, R.A., Linberg, F.A., & Ryberg, P.T., 1983, Provenance of North American Phanerozoic Sandstones in Relation to Tectonic Setting, Geol. Soc. America Bull., Vol. 94, p. 222 – 235.

Dott, R. L., Jr., 1964, Wacke, Greywacke and Matrix – What Approach to Immature Sandstone Classification?, Journal of Sedimentary Petrology, Vol. 34, p. 625 – 632.

Evans, P., 1932, Tertiary Succession in Assam, Trans. Mining & Geological Institute India, 27, p. 161– 246.

Evans, P., 1959, Stratigraphy and Tectonics of Assam Oil – fields Region, ECAFE Symposium, 1958, New Delhi, 170. (United Nations, Bangkok).

Folk, R. L., 1980, Petrology of sedimentary rocks, Hemphill's Austin, 15-60.

Force, E. R., 1980, the provenance of rutile, Journal of Sedimentary Petrology, Vol. 50, p. 485–488.

Ghosh, S., Fallick, A.E., Paul, D.K. and Potts, P.J., 2005, Geochemistry and origin of Neoproterozoic granitoids of Meghalaya, Northeast India: Implications for linkage with amalgamation of Gondwana supercontinent, Gondwana Res., Vol. 8, p. 421–432.

Hubert, J.F., 1962, A Zircon- tourmaline-rutile maturity index and the interdependence of the composition of heavy minerals assemblages with the gross composition and texture of sediments, Journal Sediment Petrol., Vol. 32, p. 440-450.

Ingersoll, R. V., Bullard, T. F., Ford, R. L., Grimm, J. P., Pickle, J. D., and Sares, S. W., 1984, The Effect of Grain size on Detrital Modes: A Test of the Gazzi-Dickinson Point-counting Method, Journal of Sedimentary Petrology, Vol. 54, p. 103–116.

Johnson, S. Y., and Alam, A. M. N., 1991, Sedimentation and tectonics of the Sylhet trough, Bangladesh, Geological Society of America Bulletin, Vol. 103, p. 1513-1527.

Medlicot, M.B., 1869, Geological Sketch of the Shillong Plateau in NE Bengal, Mem. Geol. Surv. Ind., Vol.7, pt.l, p.151-207.

Milner, H. B., 1962, Sedimentary Petrography, Vol. 2, Principles and Applications, George Allen and Urwin, London, p. 715.

Mitra, S.K., and Mitra, S.C., 2001, Tectonic setting of the Precambrian of the north-eastern India (Meghalaya Plateau) and age of the Shillong Group of rocks, Geological Survey of India Special Publication, Vol.64, p. 653–658.

Najman, Y., Mark, C., Barfod, D. N., Carter, A., Parrish, R., Chew, D., and Gemignani, L., 2019,

Spatial and temporal trends in exhumation of the Eastern Himalaya and syntaxis as determined from a multitechnique detrital thermochronological study of the Bengal Fan, Geological Society of America Bulletin, Vol. 131(9/10), p. 1607-1622.

Nandy, D. R., 2001, Geodynamics of Northeastern India and the Adjoining Region, acb Publication, Kolkata, chapter 5, p. 111-113.

Pettijohn, F. J., 1975, Sedimentary Rocks 3rd ed., New York, Harper & Row, p.628.

Pettijohn, F. J., 1984, Sedimentary Rocks 3rd ed., CBS Publishers and Distributors, New Delhi, p .628.

Pettijohn, F. J., Potter, P. E., and Siever, R., 1987, Sand and sandstone, second ed., Springer, New York, p. 553.

Poldervaart, A., 1955, Zircon in rocks, Amer. Jour. Sci., Vol. 253, p. 433 -461.

Raju, A.T.R., 1968, Geological Evolution of Assam and Cambay tertiary Basins of India, AAPG Bull. Vol. 52(12), p. 2442-2437.

Rangarao, A., 1983, Geology and Hydrocarbon Potential of a part of Assam-Arakan Basin and its adjacent area, Petroleum Asia Journal, p. 127-158.

Sah, S.C.D. and Dutta, S.K., 1968, Palynostratigraphy of the Tertiary sedimentary formations of Assam: 2. Stratigraphic significance of spores and pollen in the Tertiary succession of Assam, Palaeobotanist, Vol. 16 (2), p.177-195.

Saxena, R.K. and Tripathi, S.K.M., 1982, Lithostratigraphy of the Tertiary sediments exposed along Jowai-Badarpur Roadin Jaintia Hills (Meghalaya) and Cachar (Assam), Palaeobotanist, Vol. 39 (1), p. 34- 42.

Sein, M.K. and Sah, S.C.D., 1974, Palynological demarcation of Eocene-Oligocene sediments in the Jowai-Badarpur Road Section, Assam: In: S.C.D. Sah and A.T. Cross (Eds.): Symposium Stratigraphy and Palynology, Lucknow 1971, Spec. Publ. 3, p. 99-105., Birbal Sahni Institute of Palaeobotany, Lucknow.

Singh, R.Y., Tewari, B. S., Vimal, K. P., Modak, S. K., 1986, Stratigraphy and palynology of the Barail sediments, Jaintia Hills, Meghalaya, Bull. Geol. Min. Met. Soc. India, Vol. 54, p. 101-113.

Singh, M. P., and Singh, A. K., 2000, Petrographic characteristics and depositional conditions of Eocene coals of platform basins, Meghalaya, India, International Journal of Coal Geology, Vol. 42, p. 315-356.

Sinha, N.K., Chatterjee, B. P. and Satsangi, P.P., 1982, Status of Paleontological researches in North Eastern Region, G.S.I. Rec. 112(I).

Uddin, A., and Lundberg, N., 1998, Cenozoic history of the Himalayan-Bengal system: Sand composition in the Bengal basin, Bangladesh, Geological Society of America Bulletin, Vol. 110, p. 497-511.

Yin. A., Dubey, C.S., Webb A.A.G., Kelty, T.K., Grove, M., Gehrels, G.E. and Burgess, W.P., 2010, Geologic correlation of the Himalayan orogen and Indian Craton: Part I. structural geology, U – Pb Zircon geochronology, and tectonic evolution of the Shillong Plateau and its neighbouring regions in Northeast India, Geological Society of America Bulletin, Vol. 122(3/4), p. 336 – 359.

JOURNAL INDIAN ASSOCIATION OF SEDIMENTOLOGISTS ISSN NO 2582 – 2020
Vol. 39, Issue 2, 2022, pp. 58-68
DOI: https://doi.org/10.51710/jias.v39iII.260

Fossil Future: Why Global Human Flourishing Requires More Oil, Coal and Natural Gas --Not Less" by Alex Epstein

G. Shanmugam
Department of Earth and Environmental Sciences
The University of Texas at Arlington, USA
E-mail: shanshanmugam@aol.com

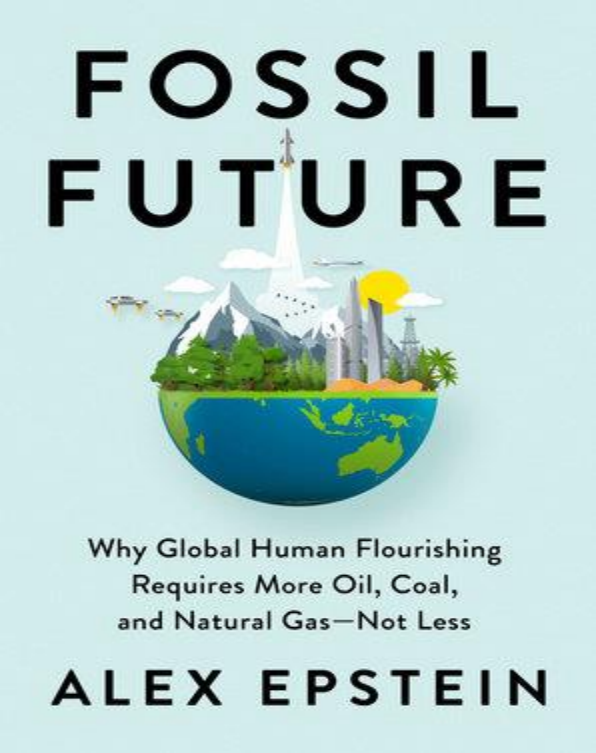

Abstract

Alex Epstein's "Fossil Future: Why Global Human Flourishing Requires More Oil, Coal, and Natural Gas--Not Less", rich in empirical data and common sense, is a timely masterpiece. It makes a compelling case for more Fossil Fuels (Oil, Coal, and Natural Gas) for the survival of the human race amid the Net–Zero ultimatum on CO_2 emission by 2050. In practice, Fossil Fuels are cheap, reliable, and necessary, whereas Renewable Energy (Wind and Solar) is expensive, unreliable, and a luxury. Petrochemicals are the building blocks of wind turbines and solar panels. At present, humans cannot collect renewable energy without petrochemical–based wind turbines and solar panels (i.e. without emitting CO_2). It is worth noting that there are 772 Pounds of petrochemical Plastics in each electric car. Therefore, the whole renewable-energy (Wind and Solar) movement is the height hypocrisy!

Introduction

The "Fossil Future" by Alex Epstein is a timely masterpiece amid the 2022–Energy Crisis in Europe. It is a well written, well researched, well reasoned, and well illustrated book. The author makes a compelling case for his argument "Why Global Human Flourishing Requires More Oil, Coal, and Natural Gas--Not Less" based on sound logic, common sense, and more importantly, empirical data.

Alex Epstein is an energy expert and founder of the Center for Industrial Progress, which offers a positive, pro–human alternative to the green movement. His New York Times best selling book, "The Moral Case for Fossil Fuels" (Epstein, 2014), has been widely praised as the most persuasive argument ever made for our continuing use of fossil fuels, winning Epstein the "Most Original Thinker of 2014" award from The McLaughlin Group. He earned a B.A. degree in Philosophy from the Duke University. The fact that Epstein is a philosopher, not a scientist, is an asset in this debate on "Fossil fuels vs. Renewable energy" that has been severely muddled by climate scientists. I, as a petroleum geologist (Shanmugam, 2006, 2012, 2021), find his book on Fossil Fuels, written by a philosopher, not only refreshing but intellectually rewarding! Therefore, I whole heartedly recommend this book to anyone who wishes to understand the problem with an open mind. I also take this opportunity to cite additional references in strengthening the case for Fossil Fuels.

Book title

My one criticism of the book is its title. As a geologist, I have difficulties with the title. In my view, "Fossil Future" should be titled "Fossil–Fuel Future". The reason is that the terms "Fossil" and "Fossil Fuel" are not one and the same. Each one conveys a totally different meaning in geology. According to the Cambridge Dictionary (2022a), the term "fossil" means "part of a plant or animal, or its shape, that has been preserved in rock or earth for a very long period". On the other hand, according to the Cambridge Dictionary (2022b), the term "fossil fuel" means "a fuel such as coal, oil, or natural gas that is produced by the gradual decaying of prehistoric plants and animals." In short, one represents a rock and the other represents a fuel.

Biased Climate Scientists

On page 63, under section "An Uncorrected Failure", Epstein points out the inherent problems and biases with climate scientists like James Hansen, Michael Mann, and Bill McKibben (see other examples by Van deer Linen, 2018; McKitrick and Christy, 2020; Koonin, S. E. (2021); Shanmugam, 2022). Climate scientists are biases and they accentuate the negative attributes of fossil fuels, such as 'CO2 emission, and totally ignore the positive attributes (See examples below).

Fossil fuels vs. Renewable energy

The central theme of the book is to emphasize the benefits of fossil fuels to humanity when compared with renewable energy types (Table 1).

Table 1. Fossil fuels vs. Renewable energy

Serial Number	Property	Fossil Fuels	Renewable Energy
1	Types	Oil Natural gas Coal	Solar Wind Hydro* Geothermal* Biomass*
2	Percentage of world's energy	80%	3%
3	Usage in critical areas, such as agriculture, production of fertilizers, heavy machinery, aviation, shipping, trucking and other ground transportation, sanitation, road construction, pipeline construction, military complexes, war machines, space industry, healthcare industry, among many others.	Yes	No
4	Petroleum products critical to modern living	>6,000 syringes, medical equipment, gloves, N─95 masks, Aspirin, antibacterial, cough syrups, lubricants, ointments (see Table 2)	0 (Zero) Petrochemicals are the building blocks of wind turbines and solar panels (Hockstad, 2016)
5	Energy density	Very high (Concentrated)	Low (Dilute)
6	Occurrence	Subsurface	Subaerial
7	Reliability	Very high	Low Sun and the wind are intermittent, uncontrollable, unreliable, sources of energy (Lawson, 2022; Schreiber, 2022)
8	Cost	Cheap	Expensive
9	Emission of CO_2	Low (Happer, 2022)	Zero
10	Damage to environment	Minimum (e.g. Emission of CO_2) (Lindzen, 2012; Happer, 2022)	Yes (e.g. killing of birds by wind turbines)
11	Group think	Low	Very high

12	Influence by International Organizations and Social Media	Accentuate the negative and ignore the positive attributes	Accentuate the positive and ignore the negative attributes
13	Research funding	Low	Very high. **German funding for renewable energy research reaches 1.31 billion Euros (Meza, 2022)**
14	Availability	Unlimited reserve with potential for new discoveries (CNOOC, 2002). Fracking of shale gas.	Unlimited
15	The ultimate effect of the Net-Zero policy	Planet Earth without humans, but with real-world earthquakes, volcanic activities, meteorite impacts, tropical cyclones, and tsunamis	Planet Earth without humans, but with real-world earthquakes, volcanic activities, meteorite impacts, tropical cyclones, and tsunamis
16	Operation	Ethical Methods of extraction of Fossil fuels do not employ renewable energy	Hypocritical Methods of extraction of renewable energy do utilize fossil fuels. 1. Wind turbines and Solar panels ─the means of collecting renewable energy─ are made with petrochemical products (Hockstad, 2016) 2. The green-energy elites, such as, Al Gore, Leonardo DiCaprio, and Bill Gates, fly to Davos in Switzerland to attend the World Economic Forum, where they promote renewable energy. However, their private jets consume enormous amounts of jet fuels emitting CO_2.

*Not the focus of this book review
Note: Epstein also emphasizes the importance of Nuclear Energy

In his books, Epstein documented that Fossil fuels (Oil, Coal, and Natural Gas) are still the dominant source of energy around the world, and growing fast—while much hyped renewable (Wind and Solar) are causing sky rocketing electricity prices and increased blackouts (Epstein, 2014). Fossil fueled development has brought global poverty to an all-time low (Epstein, 2014). While fossil fuels have contributed to the 1 degree of warming in the last 170 years, climate-related deaths are at all-time lows thanks to fossil-fueled development (Epstein, 2014). During the past 100 years, with an increasing atmospheric CO2 there has been a decreasing climate-related disaster deaths (Epstein, 2022) (Fig. 1).

Life─saving petroleum products

On page 152, Epstein reminds us that "Fossil fuel materials are also indispensable to modern medicine, with medications, syringes, medical equipment, gloves, and masks all made of oil and/ or natural gas. It's hard to find something in a hospital that isn't substantially made of oil and/or gas." The N─95 masks, which saved millions of lives during the COVID-19 Pandemic worldwide in 2020, are made mostly of petrochemicals derived from oil and natural gas (Quan, 2020). Aspirin, antibacterial, suppositories, cough syrups, lubricants, creams, ointments are some of the numerous medications that have their base in petrochemicals.

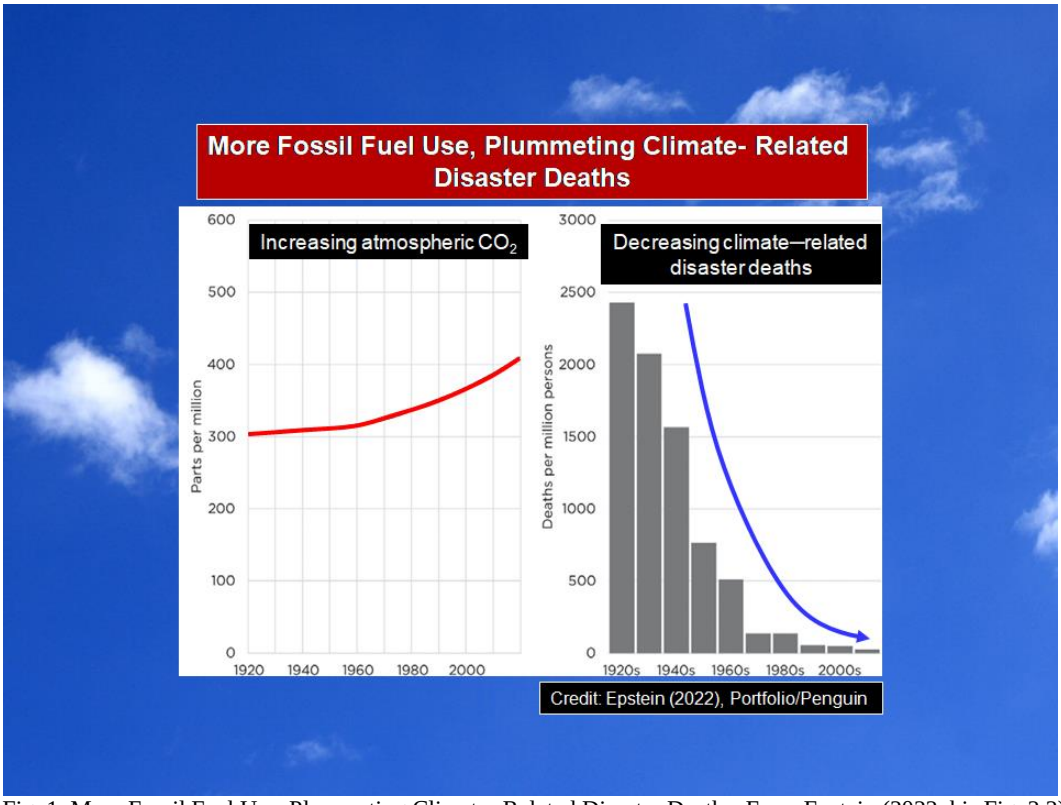

Fig. 1. More Fossil Fuel Use, Plummeting Climate- Related Disaster Deaths. From Epstein (2022, his Fig. 2.2). Additional labels by G. Shanmugam. *Sources: Scripps Institution of Oceanography; EM- DAT; World Bank Data; Maddison Project Database*

Rankin Energy Corporation (2022) stated that there are over 6,000 products. Petroleum products are an integral part of modern living, but we seldom acknowledge their importance (e.g., Floor Wax, Soap, Shoes, Toilet Seats, Shampoo, Anesthetics, Toothpaste, Gasoline, among others; see Table 2). Table 2. 144 petroleum products, among over 6,000 items, that are in use to facilitate modern living (Ranken Energy Corporation, 2022).

Infinite reserve of fossil fuels

The notion that the reserve of fossil fuels is finite is false. We continue to discover new oil and gas fields. In October 2022, CNOOC (2022) discovered a large deep─water gas field, containing 50 billion cubic meters of fuel in the South China Sea. According to the China National Offshore Oil Corp (CNOOC), the gas field called "Baodao 21─1" achieved the biggest drilling breakthrough in the Songnan─Baodao area in more than 50 years. Furthermore, innovative methods like fracking of shale gas provide endless opportunities for Infinite supply of fossil fuels. Epstein on page 55 correctly points out that "For example, using fossil─ fueled machines that "fracture" once─ useless shale rocks, today's oil and gas industry cost- effectively produces via fracking over a hundred billion gallons of oil a year that were in the past considered Unavailable."

Reliability and Research Funding

On page 115, Epstein writes that "A non─nourishing environment is one in which one toils for hours and hours a day to acquire barely enough food and water to make it to the next day." Personally, I could personally relate to this point some 70 years ago. I was born in 1944 in a small town called Sirkazhi, Madras Presidency, British India. In those days, my mother would start cooking very early in the morning using cow dung patties that would take 15─20 minutes just to heat a pot of water. Thanks to fossil─fuel generated electricity and microwave Ovens; one can accomplish the same task today in just 30 seconds. Disappointingly, one third of the world still uses wood and dung (See Epstein, 2022, his Fig. 1.5). Fossil fuels have done wonders to modern living. However, if fossil fuels were to be abolished tomorrow by the Net─Zero mandate, the modern living, as we know it in the West, will cease to exist. This is not a hollow threat, but a

real possibility. Sadly, we are already witnessing this tragedy in Europe today.

Serial Number	Petroleum Products			
1-4	Solvents	Diesel fuel	Motor Oil	Bearing Grease
5-8	Ink	Floor Wax	Ballpoint Pens	Football Cleats
9-12	Upholstery	Sweaters	Boats	Insecticides
13-16	Bicycle Tires	Sports Car Bodies	Nail Polish	Fishing lures
17-20	Dresses	Tires	Golf Bags	Perfumes
21-24	Cassettes	Dishwasher parts	Tool Boxes	Shoe Polish
25-28	Motorcycle Helmet	Caulking	Petroleum Jelly	Transparent Tape
29-32	CD Player	Faucet Washers	Antiseptics	Clothesline
33-36	Curtains	Food Preservatives	Basketballs	Soap
37-40	Vitamin Capsules	Antihistamines	Purses	Shoes
41-44	Dashboards	Cortisone	Deodorant	Shoelace Aglets
35-48	Putty	Dyes	Panty Hose	Refrigerant
49-52	Percolators	Life Jackets	Rubbing Alcohol	Linings
53-56	Skis	TV Cabinets	Shag Rugs	Electrician's Tape
57-60	Tool Racks	Car Battery Cases	Epoxy	Paint
61-64	Mops	Slacks	Insect Repellent	Oil Filters
65-68	Umbrellas	Yarn	Fertilizers	Hair Coloring
69-72	Roofing	Toilet Seats	Fishing Rods	Lipstick
73-76	Denture Adhesive	Linoleum	Ice Cube Trays	Synthetic Rubber
77-80	Speakers	Plastic Wood	Electric Blankets	Glycerin
81-84	Tennis Rackets	Rubber Cement	Fishing Boots	Dice
85-88	Nylon Rope	Candles	Trash Bags	House Paint
89-92	Water Pipes	Hand Lotion	Roller Skates	Surf Boards
93=96	Shampoo	Wheels	Paint Rollers	Shower Curtains
97-100	Guitar Strings	Luggage	Aspirin	Safety Glasses
101-104	Antifreeze	Football Helmets	Awnings	Eyeglasses
105-108	Clothes	Toothbrushes	Ice Chests	Footballs
109-112	Combs	CD's & DVD's	Paint Brushes	Detergents
113-116	Vaporizers	Balloons	Sun Glasses	Tents
117-120	Heart Valves	Crayons	Parachutes	Telephones
121-124	Enamel	Pillows	Dishes	Cameras
125-128	Anesthetics	Artificial Turf	Artificial limbs	Bandages
129-132	Dentures	Model Cars	Folding Doors	Hair Curlers
133-136	Cold cream	Movie film	Contact lenses	Drinking Cups
137-140	Fan Belts	Car Enamel	Shaving Cream	Ammonia
141-144	Refrigerators	Golf Balls	Toothpaste	Gasoline

Because of the ongoing Russia–Ukraine war that began in February 2022, sanctions were imposed on Russia. This led to shutting down of Nord Stream Pipelines 1 and 2 that were built to supply gas from Russia to Germany. According to Lawson (2022), "Nord Stream 1 is the single biggest pipeline for gas from Russia to Europe and has the capacity to deliver 55bn cubic metres (bcm) of gas a year. Continued supplies through the pipeline are seen as crucial to prevent a deepening of the energy crisis." In this context, the Germany's Deutsche Bank reported that if Russia makes deeper cuts in the supply of natural gas to Western Europe as a result of sanctions over the war in Ukraine, German households might have to turn to an alternative fuel to heat their homes, such as wood (Schreiber, 2022).

Germany is the leader in promoting renewable energy. The German government has approved 1.31 billion Euros in funding for research related to the country's energy transition, according to the federal environment ministry. In its aim to become climate-neutral and less dependent on energy imports, Germany is striving to convert its supply systems to renewable energy (Meza, 2022). However, under precarious war conditions, the only reliable energy sources are the Fossil Fuels (Oil, Coal, and Natural Gas), not renewable energy (Solar and Wind). Epstein illustrates this point in great detail on page 215 with his Fig. 6.3 using Germany as a case study.

Fossil Fuels are cheap, reliable, and necessary, whereas Renewable Energy (Wind and Solar) is expensive, unreliable and a luxury.

The role of CO_2 in generating cyclones

Epstein writes about weather extremes born of carbon usage. In the U.S., whenever a cyclone hits the Gulf of Mexico, the first you hear from the weather forecaster on TV is that tropical cyclones are the result of anthropogenic global warming and related carbon emission. Epstein tackles this fallacy head on page 277 by noting that "Long before significant CO_2 emissions, storms were taking tens and even hundreds of thousands of human lives in the unempowered world, such as the 300,000 lives lost in an 1839 India cyclone". Importantly, empirical data show that there is a decrease in storm─related deaths during the past six decades (Epstein, 2022, his Fig. 7.5) (Fig, 2).

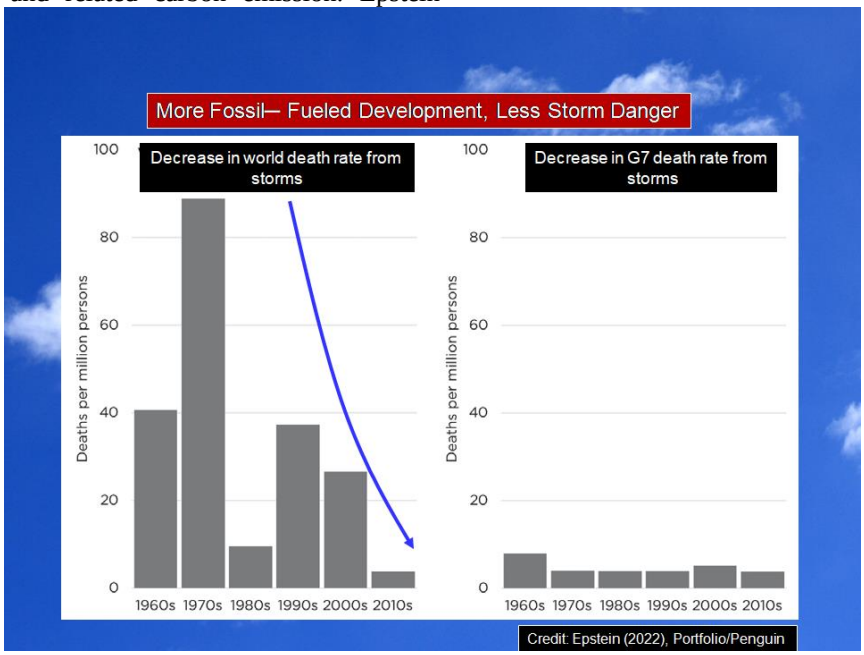

Fig. 2. More Fossil- Fueled Development, Less Storm Danger. From Epstein (2022, his Fig. 7.5). Additional labels by G. Shanmugam. *Sources: Scripps Institution of Oceanography; EM- DAT; World Bank Data; Maddison Project Database*

As a geologist, I have researched and published articles on cyclone and tsunamis in peer─reviewed international journals (Shanmugam, 2008). I find the connection between CO_2 and cyclones is unsustainable. Tropical cyclones are formed only when certain meteorological conditions are satisfied. Necessary conditions for the development of tropical cyclones are (Gray, 1979; AOML, 2007):

(1) A minimum distance of at least 500 km (311 mi) from the equator,
(2) Warm ocean waters of at least 26.5°C (80°F) to a depth of about 50 m (164 ft),
(3) An unstable atmosphere that cools fast with height,
(4) Relatively moist layers near the mid atmosphere (5 km; 3 mi),
(5) A pre─existing near─surface disturbance with sufficient vorticity and convergence,
(6) Low values (less than about 10 m s^{-1} [33 ft s^{-1}]) of vertical wind shear (i.e., the magnitude of wind change with height) between the surface and the upper troposphere, and
(7) The Coriolis force.

Clearly, CO_2 emission is not a primary factor in the genesis of cyclones.

Recent studies by Chand et al. (2022) show that the frequency of cyclones has been declining since 1850 (Fig. 3) despite global warming. Therefore, the link between Co_2 emissions and generation of tropical cyclones is not validated by empirical data.

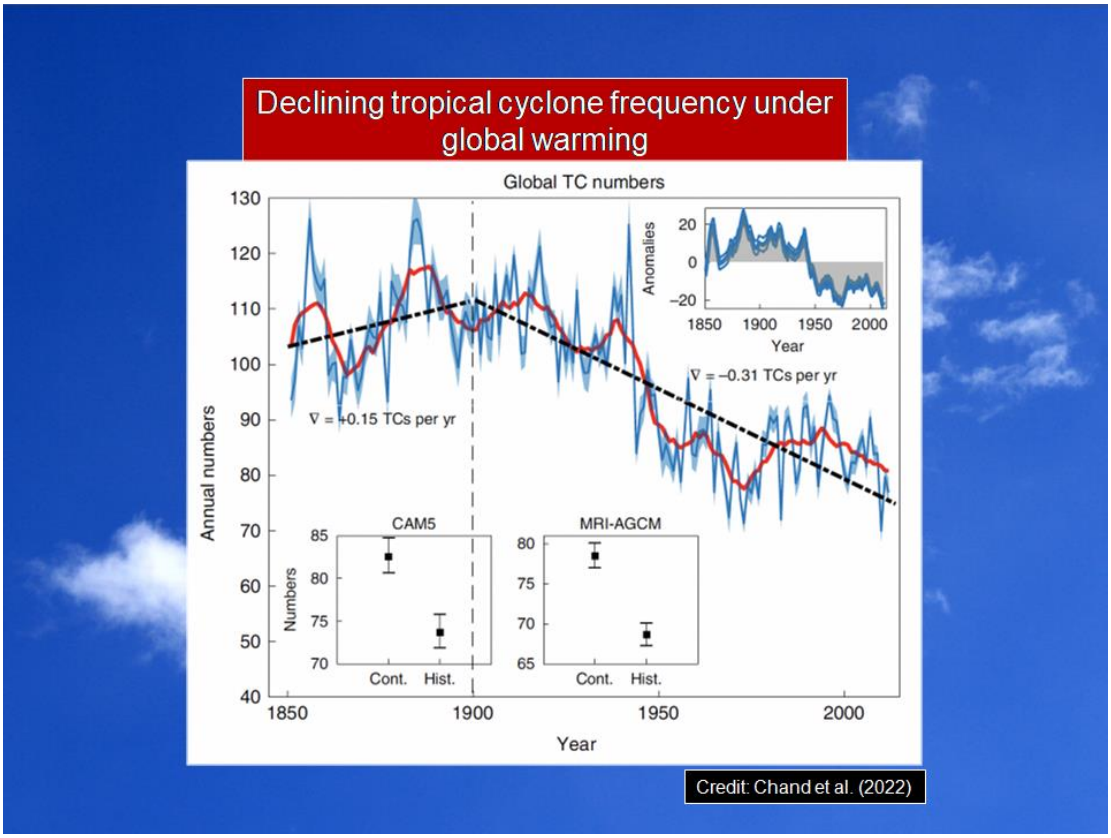

Fig. 3. Declining tropical cyclone frequency under global warming. From Chand et al. (2022). Nature Climate Change.

The Net─Zero Ultimatum

On page 394, Epstein notes that "…President Joe Biden has made it a goal for the U.S. to have "Net─Zero" CO_2 emissions from electricity by 2035 and from all forms of energy by 2050— with unreliable solar and wind as the primary means of getting there."

This mandate, if implemented, requires 100% elimination of fossil fuels by 2050.

It can realistically be achieved only by eliminating the entire human race because the human race is the only one who uses fossil fuels that emit CO_2.

Fossil fuels are the underpinning of modern civilization that relies on petroleum products.

Renewable energy sources (wind and solar) cannot produce petroleum products (Fig. 4) because wind and solar energy sources do not contain hydrogen and carbon molecules.

Therefore, modern civilization will cease to exist without fossil fuels.

Environmental, Social, and Governance (ESG) On page 396, Epstein alerts that "The aspect of the corporate anti─ fossil fuel movement that scares me the most is the "ESG" movement, which prods companies not only to advocate for fossil fuel elimination but also to commit to practicing it, independent of what the law says." He is proven correct in the case of Sri Lanka that adopted ESG policy and banned chemical fertilizer in 2021. Although Sri Lanka has an almost perfect ESG score at 98.1, Sri Lanka has drastically reduced crop yields. Furthermore, the ESG policy has damaged Sri Lanka's trade balance and has run out of fuel. The country is facing the worst economic crisis in decades (Daily Caller News Foundation, 2022), resulting in bankruptcy (Bostock, 2022). According to Follett and Cochran (2022), "Over 90 percent of Sri Lanka's farmers had used chemical fertilizers before they were banned. After they were banned, an astonishing 85 percent experienced crop losses. Rice production fell 20 percent and prices skyrocketed 50 percent in just six months."

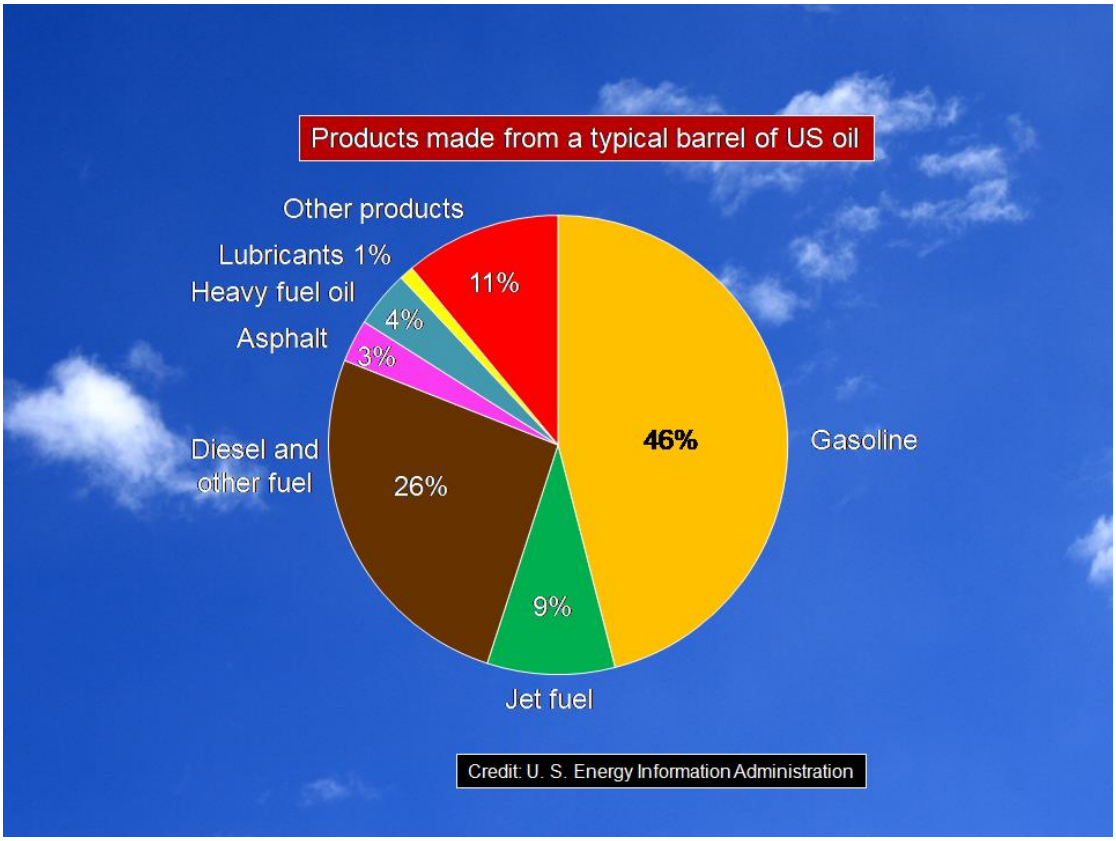

Fig. 4. A breakdown of the products made from a typical barrel of US oil. Solar and wind cannot produce these vital products necessary for human survival in the western countries.
Diagram credit: U.S. Energy Information Administration > Petroleum > Navigator > Refinery Yield

Wind turbines, Solar panels, and Electric cars: The Green Energy Myths

In chapter 6, Epstein explains why the more solar and wind grids we use, the more their electricity tends to cost. In addition to this economic problem, there is an ethical problem. Petrochemicals are the building blocks of wind turbines and solar panels (Epstein did, 2016). At present, humans cannot collect renewable energy without petrochemical─based turbines and panels (i.e. without emitting CO_2). It is worth noting that there are 772 pounds of Petro-Chemical Plastics In each electric car (Whipple, 2020). Therefore, the whole renewable─energy (Wind and Solar) movement is the height hypocrisy!

Earth in the Solar System

Epstein discusses the role of the Sun on climate change throughout the book. I would like to further emphasize that Climate Change that affects the Earth must be considered in the context of the Solar System (Fig. 5).

In the Solar System, Earth is a minor player (Fig. 5), despite its human habitants with an "inflated sense of self". For example, the global elites like Al Gore (a former U.S. Vice President) and Leonardo DiCaprio (an actor) set agenda in controlling CO_2 emissions during their annual meeting at the World Economic Forum in Davos, Switzerland, see also Table 1).

In their seminal book, Haigh and Cargill (2015) emphasize that "The Earth's climate system depends entirely on the Sun for its energy. Solar radiation warms the atmosphere and is fundamental to atmospheric composition, while the distribution of solar heating across the planet produces global wind patterns and contributes to the formation of clouds, storms, and rainfall."
We humans cannot regulate cosmic forces that control Earth's temperature and climate (Haigh and Cargill, 2015; see also Soon et al., 2015; Soon and Baliunas, 2017).

Furthermore, Venus and Jupiter may meddle with Earth's orbit and climate (Daley, 2018). In 405,000-year cycles, the tug of nearby planets causes hotter summers, colder winters and drier droughts on our Planet Earth. By comparison, the human factor in controlling Earth's climate is frivolous.

Earth's climate is controlled by CO_2 emissions by all countries (see Pie Chart in Fig. 5). Any mandate on control of emission of CO_2

must be adopted by all countries without any exceptions. However, this is not the case today.

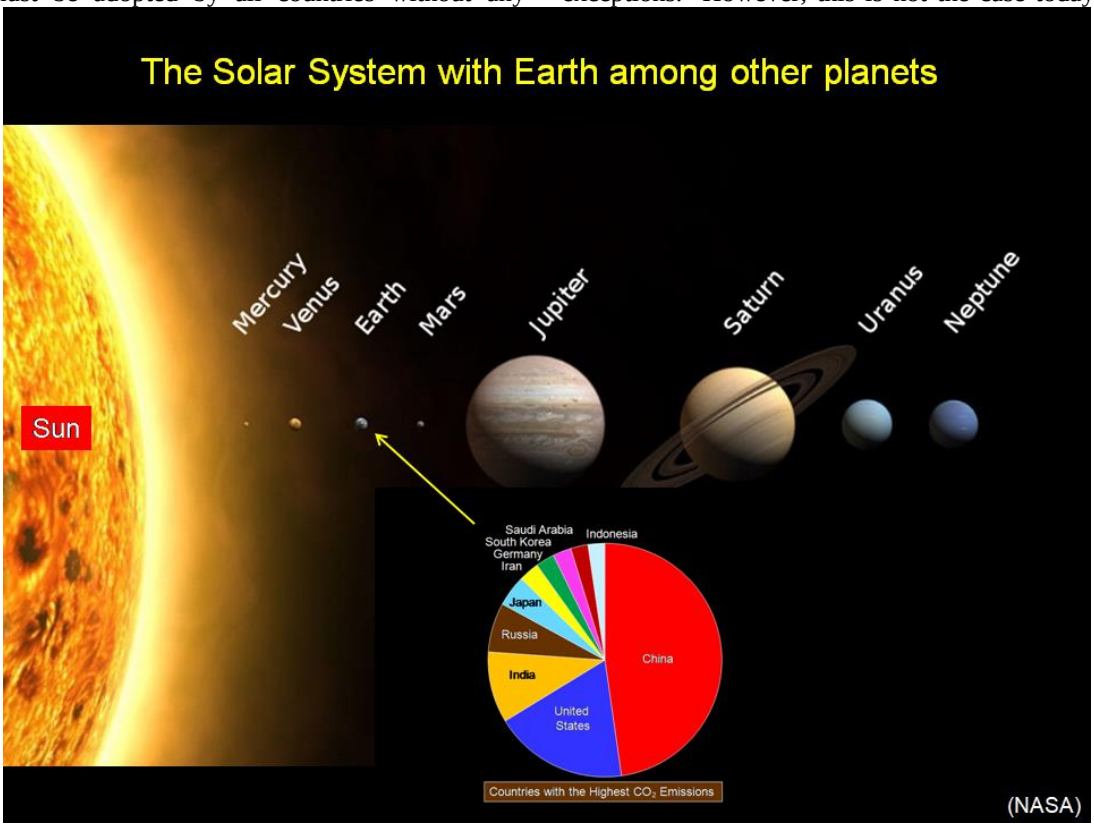

Fig. 5. Diagram showing the position of Earth among other planets in the Solar System (NASA). The pie chart at the bottom shows the top 10 countries with the Highest CO_2 emissions in the world (Unit: million tons CO_2) in 2020 (EDGAR, 2022).

China - 11,680.42 (Unit: million tons CO_2)
United States - 4,535.30
India - 2,411.73
Russia - 1,674.23
Japan - 1,061.77
Iran - 690.24
Germany - 636.8
South Korea - 621.47
Saudi Arabia - 588.81
Indonesia - 568.27

Figures, Notes, and Index

Figures are composed of histograms, pie charts, graphs and photographs. They are clearly labeled and sourced. There are 39 figures.

Notes are useful list of references and other explanations included at the end. There are 328 notes.

On pages 457─468, a comprehensive Index contains Subject and Author names.

The book ends on page 468, but the publisher erroneously claims that there are 480 pages.

I have examined both the print version and the digital (PDF) version. The Publisher: Portfolio/Penguin has done an excellent job of production.

Concluding remarks

Epstein, by applying his distinctive "human flourishing framework" (page 95) to the latest evidence, comes to the audacious conclusion that the benefits of fossil fuels will continue to far outweigh their side effects—including climate impacts—for generations to come. Epstein forcefully argues that the path to global human flourishing is a combination of using more fossil fuels, getting better at "climate mastery," (page 101) and establishing "energy freedom" (Chapter 10, page 357) policies that allow nuclear and other truly promising alternatives to reach their full long-term potential. In the final Chapter 11 (page 430), Epstein concludes the book with an optimistic note: "Sooner or later— and with your help, sooner—billions of people will see what I started seeing fourteen years ago: that for eight billion people to

live in a nourishing, safe, opportunity- filled world— a world in which, for the first time ever, global human flourishing is possible— we need more oil, coal, and natural gas, not less." Amen!

Acknowledgements

I thank Prof. G. M. Bhat, Managing Editor of JIAS, Jammu University, India, for encouraging me to submit this Boook Review. I also thank Alex Epstein for providing a PDF of the book. I thank J. E. Damuth for keeping me up-to-date on Climate Change issues. Of Course, I am indebted to the late George Devries Klein for his motivation on the topic. As always, I am grateful to my wife, Jean Shanmugam, for her general comments.

References

AOML (Atlantic Oceanographic and Meteorological Laboratory), (2007). How do tropical cyclones form?: http://www.aoml .noaa.gov/hrd/tcfaq/A15.html (accessed November 10, 2007).

Bostock, W. (2022). Sri Lanka says it is 'bankrupt' as financial crisis ravaging the country https://www.businessinsider.com/sri-lanka-says-bankrupt-financial-crisis-ravages-country-debts-default-2022-7 Retrieved November 28, 2022

The Cambridge Dictionary, (2022a). Fossil. https://dictionary.cambridge.org/us/dictionary/english/fossil Retrieved November 23, 2022.

The Cambridge Dictionary, (2022b). Fossil Fuel. https://dictionary.cambridge.org/us/dictionary/english-malaysian/fossil-fuel Retrieved November 23, 2022.

Chand, S.S., Walsh, K.J.E., Camargo, S.J., Kossin, J. P., Tory, K. J., Wehner, M. F., Chan, J. C. L., Klotzbach, P. J., Dowdy, S. J., Bell, S. S., Ramsay, H. A. and Murakami, H. (2022). Declining tropical cyclone frequency under global warming. *Nat. Clim. Chang.* **12**, 655–661. https://doi.org/10.1038/s41558-022-01388-4

CNOOC, (2022). CNOOC discovers large deep-water gas field, containing 50 billion cubic meters of fuel. Global Times, https://www.globaltimes.cn/page/202210/1277590 .shtml Retrieved November 22, 2022.

Daily Caller News Foundation, (2022). 'Complete Collapse': Here's How ESG Destroyed One Nation's Economy. https://dailycaller.com/2022/07/06/complete-collapse-esg-destroyed-nations-economy/ Retrieved November 26, 2022

Daley, J. (2018). Venus and Jupiter May Meddle With Earth's Orbit and Climate. Smithsonian Magazine. https://www.smithsonianmag.com/smart-news/venus-and-jupiter-change-earths-orbit-and-climate-405000-year-cycle-180969038/ Retrieved December 5, 2022.

EDGAR (European Union's Emissions Database for Global Atmospheric Research) (2022). Top 10 Countries with the Highest CO_2 Emissions in the World (Unit: million tons CO_2) https://worldpopulationreview.com/country-rankings/co2-emissions-by-country). Retrieved December 1, 2022.

Epstein, A. 2014. The Moral Case for Fossil Fuels. Portfolio/Penguin, 256 p.

Epstein, A. (2022). Fossil Future: Why Global Human Flourishing Requires More Oil, Coal, and Natural Gas--Not Less. Portfolio/Penguin, 480 p.

Follett, C. and Cochran, M. (2022). Sri Lanka Is a Wake-Up Call for Eco-Utopians. https://www.humanprogress.org/sri-lanka-is-a-wake-up-call-for-eco-utopians/Retrieved November 26, 2022

Gray, W. M., (1979). Hurricanes: Their formation, structure and likely role in the tropical circulation, in D. B. Shaw, ed., Meteorology over tropical oceans: Royal Meteorological Society, p. 155–218.

Haigh, J. D., Cargill, P. 2015. The Sun's influence on climate. Princeton University Press, Princeton, New Jersey. 216 p.

Happer, W. (2022). 138. Climate Physics w/Professor William Happer. October 29, 2022. https://www.google.com/search?q=harper+climate+physics+youtube&oq=harper+climate+physics+youtube&aqs=chrome..69i57j33i160l2.19747j0j7&sourceid=chrome&ie=UTF-8#fpstate=ive&vld=cid:e59ba35f,vid:5Uf_AbyG6ho Retrieved Novermber 23, 2022.

Hockstad, M. (2016). Petrochemicals: The Building Blocks for Wind and Solar Energy. AFPM (American Fuel & Petrochemical Manufacturers) https://www.afpm.org/newsroom/blog/petrochemicals-building-blocks-wind-and-solar-energy Retrieved November 26, 2022

Koonin, S. E. (2021). Unsettled: What Climate Science Tells Us, What It Doesn't, and Why It Matters. BenBella Books. 316 p.

Lawson, A. (2022). Nord Stream 1: Gazprom announces indefinite shutdown of pipeline. The Guardian. https://www.theguardian.com/business/2022/sep/02/nord-stream-1-gazprom-announces-indefinite-shutdown-of-pipeline Retrieved November 27, 2022

Lindzen, R. (2012). Reconsidering the Climate Change Act: Global Warming: How to approach the science (Climate Models and the Evidence?). Seminar at the House of Commons Committee Rooms . Westminster, London. 22nd February 2012.

https://www.telegraph.co.uk/multimedia/archive/02148/RSL-HouseOfCommons_2148505a.pdf Retrieved December 5, 2022.

McKitrick, R. Christy, J. (2020). Pervasive Warming Bias in CMIP6 Tropospheric Layers. Earth and Space Science, 7 (9), First published: 15 July 2020 https://doi.org/10.1029/2020EA00128

Meza, E. (2022). German funding for energy research reaches 1.31 billion Euros. https://www.cleanenergywire.org/news/german-funding-energy-research-reaches-131-billion-euros Retrieved November 26, 2022.

Quan, H. (2020). Petroleum in Real Life: N-95 masks. Context Energy Examined. https://context.capp.ca/articles/2020/pirl-n-95-masks/Retrieved November 27, 2022

Rankin Energy Corporation, (2022). Products made from petroleum. https://www.ranken-energy.com/index.php/products-made-from-petroleum/ Retrieved November22, 2022.

Schreiber, R. (2022). Deutsche Bank Says Germans May Need to Switch from Gas-to-Wood for Heating this Winter, is Wood-to-Gas for Cars Next? https://www.thetruthaboutcars.com/2022/07/deutsche-bank-says-germans-may-need-to-switch-from-gas-to-wood-for-heating-this-winter-is-wood-to-gas-for-cars-next/ November 26, 2022

Shanmugam, G. (2006). Deep-water Processes and Facies Models: Implications for Sandstone Petroleum Reservoirs, Amsterdam: Elsevier. 476 p.

Shanmugam, G., (2008). The constructive functions of tropical cyclones and tsunamis on deepwater sand deposition during sea level highstand: implications for petroleum exploration. *AAPG Bulletin*, 92, 443-471.

Shanmugam, G. (2012). New perspectives on deep-water sandstones: origin, recognition, initiation, and reservoir quality, 9. In Handbook of petroleum exploration and production, Amsterdam: Elsevier. 524 p.

Shanmugam, G. (2021). Mass transport, gravity flows, and bottom currents: Downslope and alongslope processes and deposits. Amsterdam: Elsevier. 608 p.

Shanmugam, G., (2022). The peer-review problem: A sedimentological perspective. Journal of the Indian Association of Sedimentologists, 39, 3─24.

Soon, W, Connolly, R & Connolly, M, (2015). Re-evaluating the role of solar variability on Northern Hemisphere temperature trends since the 19th century. *Earth-Science Reviews*, 150, 409-452.

Soon, W, Baliunas, S. 2017. A Brief Review of the Sun–Climate Connection, with a New Insight Concerning Water Vapour. https://lweb.cfa.harvard.edu/~wsoon/myownPapers-d/SoonBaliunas17-June8-FINAL-CCTF2017_Ch11_2pp.pdf Retrieved December 5, 2022.

Van deer Linen, G. J. (2018). Post-modernism and climate change. Jour. Indian Association of Sedimentologists, Vol. 35, No. 2 (2018) Special Issue dedicated to George Devries Klein in celebrating his life and achievements pp 6-12.

Whipple, T. (2020). THE GREEN ELECTRIC CAR MYTH: 772 Pounds Of Petro-Chemical Plastics In EachVehicle. https://daily.energybulletin.org/2020/07/_the-green-electric-car-myth-772-pounds-of-petro-chemical-plastics-in-each-vehicle/ Retrieved December 4, 2022.

A Report on 38th Convention of Indian Association of Sedimentologists and National Conference on "Current Understanding from the Indian Sedimentary Basins and Road Ahead"

The 38th Indian Association of Sedimentologists (IAS) convention and National Conference on the "Current Understanding from the Indian Sedimentary Basins and Road Ahead" was organized from 9 - 11 December 2022 under the aegis of IAS at the Department of Geology, University of Delhi. In the backdrop of centenary year of the University of Delhi and Azadi Ka Amrit Mahotsov the conference was conceptualized to address the various aspects of earth surface processes including resource sedimentology (water, conventional and unconventional energy resources). Considering the diversity and veracity of research topics in the subject, eight scientific themes were identified by the scientific committee of the conference: 1. Continental and marine depositional environments (Clastic and Carbonate) 2. Tectonics and volcano sedimentary system 3. Archean-Proterozoic basins: clues from early hydrosphere, atmosphere and biosphere 4. Phanerozoic sedimentation and biological processes in sedimentation 5. Recent advances in sedimentology and stratigraphic techniques 6. Quaternary and modern sedimentation systems, Vedic Saraswati River 7. Deep-time climate and environment and 8. Resource sedimentology: mineral, water, conventional and nonconventional energy resources.

In order to expose young researchers to field-based sedimentology, a post-conference field excursion was organised in the Paleoproterozoic Bayana Basin in North Delhi fold belt. The participants were exposed to the products of different continental (alluvial fan, fluvial) and shallow marine (shoreface, shelf) products in the field, their identifying criteria and basin-scale development pattern.

The inaugural session of the 38th Convention of Indian Association of Sedimentologists (IAS) and the National Conference was held at the Conference Centre of the University of Delhi. Dr. Kalachand Sain (FNS, FASc, FNASc, FTAS, FAPAS, J.C. Bose Fellow) Director, Wadia Institute of Himalayan Geology, Dehradun, Uttarakhand was the chief guest, Prof. Rajeev Gupta, Chief Executive Officer (CEO) of the Institute of Eminence (IoE), University of Delhi the Guest of honour and Prof. G. N. Nayak, President Indian Association of Sedimentologists (IAS) graced the occasion., Professor P. P. Chakraborty, Head of the Department (in-charge) and Dr. Pramod Kumar (Convener) inaugurated the Convention and National Conference.

Inaugural session: Prof. G. N. Nayak (President-IAS), Prof. Rajeev Gupta (CEO-IoE), Prof. P. P. Chakraborty (Head) Dr. Pramod Kumar (Convener) from left to right.

Prof. G. N. Nayak (President, IAS) spoke about the philosophy of conducting the 38th Convention of the Indian Association of Sedimentologists (IAS-2022) along with the National conference on 'Current understanding from the Indian the sedimentary basins and road ahead' under the same umbrella, is to bring out synergistic growth of the Association (IAS) and understanding the Indian sedimentary basins.

Dr. Kalachand Sain (Chief Guest) spoke on the clime change and its worse impact on water, energy, food and health securities. Water is life to living beings and energy is the driving force for socioeconomic growth of the country. Therefore, we need to

characterize numerous surface and subsurface processes/phenomena to provide a secured and climate-adapted future with a view to meet the overwhelming requirement of both resources and sustainability.

Prof. Anupam Chattopadhyay (Head of the Department) said it is a matter of pride for the Department of Geology, University of Delhi to host the 38th Convention of Indian Association of Sedimentologists (IAS) and the National Conference. It is a special occasion as the National conference and the IAS Cnvention coincide with the '*Centenary year celebration'* of the University of Delhi and '*Azadi ka Amrit Mahotsav'*.

Dr. Pramod Kumar (Convener) express his heartfelt gratitude to the Indian Association of Sedimentologists (IAS) for giving us an opportunity to host the 38th Annual Convention and a National Conference. Apart from the normal academic sessions, we have dedicated separate theme on energy resources, to have an industry academia interaction. For the early career scientists and research scholars we are organizing two workshops. The active response from the delegates from all the parts of the country remained the diving energy for the successful execution of the conference. Abstracts were received from all parts of the country. A total of 115 participants attended the conference; we received 95 abstract and 07 keynotes. During the two days of scientific technical themes a total of 57 oral presentation and 28 poster were presented in the conference.

Group Photographs: 38th IAS Conference Participants.

The convention address was delivered by Prof. S. K Tandon on "The evolving tale of the 'Lost' Saraswati River of northwest India: a sedimentological perspective". The Saraswati River has been described in the literature as a 'River par excellence' and in some other accounts as a 'Lost River' and a 'Prehistoric River'. Several questions surround the existence of this river with regards to its antiquity, and its association or otherwise with the different phases of the Harappan Civilization. There is also the unresolved question of when and how the decline of this large river took place through climate-driven aridity and/or tectonic processes. The causes, nature, and the timing of avulsion continue to be currently debated by researchers from different disciplinary backgrounds. Prof. Tandon discussed the key regional palaeoclimatic and tectonic evidences and their possible roles in a broad spatio-temporal framework of the Yamuna-Sutlej interfluve. He emphasized on both tectonic and climatic factors for demise of the Saraswati River.

Prof. Santanu Banerjee delivered keynote address on "Distinguishing celadonite from glauconite for environmental interpretations: a review". Celadonite and glauconite are comparable in terms of physical, chemical and mineralogical characteristics. Formation of both these minerals requires slightly oxygen-depleted depositional conditions in a semi-confined micro-environment, facilitating the uptake of Fe into the structure.

Other keynote addresses were delivered by Prof. Santosh Kumar on "Zircon typology and geochronology of magmatic and associated volcano-sedimentary lithounits from the Kumaun Lesser Himalaya: Constraints on basin depositional age and nature of provenance"; by Prof. Joydip Mukhopadhyay on "Oxygenation of atmosphere and hydrosphere: clues from Archean sedimentary rock record". Early atmosphere and hydrosphere of our planet were very much different during the Archean and Early Proterozoic; by Prof. Devesh K Sinha on "Evolution of Cenozoic Climate, Evidence from Deep Sea sedimentary Records and Polar Ice Cores". The Cenozoic Era has been a time of conspicuous waxing and waning of ice sheets and resulting ocean circulation changes; by Prof. Partha Pratim Chakraborty on "Debates and Constraints in early

atmosphere/ hydrosphere oxygenation: Clues from Indian Precambrian basins".

A two-day field visit (11 - 12 December 2022) was conducted in the Bayana basin to expose the participants to product of different sedimentary environments ranging from continental through shallow-marine to distal marine set-up beyond storm wave base.

Geological Field Excursion photographs: Paleoproterozoic Bayana basin.

Pramod Kumar, Partha Pratim Chakraborty, Vimal Singh, Ashutosh Singh and Pritam Paritosh Paul

Department of Geology, University of Delhi, Delhi-110007, India

Vol. 39 No. II pp 72-73

National Conference and 37 IAS Convention Report

National Conference on "Resource Potential of Sedimentary Basins" and 37 IAS convention was organised by the Department of Geology, University of Jammu, Jammu 26-27April, 2022 on virtual mode. The executive council of the IAS in its meeting at Hyderabad decided that the 37th IAS convention will be held at Jammu in the month of November, 2020 but due to Covid-19 pandemic the conference could not held and was postpone for 2021 but the Covi-19 situation didn't improve to conduct the same in offline mode and it was again postpone and finally the executive council of the IAS decided to conduct the same in the month of March, 2022. But due to poor response and emergence of new Covid-19 variation the committee decided to conduct the same on virtual mode on 26-27th April, 2022.

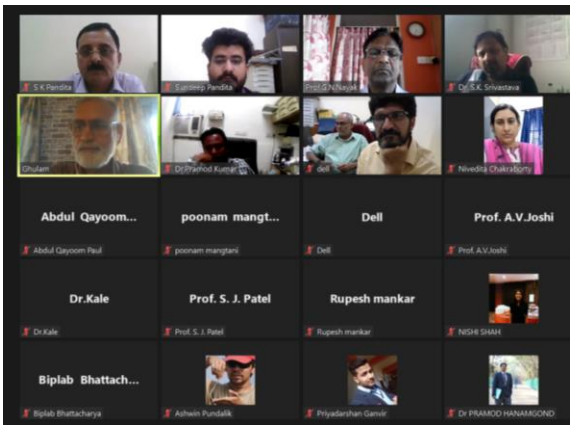

The virtual inauguration of the conference was held at 10:30 am on 26th and the chief guest of the function was Dr. Ashutosh Mondal, DDG, GSI, Jammu and the guest of the honor of the function was Dr. Ravi Misra, Executive Director, Chief Exploration & Development Directorate, Oil and Natural Gas Corporation (ONGC). Professor S K Pandita, Convener started the inauguration proceedings by introducing the different dignitaries to the audience and also presented brief background of the IAS conference and then invited Prof. G N Nayak, President of the Association to brief the audience about the various important issues taken up by the association during the last two years. Prof. Nayak during his address highlighted that "**The Journal" (JIAS)** acquired both online and print ISSN numbers and now in the UGC Care list (Category A) and obtained the DOI recognition. He also appreciated the efforts made by Prof. G M Bhat and Dr Bashir A Lone, managing editors for achieving these distinctions of the journal. He also put forth the new initiative to bring out online "IAS Magazine" which shall be "fellowship magazine" of the association with news about science, people, the society and articles of general interest and achievements of Sedimentologists of international repute and their contributions in Sedimentology. After this report by the president, the chief guest and guest of honor of the function also addressed the audience put emphasis to work for the society.

The deliberations of the two day conference "Resource Potential of Sedimentary Basins" started with the convention address of Dr Ravi Mishra on "Energy Scenario vis a vis climate change- road ahead for Hydrocarbon industry". In his address he laid emphasis on the challenges ahead in the energy sector with regard to environmental sustainability and how climate change directly have impact on various aspects of energy (supply, production) including the physical pliability of existing and future energy infrastructures.

More than 100 participants attended the conference in virtual mode from different parts of the country and abroad. A total of forty five (45) presentations were made by different researchers on themes: *Natural Resources Potential of Sedimentary Basins; Thrust Tectonics and Balanced Cross Sections, Hydrocarbon prospecting; Coastal Geodynamics: Past and present; Environment and Engineering Geology; Energy scenario vis-à-vis Global Warming and Climate Change; Groundwater Modelling.* Besides, four key note addresses were presented and the first one by Prof. Sudipta Dasgupta On "Unusual infaunal animal-sediment interactions: Unique ichnologic preservations around the Eocene shoreline of Kutch basin, Gujarat". Dr. Soumen Paul spoke on on

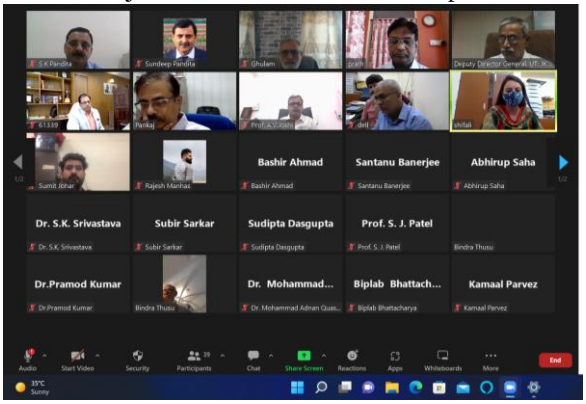

"Sequence Stratigraphy: A new paradigm". Prof. G. Shanmugam presented "Sedimentary Basins:

Processes, deposits, palaeogeography, and challenges" and Prof. Satish. J. Patel presented "Implications of Lithofacies and Ichnofacies in Sequence Stratigraphic Analysis: A Case Study from the Kachchh Sub-basins (Chorar Island-Wagad Highland)".

The valedictory function of the conference was chaired by Prof G N Nayak (President, IAS) and Prof. G M Bhat (Vice-President, IAS). They highlighted the key contribution by the presenters and congratulated the organizers for conducting a very successful conference.

Prof Pandita presented a report on the deliberations of the two day proceedings and Organizing Secretary, Dr. Yudhbir Singh presented the vote of thanks.

Dr. Yudhbir Singh

Department of Geology
University of Jammu, Jammu

JOURNAL INDIAN ASSOCIATION OF SEDIMENTOLOGISTS ISSN NO 2582 – 2020
Vol. 39, Issue 2, 2022, pp. 74-76

Obituary

Sarbani Patranabis-Deb
(13th November, 1966–31st October, 2022)

Sarbani Patranabis-Deb was an impressive multi-disciplinary earth scientist grounded on conventional scientific method of examining the rocks in the field. She was born in West Bengal, India on the 13th November, 1966 and passed away in Kolkata, on the 31st October, 2022. Sarbani was an accomplished sedimentologist, stratigrapher, sandstone petrologist, volcanic geologist, geochronologist, tectonics specialist, basin analyst, and a global geologist. She had a remarkable career in academia by joining the Indian Statistical Institute (ISI) in 1997. She was promoted to full Professor in 2020. I had the privilege of getting to know Sarbani both professionally and personally during the past 20 years since her obtaining Ph.D. from Jadavpur University in 2001. It was serendipity that the Directors of ISI requested my professional evaluation of her academic performance in 2008, 2013, and 2019 towards her career advancements at ISI. Although my research interest focuses primarily on deep-water processes (Shanmugam, 2021), Sarbani and I had many common interests of research domains, which included deltaic sedimentation, shelf sedimentation, tidal sedimentation, sequence stratigraphy, sediment deformation, tectonics, and diagenesis. We both published articles on fan deltas (McPherson et al., 1987; Patranabis-Deb and Chaudhuri, 2007).

She has research interests in sedimentology, stratigraphy, and stratigraphic basin analysis focusing on the Proterozoic cratonic basins (Purana Basins) of peninsular India and the greenstone belts underlying them.

She also worked on ancient microbial mats and their lifestyles in Precambrian sea.

She was elected fellow of West Bengal Academy of Science and Technology (WAST) 2021, received National Geoscience Award-2010, for Basic Geosciences, Ministry of Mines, Government of India (2012), Slater Fellow, Durham University, UK, 2009, BOYSCAST Fellow (DST), Post-Doctoral work on Dynamics of Indian Lithosphere at Indiana University Bloomington, USA, 2005

In 2020, the 36th International Geological Congress (36 IGC) planned for New Delhi in India was cancelled due to COVID-19 travel restrictions. This included field trips. In order to minimize disappointments from international geologists who

travelled to India to examine the Indian rocks, Sarbani organized field trips to interested geologists.

Following the Indian tradition and culture, Sarbani had always placed her family first above all else. She is survived by her husband and two sons. Her husband, Gautam Kumar Deb, is a Professor (Structural Geology) at Presidency University in Kolkata. She was always very proud of her two sons and their academic achievements.

Despite her recurrent illness during the past few years, she continued to do research and publish frequently (e.g., Patranabis-Deb, 2022; Patranabis-Deb and Saha, 2020; Patranabis-Deb et al., 2018, 2020; Kale et al., 2020; Bachhar et al., 2021; Deb et al., 2021; Banerjee et al., 2022; Slowakiewicz et al., 2022, Wabo et al., 2022, among others). She was a tenacious fighter till the end. The global geologic community will miss her.

The most recent email that I received from Sarbani was on October 22, 2022, just nine days before her passing, in which she wished me "Happy diwali dada". Dada means big brother. In the end, I have lost not only a dear sister but also a superb sedimentologist.

In the ancient Hindu culture, the name "Sarbani" represents the Mother Goddess Durga─the ultimate symbol of strength and protection. The name also means the Number # 1 (topper), reflecting leadership. I think of **SARBANI** as someone who was an amalgamation of multiple impressive traits: Stalwart (Strong), Articulate, Resourceful, Brilliant (Beautiful Bengali), Ardent, Number #1 and Intellectual (Indian)!

Please join me in celebrating Sarbani's contributions during her brief stay of 56 years on this Planet Earth. A longer version of this tribute will be published in the JIAS Magazine (Frst issue 2022)

References

Bachhar, P, Saha, D., Santosh, M., Liu, H.D., Kwon, S., Banerjee A., Patranabis-Deb, S., Deb, G.K. (2021). Mantle heterogeneity and crust-mantle interaction in the Singhbhum craton, India: new evidence from 3340 Ma komatiites. Lithos, 382-383.

Banerjee, A., Patranabis-Deb, S., Saha, D., De, S., Saha, S. (2022). Mahakut Chert Breccia in Kaladgi basin, India: Unsolved Issues Journal of the Palaeontological Society of India 67(1):12-21.

Deb, G.K., Saha, D., Patranabis-Deb, S., Banerjee, A. (2021). Coexisting Arc and MORB signatures in the Sonakhan greenstone belt, India: late Neoarchean – early Proterozoic subduction rollback and back-arc formation. The American Journal of Science 321, 1308-1349.

Kale, V.S., Saha, D., Patranabis-Deb, S., Sesha, Sai V.V., Tripathy, V., Patil-Pillai, S. (2020). Cuddapah Basin, India: A collage of Proterozoic subbasins and terranes. Proc Indian National Science Academy (PINSA) 36th International Geological Congress Special Issue. Geoscience Research in India: The Indian Report to IUGS 2016-2020. Guest Editors DM Banerjee, AK Jain Somnath Dasgupta and Sunil Bajpai. 86,137-166.

McPherson, J.G., Shanmugam, G., Moiola, R.J. (1987). Fan-deltas and braid deltas: varieties of coarse-grained deltas. Geol. Soc. America Bulletin, 99, 331–340.

Patranabis-Deb S. (2022). Preface to the thematic issue "Mesoproterozoic Basins recording Earth's Middle Age". Geological Magazine 159, 177-178 doi.org/10.1017/S0016756821.

Patranabis Deb, S. and Chaudhuri, A.K. (2002). Stratigraphic architecture of the Proterozoic succession in the eastern Chattisgarh basin: its tectonic implication. Sedimentary Geology, 147, 105-125.

Patranabis-Deb, S. and Chaudhuri, A.K. (2007). A retreating fan delta system in Proterozoic Chattisgarh basin, central India: facies analysis and palaeotectonic implications. AAPG Bulletin 91, 1-24.

Patranabis-Deb, S., Majumder, T; Khan, S. (2018). Lifestyles of the Palaeoproterozoic stromatolite builders in the Vempalle Sea, Cuddapah Basin, India. Journal of Asian Earth Sciences in special issue: The Asian continental collage (Editors) E. Shaji, Kwon S., Yang Q., 157, 360-370.

Patranabis-Deb, S., and Saha, S. (2020). Geochronology, paleomagnetic signature and tectonic models of cratonic basins of India in the backdrop of Supercontinent amalgamation and fragmentation. 36th International Geological Congress Legacy Volume, "Geodynamic evolution of the Indian subcontinent". Guest Editors: Fareeduddin, Pant, N.C., Gupta S., Chakraborty P.P., Sensarma S., Prasad G.V.R., Srivastava P, Jain A.K., Rajan R., and Tiwari V.M. Episodes 43.

Patranabis-Deb, S, Saha, D. and Santosh, M. (2020). Tracking India Within Precambrian Supercontinent Cycles. Chapter 3, in Gupta N.S. and Tandon S.K., (ed.) Geodynamics of the Indian Plate: Evolutionary Perspectives. 105-143. Springer Nature, Switzerland

Shanmugam, G. (2021). Mass transport, gravity flows, and bottom currents: Downslope and alongslope processes and deposits. Elsevier, Amsterdam, **ISBN:** 9780128225769, p. 608.

Slowakiewicz, M., Banerjee, A., Patranabis-Deb, S., Deb, G.K., Tucker, M. (2022). Sinuous stromatolites of the Chandi Formation, Chattisgarh Basin, India: their origin and implications for Mesoproterozoic seawater. Geological Magazine. 159(2):279-292

Wabo, H., Beukes, N.J., Patranabis-Deb, S., Saha, D., Belyanin, G. Kramers, J.D. (2022). Paleomagnetic and Ar/ Ar age constraints on the timing of deposition of deep-water carbonates of the Kurnool Group (Cuddapah basin) and correlation across Proterozoic Purana successions of Southern India. Journal of Asian Earth Sciences 223, Article 104984 doi.org/10.1016/j.jseaes.2021 .104984.

G. Shanmugam
Department of Earth and Environmental Sciences
The University of Texas at Arlington
Arlington, TX 76019, USA
Email: shanshanmugam@aol.com